Hydraulic Backbone of CB1 to CB3 Boreholes in the Bedretto Underground Lab

Master Thesis

Author(s):
Münger, Andri

Publication date:
2020

Permanent link:
https://doi.org/10.3929/ethz-b-000469250

Eidgenössische Technische Hochschule Zürich
Swiss Federal Institute of Technology Zurich

D ERDW
EARTH SCIENCES

Master Thesis

Hydraulic Backbone of CB1 to CB3 Boreholes in the Bedretto Underground Lab

Submitted at the Department of Earth Sciences at the ETH Zurich
Geological Institute, Chair of Engineering Geology

Supervised by
Prof. Dr. Simon Löw, Geological Institute, ETH Zurich
Dr. Nima Gholizadeh Doonechaly, Geological Institute, ETH Zurich

Submitted by
Andri Münger
15-928-658

Zurich, 03.10.2020

ABSTRACT

In collaboration with the Swiss Competence Center for Energy Research – Supply of Electricity (SCCER-SoE), ETH Zurich conducts innovative and sustainable research in the field of geo-energy and hydropower. Parts of the research is conducted in the Bedretto Underground Laboratory for Geoenergies (BULG) – a Deep Underground Geoscience Laboratory – located in crystalline rocks of the Swiss Central Alps and concentrates on Enhanced Geothermal Systems (EGS). This thesis contributes to a strong geological and hydrogeological model at the BULG, which is of high importance for further researches within this major project.

Single well and cross-hole hydraulic tests with a multipacker system were performed in three long (191 – 302 m) research boreholes (CB1, CB2, CB3) in the BULG, in the Swiss Alps. The analyses mainly consisted of iterative non-linear optimization curve fitting applying the Theis Solution and the Generalized Radial Flow model on the single well test data and the Theis and the Agarwal solution on the cross-hole response data. Further, geological and geotechnical core logs at the scale of 1:1'000 are presented for the boreholes in which the transient pressure testing took place.

The tested crystalline fractured rock (Rotondo granite) is hydrologically heterogeneous and shows a strong scale effect regarding its transmissivity. At medium scale (several meters) recorded transmissivities range in five orders of magnitude (10^{-11} – 10^{-7} m^2/s), depending on the tested structure. At large scale all packed and tested structures showed approximately the same transmissivity (~10^{-6} m^2/s). The existence of a hydraulic backbone with a transmissivity of 10^{-7} m^2/s at medium scale is suggested. The suggested hydraulic backbone intersects CB2 at BM 159 (ATV log as reference). The exact intersection depth of CB1 and CB3 with the hydraulic backbone could not be conclusively determined, as no multipacker systems were installed in CB1 and CB3. Nevertheless, an intersection depth in CB1 at BM 181 and in CB3 at BM 151 is suggested based on borehole logs, GPR data and observation during core logging. The hydraulic backbone is characterized by hydrothermally altered fractures with vuggy porosity and has an orientation of 58/329. The hydraulic backbone appears to follow a healed fracture zone of Alpine age.

TABLE OF CONTENTS

1 INTRODUCTION 1

1.1 Bedretto Reservoir Project 1

1.2 Research Goal 3

2 STUDY SITE 4

2.1 Bedretto Underground Lab for Geoenergies (BULG) 4

2.1.1 General Information 4

2.1.2 Boreholes CB1, CB2, CB3 4

2.2 Geological Setting 5

2.2.1 General Information 5

2.2.2 Core Log CB1, CB2, CB3 6

2.3 Hydrological Setting 15

3 TRANSIENT PRESSURE TESTING METHODS 16

3.1 Multipacker System 17

3.1.1 Possible Packer Installation Intervals 18

3.1.2 Zones of Interest 19

3.1.3 Final Multipacker System Setup 20

3.2 Equipment and Test Design 26

3.2.1 Equipment 27

3.2.2 Pulse Test 29

3.2.3 Constant Rate Test 29

3.3 Test Analysis 31

3.3.1 Pulse Test 32

3.3.2 Constant Rate Test 33

3.3.3 Constant Rate Test: Single Well Test Analysis 34

3.3.4 Constant Rate Test: Cross-Hole Test Analysis 36

4 TRANSIENT PRESSURE TESTING RESULTS 39

4.1 Pulse Test 39

4.2 Constant Rate Test: Single Well 39
4.2.1 Qualitative Observations 40
4.2.2 Initial Pressure 42
4.2.3 Diagnostic Plots 43
4.2.4 Transmissivity 45
4.2.5 Storativity 46
4.2.6 Flow Dimension 47
4.3 Constant Rate Test: Cross-Hole 48
4.3.1 Qualitative Observations 50
4.3.2 Response Times 51
4.3.3 Diagnostic Plots 54
4.3.4 Transmissivity 54
4.3.5 Storativity 55
4.3.1 Skin Effect 57
4.4 Comparison: Single Well Test and Cross-Hole Response Analysis 58
4.4.1 Transmissivity 58
4.4.2 Storativity 59
4.4.3 Diffusivity 60

5 INTERPRETATION AND DISCUSSION 63
5.1 Single Well Test Analysis 63
5.1.1 Qualitative Observations 63
5.1.2 Initial Pressure 63
5.1.3 Diagnostic Plots 64
5.1.4 Transmissivity 65
5.1.5 Storativity 67
5.1.6 Flow Dimension 67
5.2 Constant Rate Test: Cross-Hole 69
5.2.1 Qualitative Observation 69
5.2.2 Response Times 70

5.2.3 Diagnostic Plots 71
5.2.4 Transmissivity 71
5.2.5 Storativity 72
5.2.6 Skin Effect 74
5.3 Comparison Single Well Test and Cross-Hole Response Analysis 75
5.3.1 Transmissivity 75
5.3.2 Storativity 75
5.3.3 Diffusivity 75

6 CONCLUSION 77

7 ACKNOWLEDGEMENT 80

8 REFERENCES 81

9 DECLARATION OF ORIGINALITY 84

10 APPENDIX 85

LIST OF FIGURES

Fig. 1.1. Location of the Bedretto Underground Laboratory for Geoenergies (BULG) and geological situation (modified after Keller & Schneider, 1982)..... 2

Fig. 2.1. Trajectories of CB1, CB2 and CB3. The dashed line indicates the extrapolated continuation of CB3 as the trajectories are based on the borehole logging, which did not reach the bottom of CB3. Left: Sideview, looking NW. Right: Topview 5

Fig. 2.2. Geological cross-section along the Bedretto tunnel alignment. Location of the Bedretto Underground Laboratory for Geoenergies (BULG) is indicated in red (modified after Keller & Schneider, 1982). 5

Fig. 2.3. Simplified composite core log of CB1. Legend shown in Fig. 2.6. 8

Fig. 2.4. Simplified composite core log of CB2. Legend shown in Fig. 2.6. 9

Fig. 2.5. Simplified composite core log of CB3. Legend shown in Fig. 2.6. 10

Fig. 2.6. Legend for column simplified geological core log in Fig. 2.3 – Fig. 2.5. 11

Fig. 2.7. Photos of specific features in the cores of the test volume in BULG. A: Broken healed fracture, B: Slickensided fracture with chloritic and sericitic infilling (core diameter for scale), C: Aplitic dike, D: Open joint, E: Foliated Granite (Type 1) with ductile shear zones, F: Hydrothermal altered fracture with newly formed minerals and vuggy porosity, G: Brittle fault zone. 14

Fig. 3.1. Schematic representation of a single packer used to set up the multipacker system. Two generations of packers (old/new) were used, both had an inflatable rubber part of 1 m length. 18

Fig. 3.2. Result of the evaluation of several data sets for the determination of possible packer installation location and zones of interest. For CB2 the definitive packer installation locations are given. 23

Fig. 3.3. Stereoplots (lower hemisphere) for each interval in CB2 with the fractures mapped in the ATV log by Krietsch (2019). The bold plane indicates orientation of the presumably most conductive structure in the considered interval. 25

Fig. 3.4. Graphical representation (not at scale) of the testing setup of the transient pressure tests in CB1, CB2 and CB3, with the multipacker system in CB2. In the first row of the flow board the interval pressure sensors are located, in the second row the manometers for pressure control in the packers and in the third row the lines for possible tracer injection into the intervals. 28

Fig. 3.5. An example for a plot created by hytool reporting the results of the analysis with Theis (1935). Shown is the report of the single well test analysis of the buildup phase of the constant rate test in Interval 4-2. 31

Fig. 3.6. Diagnostic plot showing different indicative sections (wellbore storage, infinite acting and boundary), as well as the critical 1.5 log cycles (modified after Horne, 1990). 33

Fig. 3.7. Graphical representation of subradial and radial flow in a fractured media. The red dots indicate pumping/injection locations (Brixel et al., 2020b). 36

Fig. 4.1. Oscillating pressure in Interval 5&6 during the drawdown phase of the constant rate test. 41

Fig. 4.2. Oscillating flow rate during the constant rate test in Interval 5&6, shown by a section of the flow measurements during the test. 41

Fig. 4.3. A section of the pressure curve in Interval 2 during the buildup in CB1 as an example for the oscillating pressure in Interval 2. 42

Fig. 4.4. Compilation of transmissivity values resulted from the single well analysis of the constant rate tests on log scale. 46

Fig. 4.5. Compilation of storativity values resulted from the single well analysis of the constant rate tests. 47

Fig. 4.6. Compilation of flow dimension values resulted from the single well analyses of the constant rate tests applying the GRF model. 48

Fig. 4.7. Pressure data during the constant rate test in CB1 (smoothed pressure curve for CB1). 49

Fig. 4.8. Pressure data during the constant rate test in CB3 (smoothed pressure curve for CB3). 49

Fig. 4.9. Example for the apparency of the Noordbergum effect in Interval 2 caused by the shut-in in CB1. 51

Fig. 4.10. Normalized pressure responses in all intervals and CB3 to the withdrawal in CB1. 53

Fig. 4.11. Normalized pressure responses in all intervals and CB1 to the recovery in CB3. .. 53

Fig. 4.12. Compilation of transmissivity values resulted from the cross-hole response analysis of the constant rate tests in CB1 and CB3. 55

Fig. 4.13. Compilation of storativity values resulted from the cross-hole response analysis of the constant rate tests in CB1 and CB3. 56

Fig. 4.14. Compilation of wellbore skin effect values resulted from the analysis of cross-hole responses to the constant rate tests in CB1 and CB3. 57

Fig. 4.15. Compilation of transmissivity mean values (with standard deviation) resulted from pulse test, single well test and cross-hole response analysis..... 58

Fig. 4.16. Compilation of storativity mean values (with standard deviation) resulted from the single well and cross-hole response analysis. No standard deviation is reported for the values resulted from the analyses of the cross-hole responses in Intervals 2 and 3, and for the value resulted from the single well test analysis of Interval 7, as the standard deviations are greater than the corresponding mean values, which cannot be represented on a log scale plot. 59

Fig. 4.17. Plotted are the response times vs. distances to the active well (colored dots) at log-log scale and the normal diffusion for varying diffusivity values (dashed lines). ... 60

Fig. 4.18. Compilation of the diffusivity values resulted from single well test analyses and cross-hole response analyses as well as the values obtained from the diffusion plot. 62

LIST OF TABLES

Tab. 2.1. General information about the three boreholes CB1, CB2 and CB3. 4

Tab. 3.2. Packed intervals in CB2. 21

Tab. 3.1. Packer installation depths in CB2. 21

Tab. 3.3. Characteristics of packed intervals in CB2 and information about presumably most conductive structures for each interval. 24

Tab. 3.4. Timetable giving an overview of the tests conducted in CB1, CB3 and the Intervals 1 to 7 in CB2. 26

Tab. 3.5. Details of pulse tests performed in the intervals in CB2. 29

Tab. 3.6. Details of all successfully performed and analyzed constant rate tests in chronological order. 30

Tab. 3.7. Shortest connection between the intervals and CB1 and CB3, respectively 37

Tab. 4.1. Results of the pulse tests performed in the intervals in CB2 analyzed with the Neuzil (1982) solution and the proposed flow rate for the constant rate tests. 39

Tab. 4.2. Initial pressures derived from the straight line fitting in the Horner plots of the buildup data from the constant rate tests. 43

Tab. 4.3. Indicating which interval/borehole responded to each other's constant rate tests responses interval/borehole. 50

Tab. 4.4. Response times regarding the start of the withdrawals in 52

1 INTRODUCTION

1.1 Bedretto Reservoir Project

In 2017, Swiss voters approved the new energy law, which states that energy consumption in Switzerland should be reduced, energy efficiency increased and renewable energies promoted.

How this objective is going to be achieved is specified in the Energy Strategy 2050 (SFOE, 2018). In the context of the energy strategy 2050 the Swiss Competence Center for Energy Research – Supply of Electricity (SCCER-SoE) was founded with the aim to carry out innovative and sustainable research in the areas of geo-energy and hydropower (SSCER-SoE, 2020). Together with the ETH Zurich, the SCCER-SoE conducts research in the field of Enhanced Geothermal Systems (EGS). Parts of the tests are executed in the Bedretto Underground Laboratory for Geoenergies (BULG) which is a Deep Underground Geoscience Laboratory (DUGLab). The BULG is located the Swiss Central Alps in the Bedretto Tunnel, an abandoned access tunnel to the Furka railway tunnel (Fig. 1.1) which was constructed in the years from 1971 to 1983.

EGS use the naturally increased temperatures in the earth's interior to generate electricity. The natural, average temperature gradient in the earth's interior is 25 – 30°C/km, although this value can vary from region to region. Temperatures from 150°C upwards are suitable for EGS. Therefore, a depth of 4 – 5 km needs to be reached in a region with an average temperature gradient. For a beneficial EGS, an effective heat exchange between rock and fluid is required and therefore a disperse flow through the rock body is necessary.

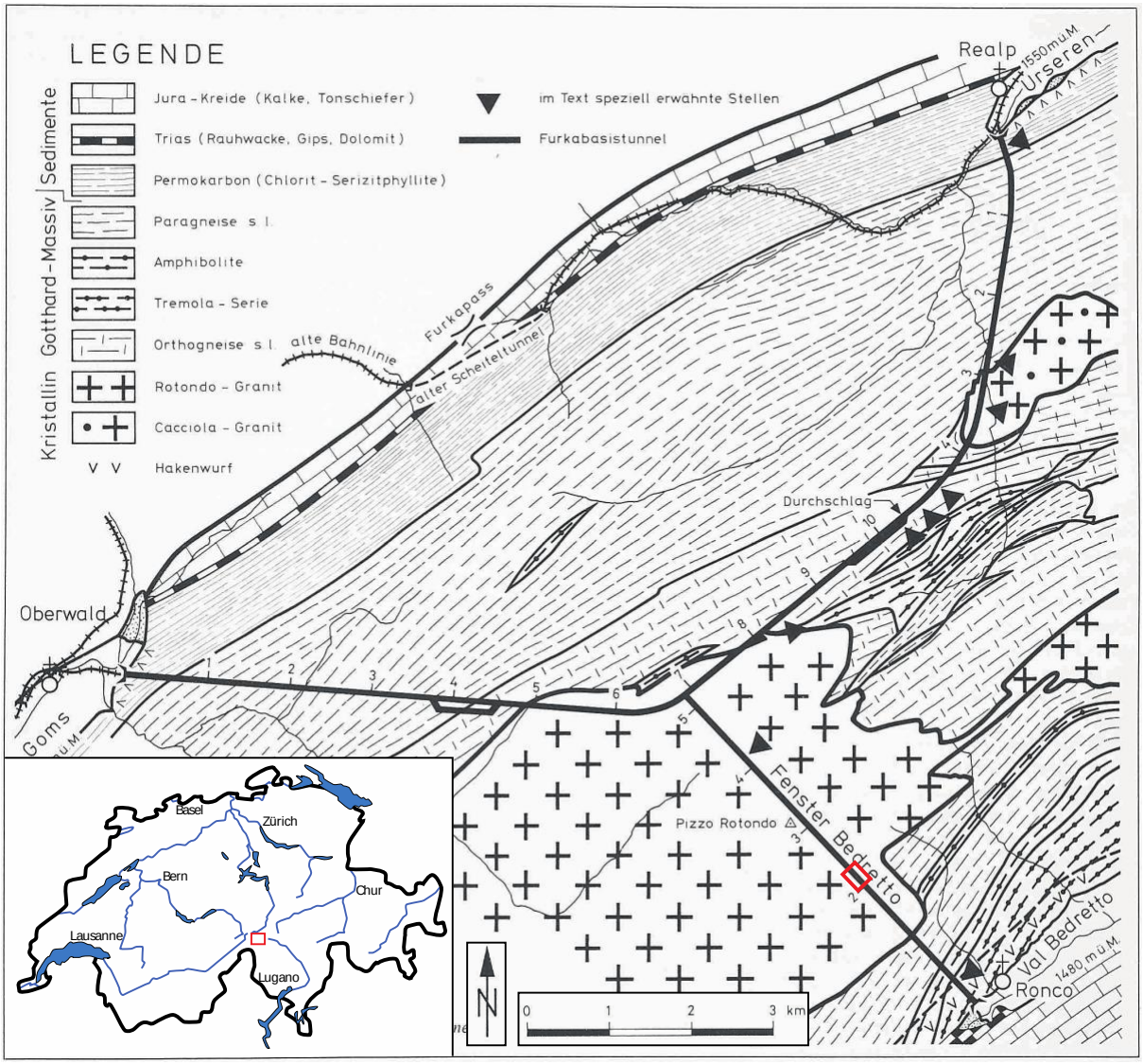

Fig. 1.1. Location of the Bedretto Underground Laboratory for Geoenergies (BULG) and geological situation (modified after Keller & Schneider, 1982).

The low transmissivity of 10^{-14} – 10^{-11} m^2/s (e.g. Brixel et al., 2020; Wenning et al., 2018) of crystalline rocks such as Rotondo granite do not allow a considerably amount of water to flow through its matrix. Groundwater flow in crystalline rocks is therefore concentrated along discrete structures with secondary porosities such as fractures and fault zones. In the Grimsel Test Site (GTS) fracture and fracture zone transmissivities of 10^{-13} – 10^{-6} m^2/s. (with a log-normal distribution around a mean value of 10^{-8} m^2/s) were found (Brixel et al., 2020). Due to the discrete flow paths in crystalline rock, hydraulic stimulation is required to create a disperse flow path network for an effective heat exchange from rock to fluid. For the design of the

hydraulic stimulation, the identification and characterization of the natural main flow paths in the rock body in which the geothermal reservoir is planned are crucial.

1.2 Research Goal

The final goal of this thesis is to contribute to the refinement of the geological and hydrogeological model of the Rotondo granite in the BULG. In more detail, the hydraulic properties of the structures intersecting the tested reservoir as well as their scale dependency are investigated. The homogeneity and isotropy of the tested reservoir is assessed. In addition, a possible hydraulic backbone is identified and characterized. Furthermore, the conductive structures in the tested reservoir are identified, characterized and geologically described.

2 STUDY SITE

2.1 Bedretto Underground Lab for Geoenergies (BULG)

2.1.1 General Information

The Bedretto tunnel is oriented NW–SE, has a total length of 5.2 km and a diameter of about 3 m. The BULG is located in a 100 m long niche starting at tunnel meter (TM) 2000 measured from the tunnel entrance near the Ronco village. The nice in which the BULG is located has height of about 3 m and a width of about 6 m. The overburden at the BULG is about 1 km (Fig. 2.2).

2.1.2 Boreholes CB1, CB2, CB3

The three boreholes (CB1, CB2, CB3) with a core diameter of 96 – 98 mm were drilled in the period of August to November 2019 by Züblin Spezialtiefbau Ges.m.b.H. For CB1 and some parts of CB2 and CB3 the double barrel with core catcher method was applied. For CB2 and CB3 mainly the counter flush method was applied. The extracted cores are cut in 1 m long pieces and stored in core boxes. More details about CB1 to CB3 can be found in Tab. 2.1. The trajectories of the three boreholes are illustrated in Fig. 2.1.

Tab. 2.1. General information about the three boreholes CB1, CB2 and CB3.

	CB1	**CB2**	**CB3**
Location Borehole Mouth	TM ~2050	TM ~2043	TM ~2037
Total Length	302 m	222.5 m	191.5 m
Diameter	98 cm	96 cm	96 cm
Dip (at wellhead)	45°	50°	40°
Dip Direction (from North)	225°	225°	225°
Angle to the tunnel alignment	90°	90°	90°
Standpipe, cemented	BM 0 – 15	BM 0 – 15.7	BM 0 – 16

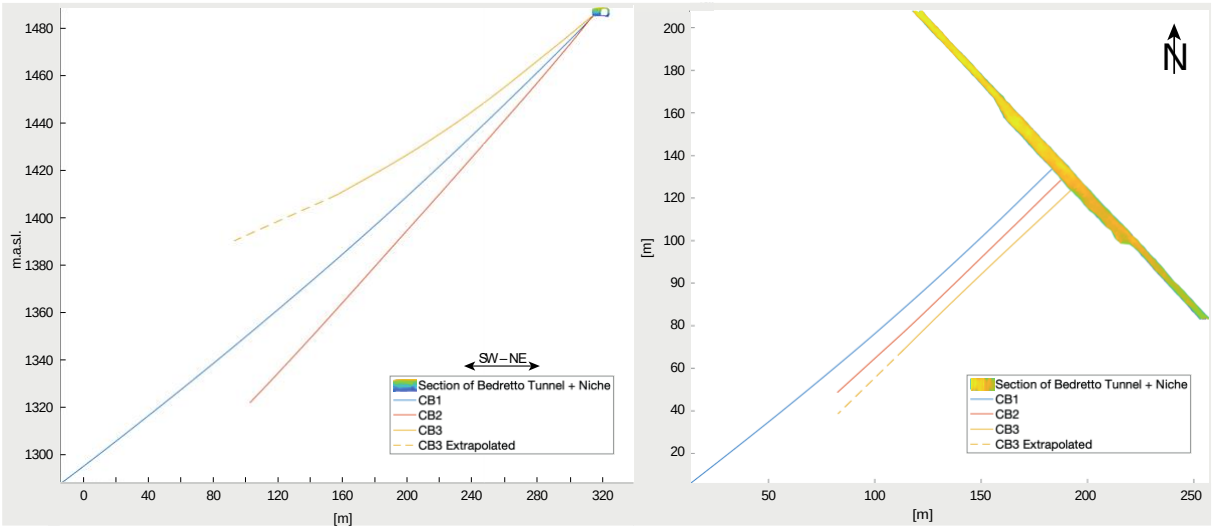

Fig. 2.1. Trajectories of CB1, CB2 and CB3. The dashed line indicates the extrapolated continuation of CB3 as the trajectories are based on the borehole logging, which did not reach the bottom of CB3.
Left: Sideview, looking NW. Right: Topview

2.2 Geological Setting

2.2.1 General Information

A detailed geological mapping (Fig. 1.1) and creation of geological cross-sections along the Bedretto tunnel (Fig. 2.2) and the Furka railway tunnel was conducted by Keller and Schneider (1982).

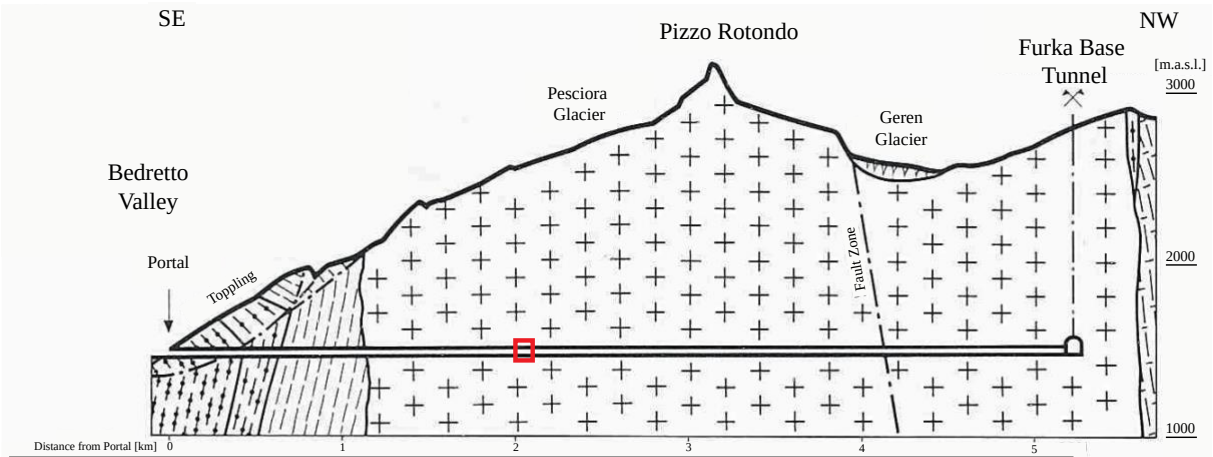

Fig. 2.2. Geological cross-section along the Bedretto tunnel alignment. Location of the Bedretto Underground Laboratory for Geoenergies (BULG) is indicated in red (modified after Keller & Schneider, 1982).

The geology along the Bedretto tunnel can roughly be subdivided in three sections. The first ~450 m meters from the tunnel portal is dominated by hornblende-gneisses, hornblende-schists, mica-gneisses and mica-schists which are indicative for the Tremola series. The TM ~450 to ~1150 are dominated by banded hornblende-schists and amphibolites in the South (TM ~450 to ~650) and bright two-mica gneisses and -schists further North (TM ~650 to ~1150). The characteristics of the TM ~450 to ~1150 are typical for the Prato series (Hafner, 1958; Steiger, 1962). The slope at the Ronco village is characterized by toppling. At the height of the Bedretto tunnel the effect reaches ~350 m into the mountain (Keller & Schneider, 1982).

At TM ~1150 a sharp boundary between the Prato series and the Rotondo granite can be observed. From TM ~1150 the Rotondo granite continues through to the end of the Bedretto tunnel (TM 5221), where it meets the Furka railway tunnel. Thus, the BULG is located completely in the Rontondo granite, which intruded in the late Vascican (Sergeev et al., 1995). The Rotondo granite—to a large extent—consists of a massive, equigranular, fine to medium grained granite (25 – 35% quartz, 25 – 35% alkali feldspar, 20 – 40% plagioclase 3 – 8% biotite) with accessories as garnet, phengite, chlorite, epidote, apatite and zircon. Few aplitic and lamprophyre dykes cross the Rotondo granite (Hafner, 1958). The granite is mostly undeformed, however, in some areas it experienced ductile deformation during the Alpine deformation (Marquer, 1990) and shows gneissic or even schistous texture. In a late stage of the alpine deformation brittle deformation occurred, whereby fault zones often formed along the previously formed ductile shear zones (Lützenkirchen, 2002). A detailed tunnel wall mapping and analysis of the found structures was performed for TM 1140 – 2800 in the context of the Master's thesis of Jordan (2019).

2.2.2 Core Log CB1, CB2, CB3

Core logs (Appendix A) for the boreholes CB1, CB2 and CB3 have been prepared at the scale of 1:1'000 in collaboration with Matthias Meier (2020) (accompanying master thesis in the BULG). Simplified composite core logs for the boreholes CB1, CB2 and CB3 can be seen in Fig. 2.3, Fig. 2.4 and Fig. 2.5, respectively. Raw data at the scale of 1:150 of the core logs, as well as additional photos of the cores can be obtained from Münger and Meier (2020).

The classifications of the Rotondo granite and the associated structures by Laws (2001), Lützenkirchen (2002) and Jordan (2019) on which the core log is based can be seen in Appendix B. In addition, a manual by Dr. Peter Guntli (Sieber Cassina + Handke AG, 2019)

was used. The core log is intended to provide a geological and geotechnical overview of the test volume, showing the most important structures and the variability of the rock mass along and between the boreholes. Further, the cores are used to identify features which might dominate the hydrogeological behavior of the test volume.

The composite core logs for the boreholes CB1 (Fig. 2.3), CB2 (Fig. 2.4) and CB3 (Fig. 2.5) includes a simplified geological core log, rock type, cumulative water inflow, RQD, discing, core loss, number of open fractures and porosity. In the simplified geological core log, the mapped geological structures are presented in a schematic way, to give an idea about the appearance and the most important features in the core (Fig. 2.7). The rock type column indicates the depths at which the different types can be found. In Appendix A, the geotechnical description with the texture, mineralogy and discontinuities is noted in this column. The presented field estimates of uniaxial compressive strength are used from Hoek and Brown (1997). In the cumulative water inflow column, the flow measurements during drilling are shown in l/min. The RQD (Deere & Deere, 1988) value is determined for each meter, whereby the drilling induced fractures and discing is not considered, thus, the core is considered to be intact at these positions. In the log the range from the minimum to the maximum value within 10 meters is indicated. Discing (Obert & Stephenson, 1965) is recorded, when the core is broken in many thinner disks (0.5 – 4 cm). It can be assumed that these discs are a result of high in situ stress magnitudes relative to the rock strength (Lim & Martin, 2010) in combination with the orientation of the borehole. The core loss column indicates where no core could be recovered. In this case, core loss is most likely caused by the drilling process (and not by a fault zone), whereby a core piece could have jammed during drilling and grinded the following rock. This conclusion is based on the shape of the lowest core piece before the core loss section and the study of the ATV log (Krietsch, 2019) which does not show any fault zone like structures in the corresponding section of the borehole. The number of open fractures is given for sections of 10 meters in length. As open fractures are counted slickensided fractures, fractures along which newly formed minerals are found as well as discontinuities with vuggy porosity. Two types of hydrothermal porosity are found in the cores, "unconnected" and "connected" porosity. Unconnected porosity stands for small pores (0.5 – 3 mm) which are more or less regularly dispersed in the rock. Connected porosity stands for several pores with diameter of ~1 mm which have oriented themselves in the core along a plane and are partially connected. This description of porosity is not conclusive and not quantitative.

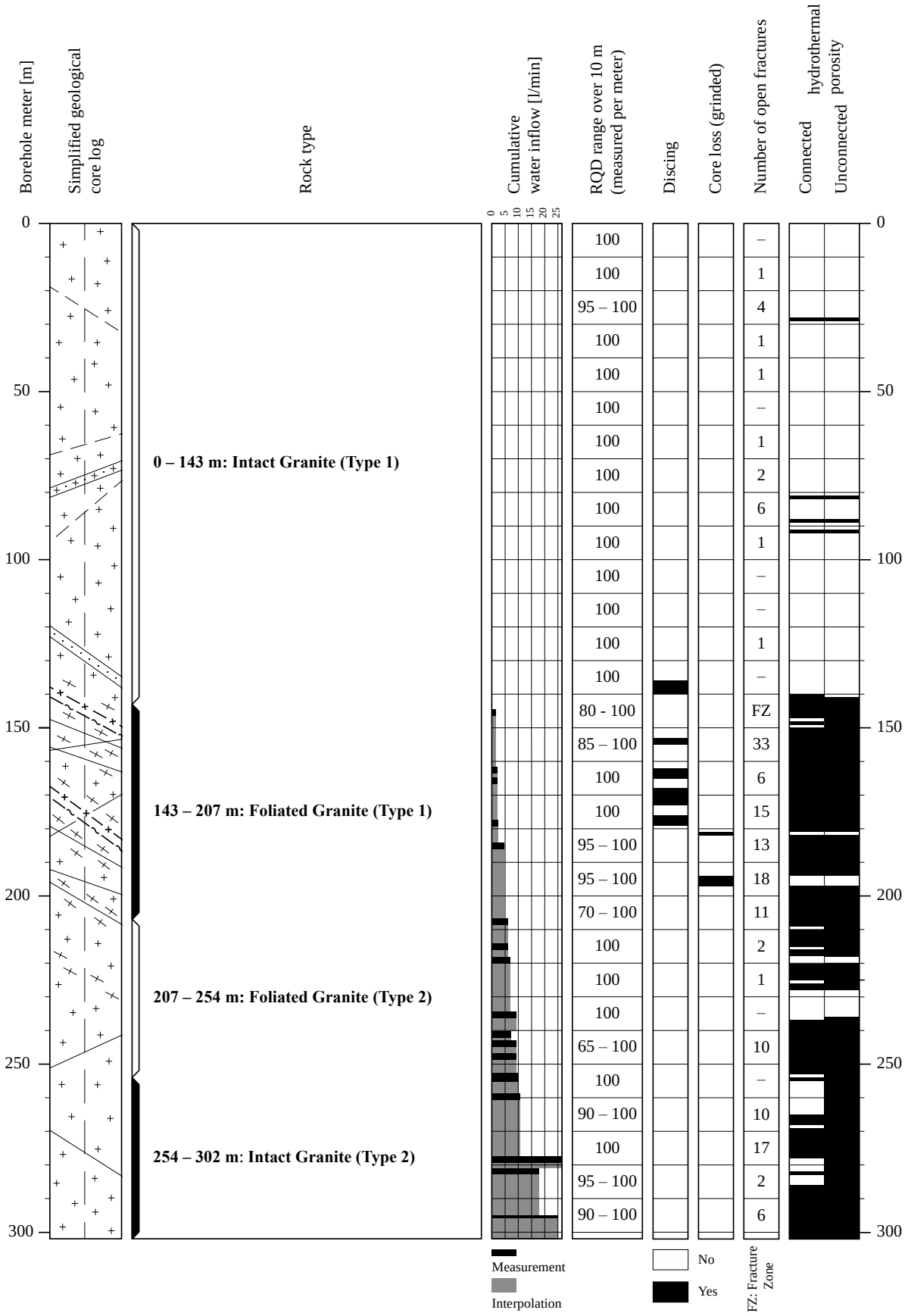

Fig. 2.3. Simplified composite core log of CB1. Legend shown in Fig. 2.6.

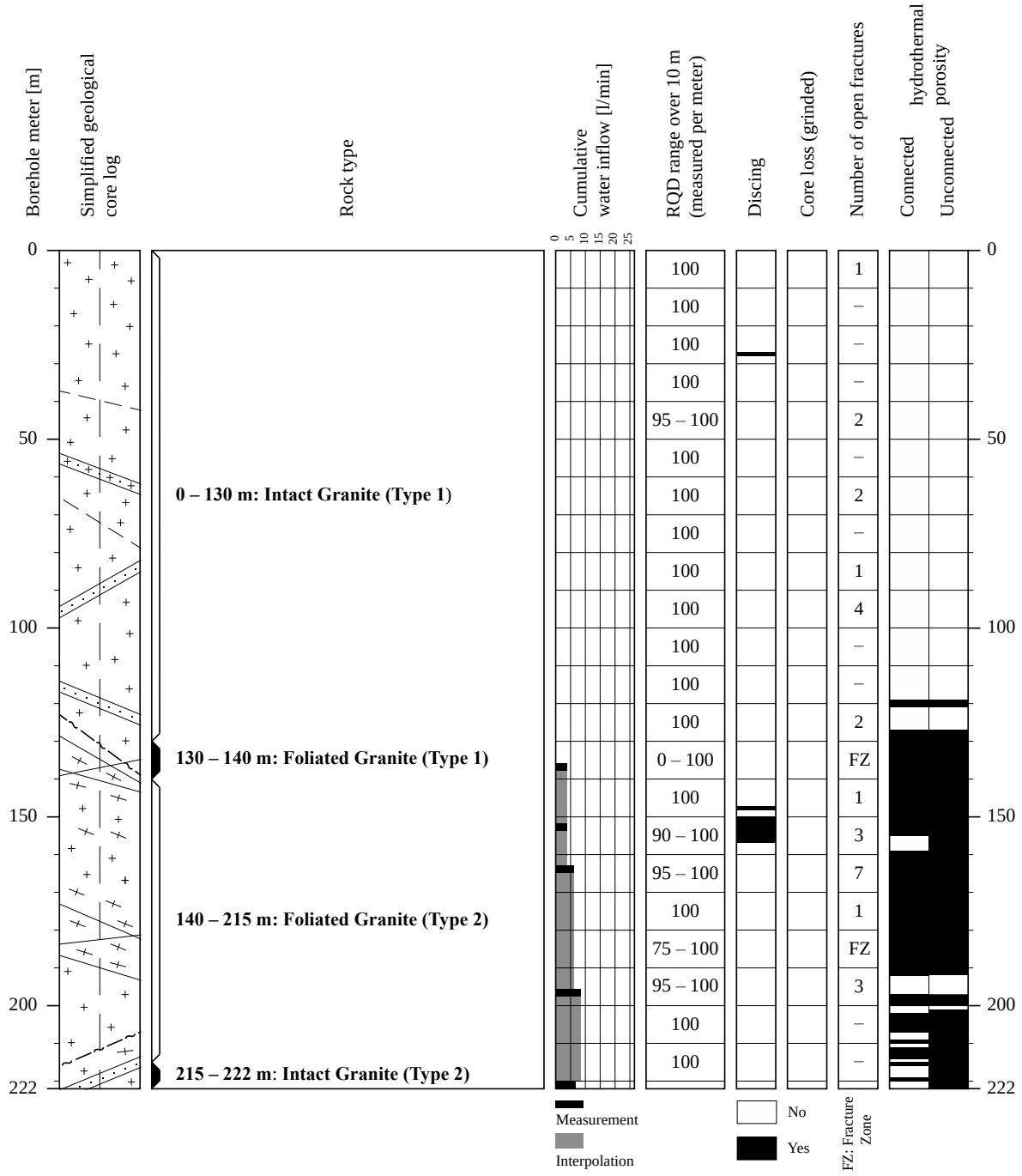

Fig. 2.4. Simplified composite core log of CB2. Legend shown in Fig. 2.6.

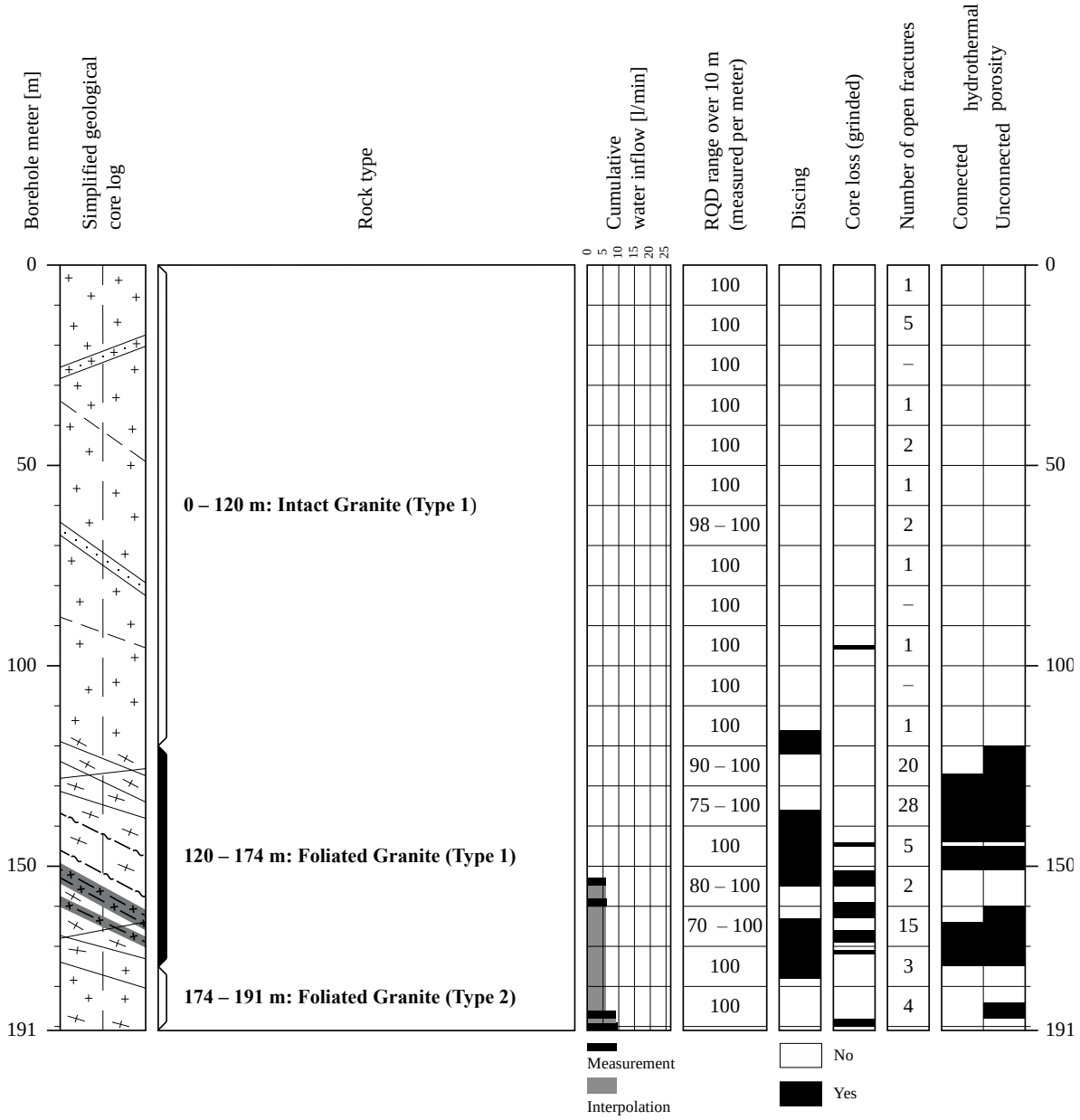

Fig. 2.5. Simplified composite core log of CB3. Legend shown in Fig. 2.6.

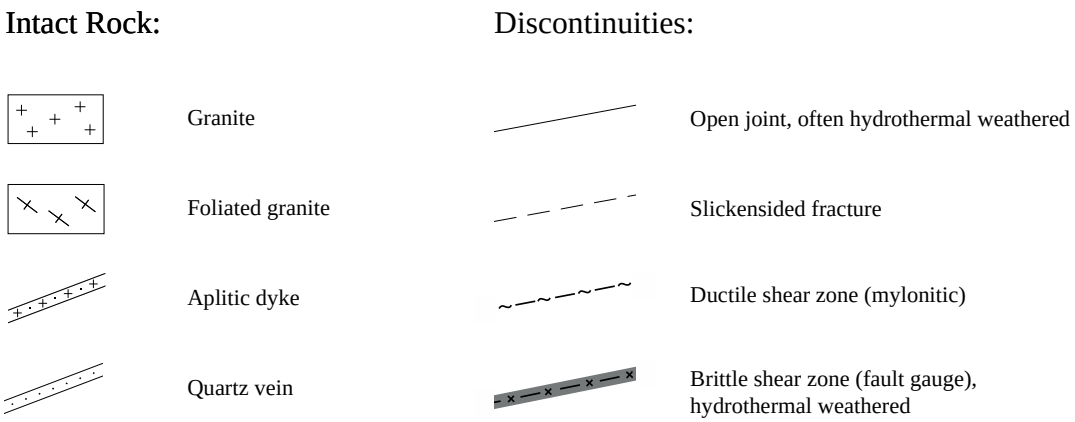

Fig. 2.6. Legend for column simplified geological core log in Fig. 2.3 – Fig. 2.5.

The three cores show sections with strong similarities. In order to provide a better comparison between the three boreholes four rock types have been elaborated. The types are the Intact Granite (Type 1 and 2) and the Foliated Granite (Type 1 and 2). These are described in more detail in the following sections. In all boreholes the Intact Granite (Type 1) is encountered first and then the Foliated Granite (Type 1 and 2). The Intact Granite (Type 2) occurs in the lowest section of the boreholes CB1 and CB2. A graphical representation of the depths of the rock types in each borehole can be seen in description column of the corresponding core log.

The Intact Granite (Type 1) is found in CB1 at borehole meter (BM) 0 – 143, in CB2 from BM 0 – 130 and in CB3 from BM 0 – 120. Figures 2.7 A and B show the Intact Granite (Type 1) at BM 84 in CB1. The Intact Granite (Type 1) can be described as homogeneous, massive, light-grey, medium to coarse-grained granite with plagioclase (often saussuritized), alkaline feldspar, quartz, white mica, biotite (in nests) and garnet (1 – 2 mm diameter). This Intact Granite is unweathered and extremely strong. Existing healed fractures have a thickness of 1 – 3 mm (sporadically 1 cm) and are usually containing biotite, muscovite (or phengite), partly chlorite, epidote or calcite (Fig. 2.7 A). The healed fractures have a frequency of 0.2 – 4 per meter and no systematic orientation is recognized. However, the core tends to fail along these healed fractures. Existing slickenside fractures have chlorite on the sliding surface, but no systematic orientation or rake is recognized (Fig. 2.7 B). In this rock type the frequency of the slickensided fractures is >/~0.1 per meter (depending on the borehole). Few quartz veins and few aplitic zones (Fig. 2.7 C) are present in this rock type. During drilling, no water inflow has been recorded along the entire length of this rock type. The RQD is almost constantly 100,

occasionally it decreases to 95. The Intact Granite (Type 1) very rarely shows discing, connected or unconnected porosity.

The Foliated Granite (Type 1) is found in CB1 at BM 143 – 207, in CB2 from BM 130 – 140 and in CB3 from BM 120 – 174. The Foliated Granite (Type 1) can be described as foliated (gneissic), grey, medium grained granite (Fig. 2.7 E) and has a similar mineralogy as Intact Granite (Type 1). In CB1 and CB3 the foliated granite is intersected by homogenous massive granite (10 – 100 cm long sections). Foliation occurs by oriented mica and fine quartz layers (1 – 3 mm thick). The distance of (shear) foliation is 0.1 – 1 cm (sericitization). The foliated granite is very strong (locally decreased). Occurring healed fractures of the foliated granite are analogue to Intact Granite (Type 1). The existing open joints have an increased frequency (1 – 3 per m) compared to Intact Granite (Type 1) or are even forming a fracture zone with more than 10 per m (Fig. 2.7 D). The open joints often occur along the foliation. The surfaces are often hydrothermally altered and show porosity (Fig. 2.7 F). In few open fractures fault gauge is visible. The slickensided fractures are rare compared to Intact Granite (Type 1) and have properties analogue to Intact Granite (Type 1). In this rock type, ductile shear zones appear. These are characterized by very fine grained (mylonitic), matrix dominated, recrystallized, dark grey-green sections, sometimes accompanied by little fault gauge. Ductile shear zones are found at BM 143 and BM 172 in CB1, between BM 130 and 140 in CB2 and at BM 142 m and BM 147 in CB3. Brittle fault zones also occur, especially in the foliated (gneissic) sections, located near ductile shear zone and with little fault gauge. In the CB3 from BM 155 – 160 and BM 163 – 165 there are brittle fault zones (Fig. 2.7 G), which can be described as cohesive cataclasites with grey matrix and rock fragments (quartz and plagioclase) with sizes of <1 cm (rarely up to 3 cm). These zones are weak to medium strong. It can be assumed that during drilling this rock type caused the first inflow to each borehole. The RQD is often 100, but sometimes it is decreased to 75 and once to 0. Discing was frequently encountered in the Foliated Granite (Type 1). From this rock unit onwards, connected and unconnected porosity is frequently encountered. This is possible due to the increased water content in this rock type and the associated hydrothermal weathering of the rock.

The Foliated Granite (Type 2) is found in CB1 at BM 207 – 254, in CB2 from BM 140 – 215 and in CB3 from BM 174 – 191. The Foliated Granite (Type 2) is a massive granite, intersected by foliated, gneissic Granite (similar to Foliated Granite (Type 1)). The mineralogy is similar to Intact Granite (Type 1) with addition of newly formed white mica on schistosity

and granitic matrix (sericitization). The Foliated Granite (Type 2) is very strong to extremely strong. The healed fractures are similar to Intact Granite (Type 1). Existing open joints have a decreasing frequency (0 – 1 per m) relative to the Foliated Granite (Type 2). Some surfaces are hydrothermally altered and show newly formed minerals (Fig. 2.7 F). The RQD is typically 100, occasionally it is decreased to 65. For the Foliated Granite (Type 2), discing was only recorded in CB2. Both connected and unconnected porosity was found in the foliated gneissic sections. The unconnected porosity is often found in the intact sections.

The Intact Granite (Type 2) is found in CB1 at BM 254 – 302 m and in CB2 at BM 215 – 222 m. This type of granite was not found in CB3. The Intact Granite (Type 2) is a massive granite with a mineralogy similar as Intact Granite (Type 1). Muscovite is present as in Foliated Granite (Type 2). Relative to the Intact Granite (Type 1), the plagioclase is more often saussuritized. The Intact Granite (Type 2) is extremely strong. The healed fractures are analogue to the Intact Granite (Type 1). In CB1 the open joints have an opening of 0 – 10 mm and are often hydrothermally altered and show newly formed minerals. However, they are not always penetrative continuous. The open joints show a frequency of 0 – 2 per m. Slickensided surfaces are rarely found. The RQD is typically 100, occasionally it is decreased to 90. No discing was recorded in the Intact Granite (Type 2). Connected porosity was encountered regularly and almost always unconnected porosity.

The test volume in the BULG can be assumed to be very heterogeneous and the thickness of the structures can change significantly over a small distance (in order of meters). In particular, this is evident in the brittle-ductile shear zone, which occurs in CB3 but is not as prominent in the boreholes CB1 and CB2. It can be assumed that the same structures (aplitic zones, mylonites or shear zones (ductile and brittle)) are encountered in different boreholes.

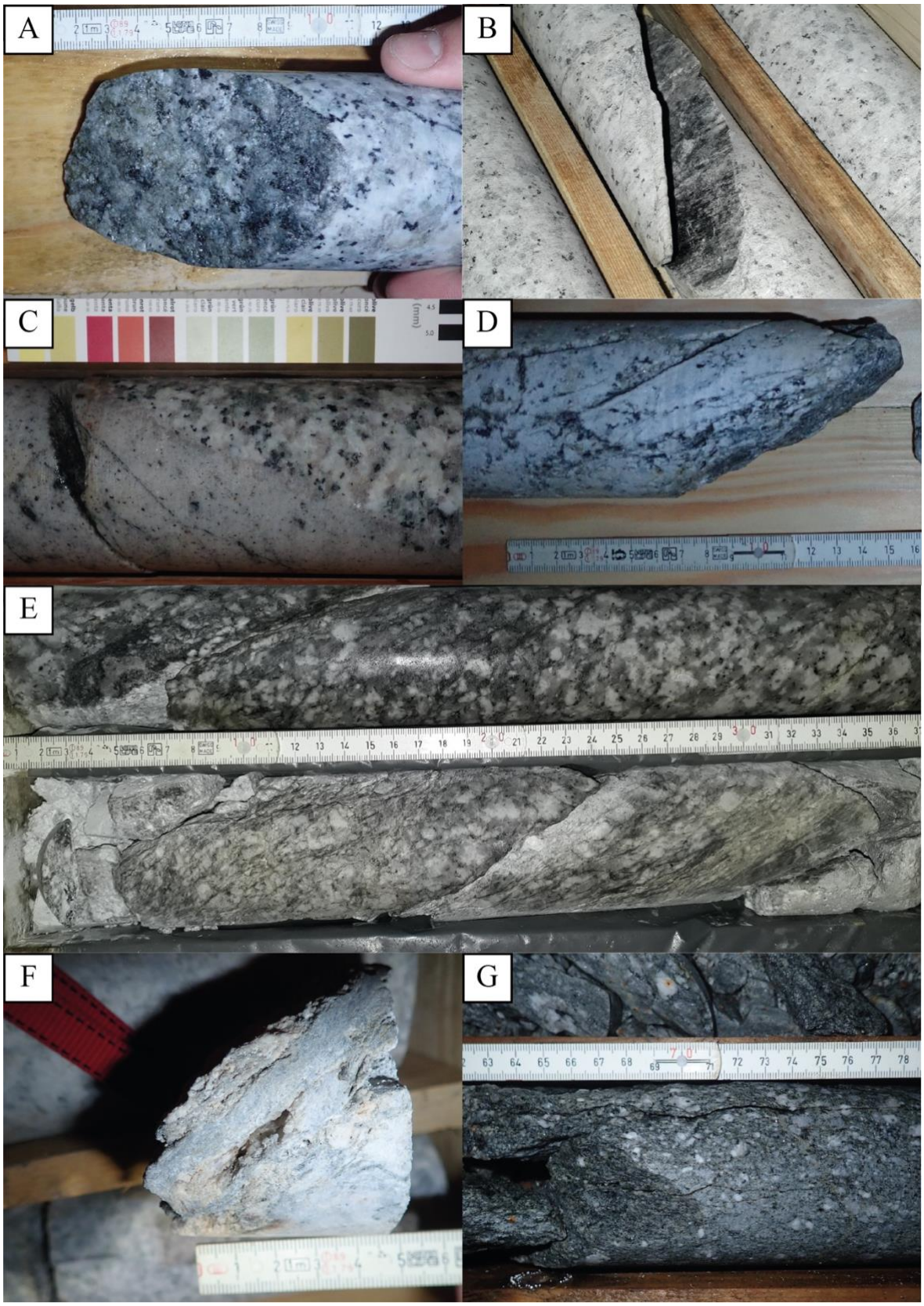

Fig. 2.7. Photos of specific features in the cores of the test volume in BULG. A: Broken healed fracture, B: Slickensided fracture with chloritic and sericitic infilling (core diameter for scale), C: Aplitic dike, D: Open joint, E: Foliated Granite (Type 1) with ductile shear zones, F: Hydrothermal altered fracture with newly formed minerals and vuggy porosity, G: Brittle fault zone.

2.3 Hydrological Setting

It can be assumed that before the construction of the Bedretto tunnel the groundwater table was near surface. The construction of the Bedretto tunnel lowered the regional hydraulic head probably by several hundred meters, hence, the Bedretto tunnel acts as a drainage to the reservoir around it. This results in a hydraulic head which generally increases with radial increasing distance to the Bedretto tunnel (artesian conditions in all directions) and therefore, the direction of water flow is from the aquifer towards the tunnel.

Lützenkirchen and Loew (2011) have found that large parts of the total water inflow into the Bedretto tunnel comes from few fault zones. The tunnel wall mapping by Jordan (2019) confirmed major water inflows along fault zones: Along the TM 1140 – 2800, fault zones seem to be the most important structures for water flow within the Rotondo granite. Also single slickensided discontinuities are occasionally water-bearing, but mostly forming only dripping zones (Jordan, 2019).

3 TRANSIENT PRESSURE TESTING METHODS

For the hydrological characterization of the rock volume around the BULG, transient pressure tests were conducted in the boreholes CB1, CB2 and CB3. The determination of hydrological parameters of structures of different types (e.g. single fractures and fracture zones) is important. The hydrological parameters determined in this thesis are Transmissivity (T) Storativity (S). The transmissivity of a confined aquifer is the rate of flow under a unit hydraulic gradient through a unit width of the aquifer (over the entire thickness of the confined aquifer). The storativity of a confined aquifer is defined as the volume of water released from storage per unit surface area of the aquifer per unit decline in hydraulic head. Storativity is also known by the terms coefficient of storage and storage coefficient.

For the determination of the transmissivity and storativity of different structures in the BULG reservoir, a multipacker system was designed (Chapter 3.1) and installed in CB2 which packs off zones of interest. CB2 was chosen for the installation of the multipacker system because its inclination of 45° makes a successful multipacker system installation possible, an ATV log was successfully performed (needed to find possible installation locations) and has no history of stuck logging tools. Only CB2 meets all the mentioned criteria. Transient pressure testing was conducted in CB1, CB3 and all intervals packed by the multipacker system in CB2 (Chapter 0). Pulse tests, constant rate tests – both single well and cross-hole responses – were analyzed applying different flow models (Chapter 3.3).

With the applied procedure in this thesis, statements can be made about the heterogeneity and anisotropy of the tested reservoir, as well as about possible scale effects. Furthermore, a possible hydraulic backbone can by identify.

In a final step, the results from the transient pressure testing can be correlated with geological structures using the core logs on a scale of 1:150 (Münger & Meier, 2020) and the tunnel wall mapping by Jordan (2019).

3.1 Multipacker System

For transient pressure tests with a multipacker system, a proper distribution of the packers along the tested borehole is crucial for informative results, whereby several factors play a role. Desirable are test intervals (borehole sections between two packers), which seal off and separate zones of interest (Chapter 3.1.2).

First of all, possible packer installation locations need to be found. Possible location are borehole sections where it is unlikely that the packers will be damaged and where they can seal the borehole completely. Therefore, borehole sections with no large roughness and inflow zone, such as borehole breakouts, fracture zones or fault zones need to be found. Furthermore, the zones of interest must be defined. Then, the available number of packers need to be distributed in the borehole in such a way that the zones of interest (zones with increased transmissivity) are separated by two the packers, so that these zones can be tested independently of the others. For CB1, CB2 and CB3 possible packer installation intervals and zones of interest are evaluated. For CB2 a multipacker system is then set up, installed and testing is conducted with it. The installed packers have an inflatable rubber part of 1 m length and 8.3 cm diameter (Fig. 3.1). Three tubing lines with an inner diameter of 3 mm and an outer diameter of 6 mm lead to each packer. One tubing line for water flow for withdrawal tests in the interval below the respective packer, one tubing line for pressure measurement and one for inflating/deflating the packer. Due to the inner diameter of the rods and the diameter of the tubing lines used, the number of packers is limited to seven. In order to monitor the pressure within the packer a manometer is connected to each tubing line used for inflating the packers. The pressure in the packer is kept between 40 and 70 bar.

Fig. 3.1. Schematic representation of a single packer used to set up the multipacker system. Two generations of packers (old/new) were used, both had an inflatable rubber part of 1 m length.

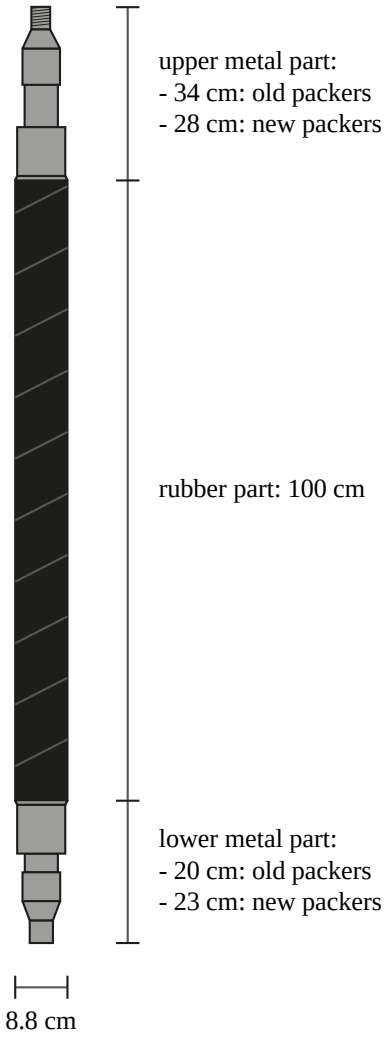

3.1.1 Possible Packer Installation Intervals

The identification of possible packer installation intervals was done by evaluating the Optical (OPTV) and Acoustic (ATV) TeleViewer logs as well as (three arm) caliper log data collected by Krietsch (2019). The precision of the indicated depth in the logs is ±10 cm. ATV logs were available for the borehole CB1 (BM 14 – 295.2) and CB2 (BM 16 – 214). OPTV logs are available for the borehole CB1 (BM 14 – 296) and parts of CB3 (BM 17 – 152). In CB1 and CB2 borehole wall defects were found by evaluating the Centralized ATV (travel time) log. In CB3 borehole wall defects were found by evaluating OPTV and caliper log data. As the caliper and OPTV logs contains much less detail than ATV logs regarding borehole wall

defects, the evaluation is not very reliable and must be handled with caution. In particular, it is likely that borehole breakouts are not identified.

The identified anomalies in the ATV travel time log are assigned to three categories (examples in Appendix C): small anomaly (1), single fracture, fracture zone or fault zone (2) and borehole breakout (3). Since “small defects” – like small anomalies and single fractures – do not necessarily exclude packer placement, an additional term has been introduced called "large defects", meaning the following defects: borehole breakout, fracture zone and fault zone. The level of detail of the defect identification is 10 cm. In Appendix D, a graphical representation for CB1, CB2 and CB3 can be found, which shows at what depth which kind of borehole wall defect is found.

To make sure that packers are installed in a place where they are not damaged and they can seal the borehole completely, intact sections longer than 2 m are determined (Fig. 3.2, columns “Possible Packer Locations, All Defects”). In order to see if only a small anomaly prevents a packer installation, graphs are created including only large defects (Fig. 3.2, columns “Possible Packer Locations, Lager Defects Only”). This offers more flexibility when setting up the multipacker system. The depths in numbers of the possible packer installation locations can be found in Appendix E.

3.1.2 Zones of Interest

Sections where an increased transmissivity is expected, are interesting zones to conduct hydrological test on to identify and characterize a possible hydrological backbone. To identify sections with an increased transmissivity, results from several investigations conducted in the BULG have evaluated (A compilation of the evaluated data sets can be seen in Fig. 3.2.):

- Flow rate during drilling (Meier, 2020)
  Major flow zones can be identified with an accuracy of about 10 m. The resulting resolution is highly depending on the number of measurements conducted and therefore variable. Flow rate during drilling data is available for all three boreholes (CB1, CB2, CB3).
- Borehole logging (ATV, OPTV, Caliper) (Krietsch, 2019)
  Single open fractures and fracture zones with open fractures can be identified by looking at the travel time of the ATV log. The accuracy is about 10 cm and the resolution 1 cm. As in the first meters of all three boreholes standpipes are installed (Tab. 2.1), the logs start only at a certain depth. Due to the sampling technique, at the lower end of the boreholes

about six meters of log are missing. ATV logs are available for the borehole CB1 (BM 14 – 295.2) and CB2 (BM 16 – 214). OPTV logs are available for the borehole CB1 (BM 14 – 296) and parts of CB3 (BM 17 – 152 m)

- Ground Penetration Radar (GPR) data (Shakas, 2020)
  Water-bearing structures can be identified. Smaller structures such as single fractures cannot always be identified, because their reflection is obscured by the reflections of larger structures. The resolution of the structure identification with GPR data is order of meters. GPR data is available for all three boreholes.
- Fault zones identified by core logging (Castilla & Krietsch, 2019)
  Fault zones have been identified by Castilla logging the cores of the three boreholes. The resolution of the identified structures is about 1 m. Logs are available for all three boreholes.

The analyzed results about the individual flow rate of inflow zones from heat dilution tests (Meier, 2020) were available only after the completion of the final multipacker system setup. Nevertheless, a visual analysis of the raw data of the heat dilution test in CB2 was used to see if major inflow zones were overseen by looking at the other data sets mentioned above. With heat dilution tests, inflow zones (> 0.25 l/min) can be identified (Meier, 2020). Borehole sections with an increased transmissivity but no flow cannot be detected with the heat dilution test, as the test only detects flow from the formation into the borehole.

3.1.3 Final Multipacker System Setup

From the combination of the possible packer installation intervals (Chapter 0) and zones of interest (Chapter 3.1.2) seven packers were distributed in CB2 (Tab. 3.1 and Tab. 3.2). After the packer installation, it turned out either Packer 5 or the tubing line leading to it is damaged, resulting in a pressure decrease in Packer 5 that made it impossible to seal the borehole at this location. This resulted in a direct hydraulic connection between Interval 5 and 6. Therefore, the designation „Interval 5&6" is used in the following.

Tab. 3.2. Packer installation depths in CB2.

Packer Number	Depth of Packer Center [BM]
1	199.03
2	196.02
3	176.51
4	166.03
5	155.49
6	140.92
7	124.44

Tab. 3.1. Packed intervals in CB2.

Interval Number	Interval Depths [BM]	Interval Length [m]
1	199.53 – 222.00	22.47
2	196.52 – 198.53	2.01
3	177.01 – 195.52	18.51
4	166.53 – 176.01	9.48
5&6	141.42 – 165.53	24.11
7	124.94 – 140.42	15.48

An illustration of the packer distribution in CB2 can be seen in Fig. 3.2. As a backup plan, packer distribution for multipacker systems in CB1 and CB3 are proposed (Fig. 3.2). The same selection criteria as for the multipacker system in CB2 are used.

For each interval in CB2 the presumably most conductive structure was determined and characterized during the core logging process, by relying on different data sets such as ATV log (Krietsch, 2019), GPR (Shakas, 2020), flow and pressure measurements during drilling (Meier, 2020). From pressure measurements during drilling the depths of major connections (and therefore conductive structures) between a completed borehole (where the pressure measurement takes place) and the newly drilled borehole can be identified. This is possible due to the open condition during drilling which affects the pressure in the completed (and shut-in) borehole as soon as the drilling reaches the connecting structure. In Tab. 3.3 characteristics of the presumably most conductive structures can be seen. In Appendix F ATV log sections and core photos from the BM in which the presumably most conductive structures are located can be seen. The column “Rock Type” in Tab. 3.3 refers to the core log description in Chapter 2.2.2. It can be seen, that the intervals are located in either Foliated Granite (Type 1) or Foliated Granite (Type 2). Neither in Intact Granite (Type 1) nor in Intact Granite (Type 2) an interval was positioned because none of the considered data sets (Chapter 3.1.2) indicated a structure with presumably high transmissivity.

Krietsch (2019) mapped the fractures recognizable in the ATV log and determined their orientation. In Fig. 3.3 stereoplots for each interval are shown, whereby the bold planes indicate

the orientation of the presumably most conductive structures in each interval. Stereoplots showing the poles of all mapped structures CB1, CB2, CB3 can be seen in Appendix G.

Jordan (2019) defined four sets according to their orientations (mean set planes are given in dip and dip direction): tunnel perpendicular (75/324), E-W striking (67/001), N-S striking (79/271) and a tunnel parallel (84/220). According to Jordan (2019), the tunnel perpendicular fracture set's orientation is subparallel tot the alpine foliation locally observed in the Rotondo granite. All intervals – except Interval 2 – are dominated by fractures which can be assigned to the fracture set "tunnel perpendicular ". In all intervals – except Interval 3 – the presumably most conductive structure seems to belong to the fracture set "tunnel perpendicular ". The presumably most conductive structure in Interval 3 is E-W striking. Intervals 5&6 and 7 are the only two intervals that has fractures that belong to the set "tunnel parallel". Interval 2 and 5&6 both show structures that are N-S striking. Further, Jordan (2019) states that the largest water inflows into the tunnel were observed along structures belonging to the fracture set "tunnel perpendicular" or that are E–W striking. Besides the structures perpendicular to the tunnel and the E–W striking ones, only fractures with a strike orientation of N-S showed inflow into the tunnel. However, the N–S striking fractures only formed dripping zones and are rarely found in CB2 (only in Intervals 2 and 5&6). In addition, no slickensided structure was found in Interval 2 during core logging and in Interval 5&6 structures with vuggy porosity were found, which most likely dominate the flow in the Interval 5&6. Therefore, it is expected that the N–S striking fractures do not have a significant effect on the results of the transient pressure measurements.

Thus, structures with the same orientation as the ones with the largest water flows into the tunnel are well represented in the intervals. This suggests that the most conductive structures and therefore a possible backbone is most probable characterized by the transient pressure tests. On the other hand, in none of the intervals an N–S striking or a tunnel parallel structure was identified as the presumably most conductive structure. Thus, the hydraulic parameters of the N–S striking and the tunnel parallel structure sets are not defined by the transient pressure tests.

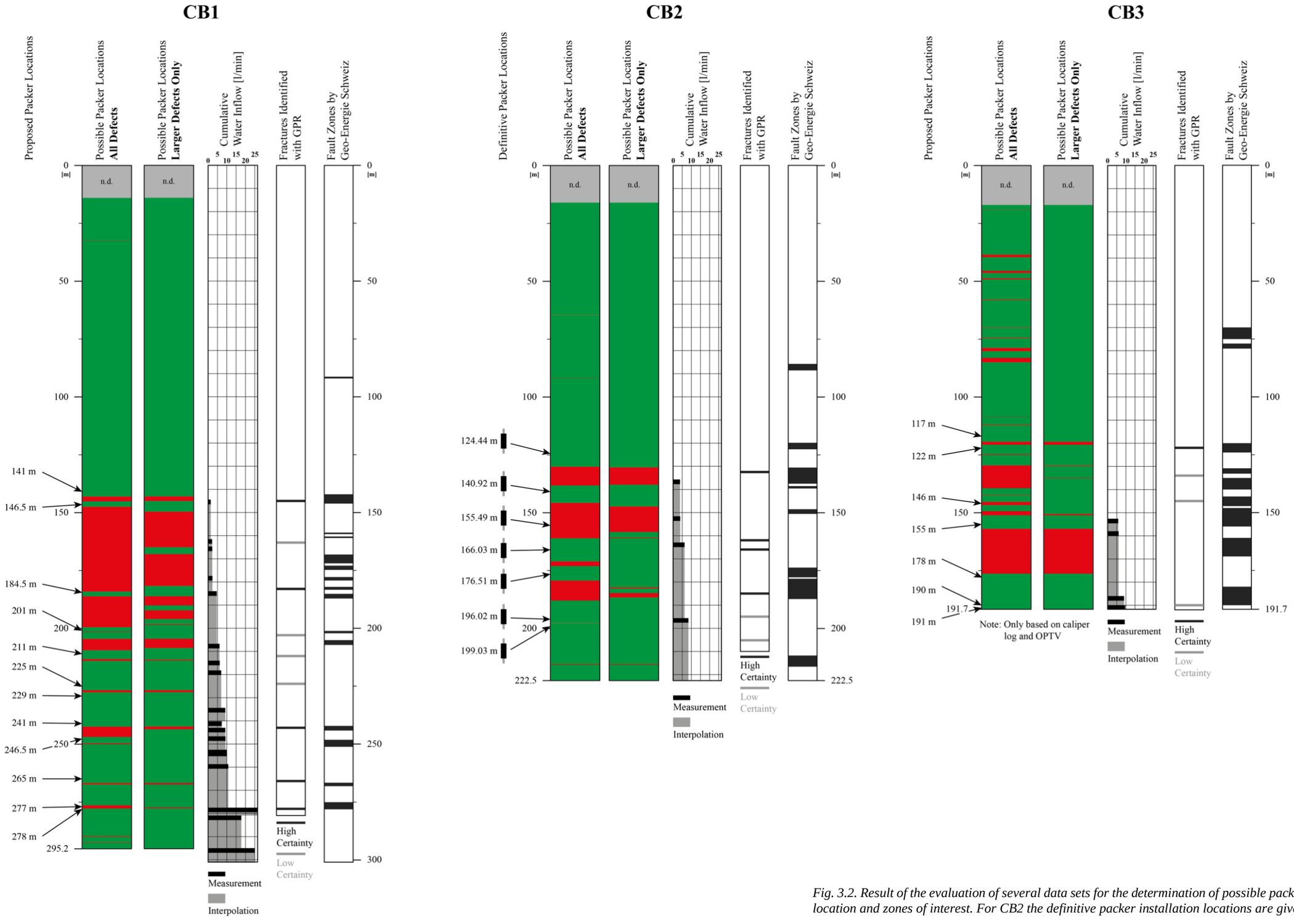

Fig. 3.2. Result of the evaluation of several data sets for the determination of possible packer installation location and zones of interest. For CB2 the definitive packer installation locations are given.

Tab. 3.3. Characteristics of packed intervals in CB2 and information about presumably most conductive structures for each interval.

Interval in CB2	Rock Type	Number of Fractures (ATV)	Number of Open Fractures (Core Log)	Type of Most Conductive Structure	Orientation of Most Conductive Structure [dip angle / dip direction]
1	(mostly) Foliated Granite (Type 2)	3	2	Discontinuity with "connected" porosity	77/333
2	Foliated Granite (Type 2)	4	1	Discontinuity with "connected" porosity	50/326
3	Foliated Granite (Type 2)	19	FZ (20 cm) + 18	fracture with vuggy porosity and newly formed minerals	49/349
4	Foliated Granite (Type 2)	11	5	fracture with vuggy porosity	42/315
5&6	Foliated Granite (Type 2)	38	6	fracture with vuggy porosity and newly formed minerals	58/329
7	Foliated Granite (Type 1)	15	FZ (80 cm) + 9	Hydrothermal altered fracture zone	80/334

FZ: Fracture Zone

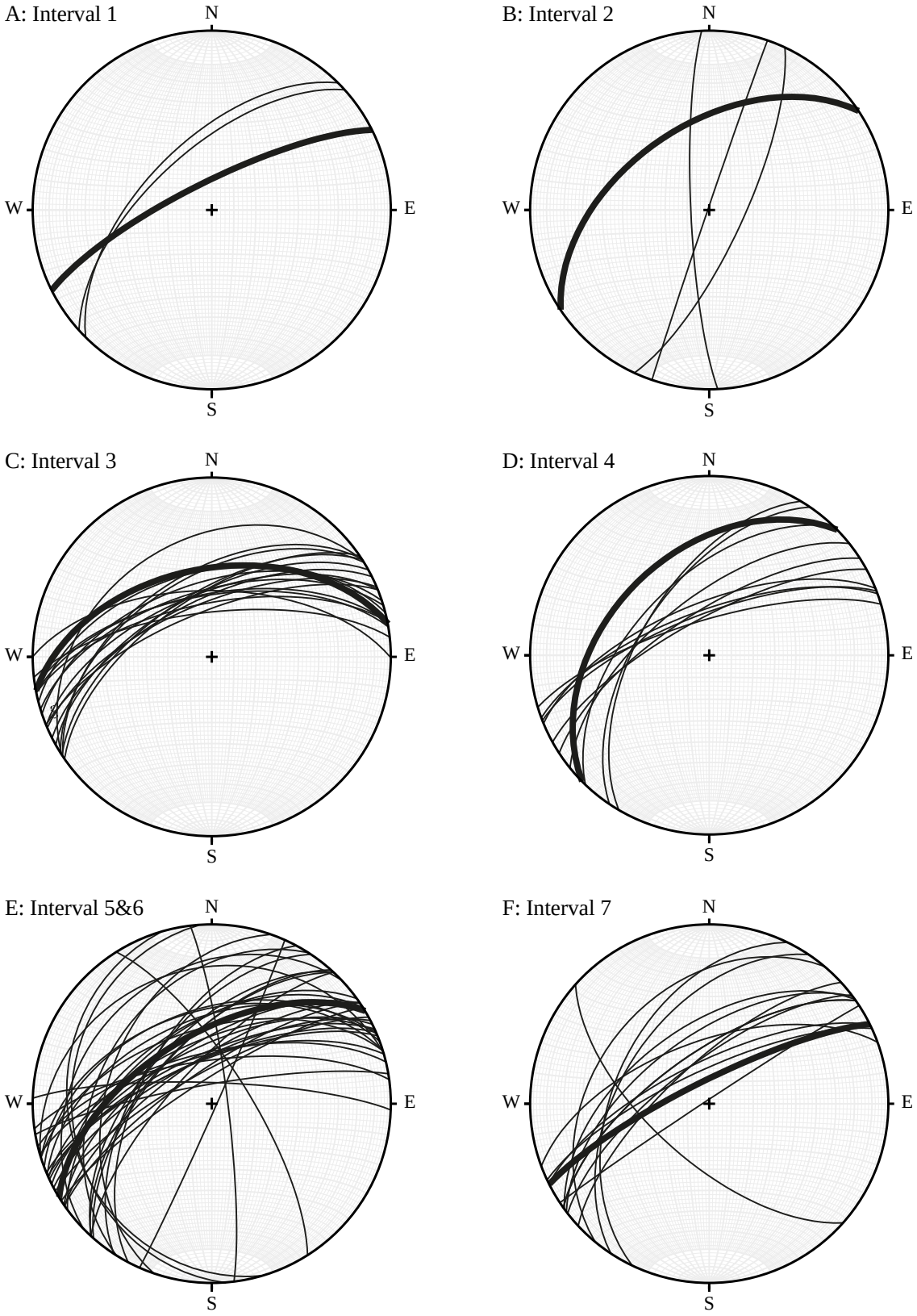

Fig. 3.3. Stereoplots (lower hemisphere) for each interval in CB2 with the fractures mapped in the ATV log by Krietsch (2019). The bold plane indicates orientation of the presumably most conductive structure in the considered interval.

3.2 Equipment and Test Design

After drilling was completed, the boreholes experienced several periods of open conditions as logs and tests (e.g. ATV log, GPR, heat dilution test) were performed in them. After the installation of the multipacker system, CB1, CB3 and all intervals in CB2 were closed for two weeks before the first test started. In Tab. 3.4 the relative order of all events in CB1, CB3 and the intervals can be seen. In Appendix H more detailed list of all events in CB1, CB3 and the interval can be seen. In each interval a pulse test was performed before the constant rate test. From pulse test analyses transmissivity values can be estimated (Chapter 3.3.1). From the estimated transmissivity values a suitable flow rate for the constant rate tests in the intervals can be determined (Chapter 3.2.3).

Tab. 3.4. Timetable giving an overview of the tests conducted in CB1, CB3 and the Intervals 1 to 7 in CB2.

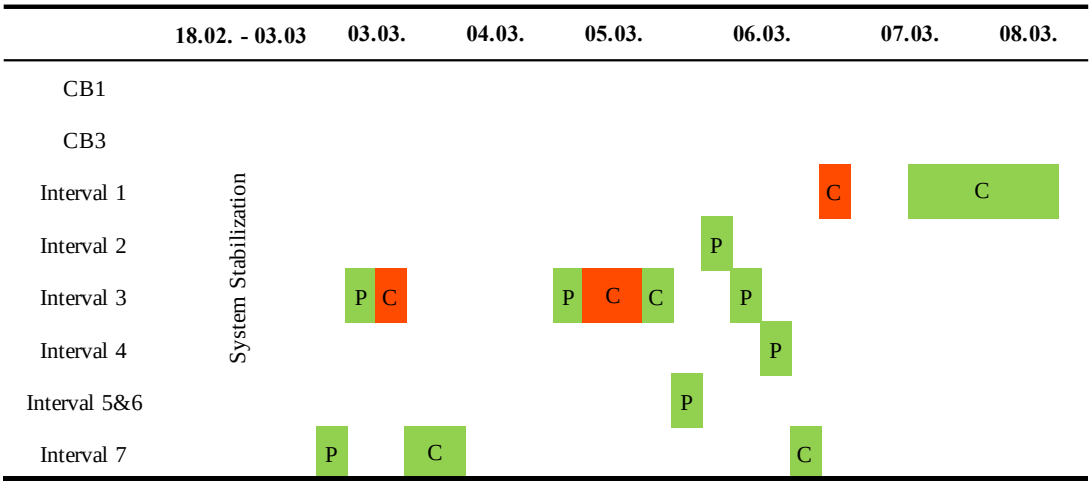

P: pulse test; C: constant rate test; green: test was analyzed; red: test had to be repeated

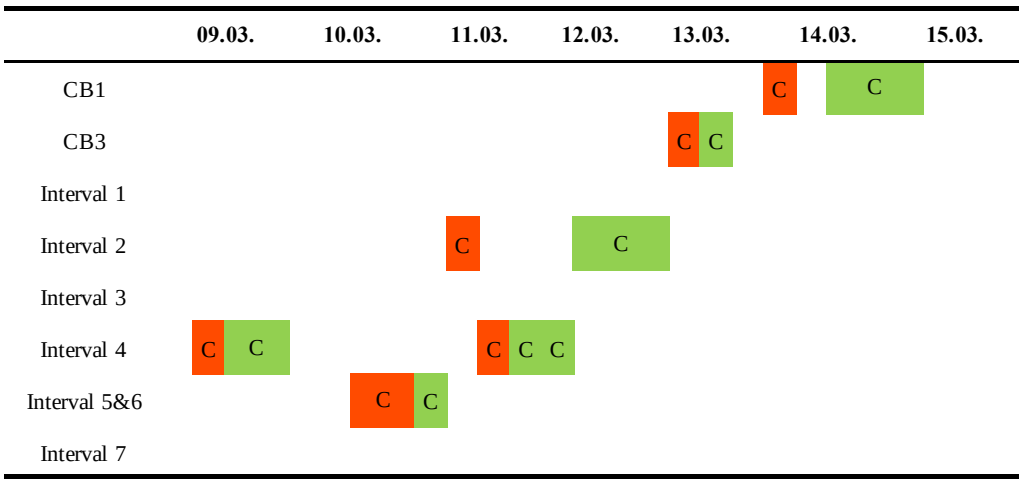

P: pulse test; C: constant rate test; green: test was analyzed; red: test had to be repeated

3.2.1 Equipment

Since artesian conditions were present in all intervals as well as in the boreholes CB1 and CB3, no pump was required neither for the pulse test nor constant rate tests. The amount of produced water during pulse tests was measured with a scale (precision ±0.1 g). The production time was measured manually with a stopwatch (precision ±0.1 s). For the pressure measurements high-precision surface pressure sensors (see below) were used. A schematic representation of the testing set up for the transient pressure tests in the three boreholes with multipacker system in CB2, flow controllers and pressure sensors can be seen in Fig. 3.4. Technical data of the mentioned equipment and more detail about the setup is given in the following.

To ensure a constant flow during the tests, three high-precision Bronkhorst CORI-FLOWTMmass flow controllers (flow meters with integrated automatic valves) and the Bronkhorst software FlowPlot (version 3.35) were used. Three flow controllers with stated accuracies of 0.2% and different capacities were in use: Device A (M15: 0.8 – 40 l/h), Device B (M13: 0.02 – l/h), Device C (M12: 0.002 – 0.1 l/h). The flow meter devices can handle a differential pressure of 2 – 10 bar. In order to keep the differential pressure in the required range, a manual pressure regulator was used. The three flow meters were connected through an RS232/FLOW-BUS interface to the main computer unit on which FlowPlot run. The desired flow rate can be entered in FlowPlot and the production can be started and stopped with FlowPlot. Due to remote access on the computer on which FlowPlot run, it was possible to start and stop the production remotely. The production was stopped when the pressure in the tested interval or borehole appeared to be stabilized. During the test the flow meter measured the flow, transmitted the measurement to FlowPlot which controls the automatic valve. The three flow meters were mounted on a flow board (Appendix I). Before the test, the desired flow rate needed to be known so that the device with the appropriate capacity could be connected.

During the pulse tests and the constant rate tests pressure is measured in CB1, CB3 and all intervals in CB2 every second. The pressure measurements surface pressure sensors "Series 33X G1/4 thread" from Keller (2020) were used. The Serie 33X sensors have an accuracy of ±0.05% full scale (FS) in the temperature range of 10 – 40°C. The Keller software Control Center Serie 30 was used in this study to save and display the measurements continuously.

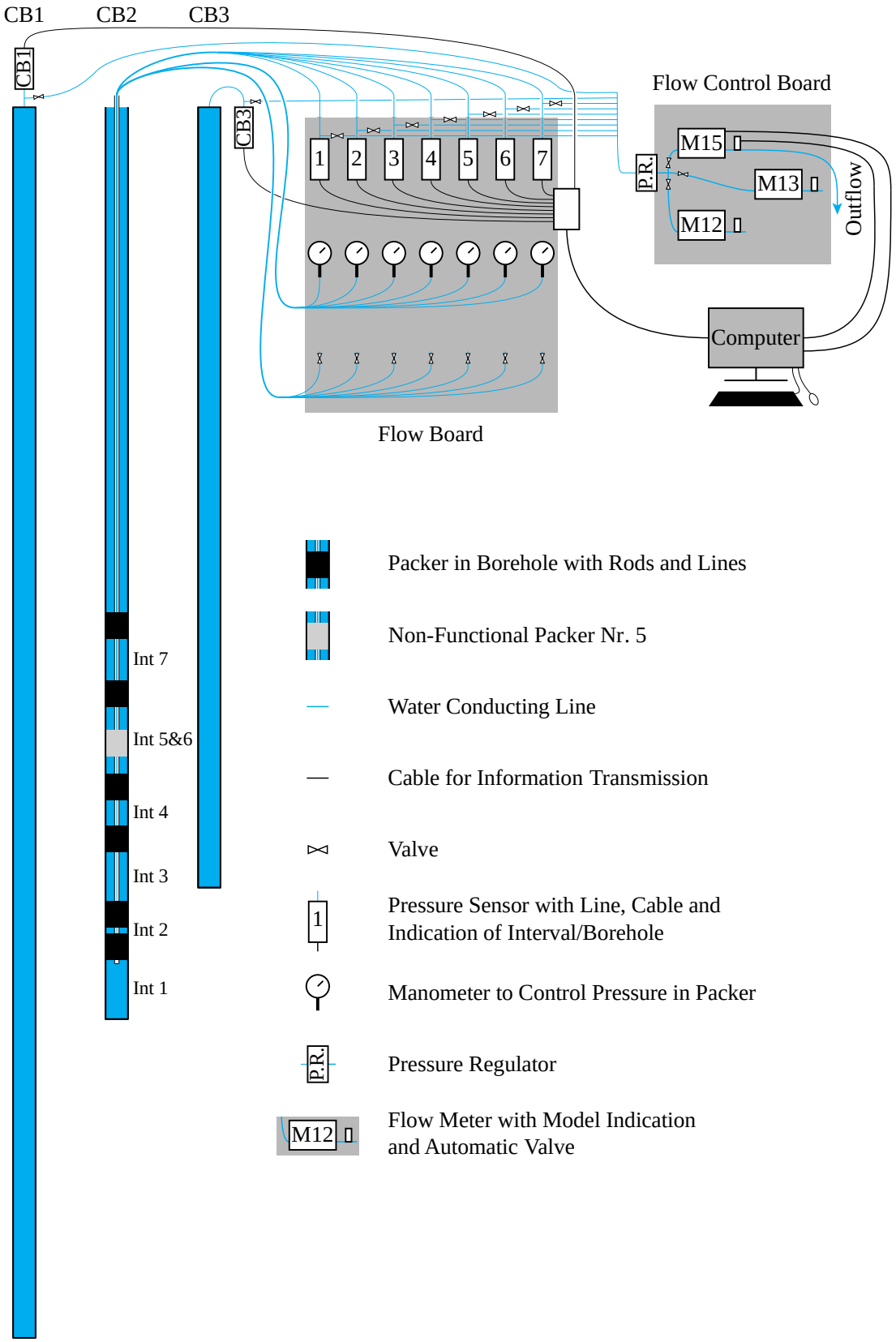

Fig. 3.4. Graphical representation (not at scale) of the testing setup of the transient pressure tests in CB1, CB2 and CB3, with the multipacker system in CB2. In the first row of the flow board the interval pressure sensors are located, in the second row the manometers for pressure control in the packers and in the third row the lines for possible tracer injection into the intervals.

3.2.2 Pulse Test

In all intervals in CB2 a pulse test was performed. In CB1 and CB3 no pulse tests were performed as the small diameter of the discharge line connected to the boreholes do not allow flow rates high enough to overcome the wellbore storage effect as well as friction inside the discharge lines. The pulse test was only started when the pressure is stable in the corresponding interval. To carry out the pulse tests the valve of the respective interval was opened to atmospheric pressure manually. A pressure drop of more than 90% of the initial pressure was targeted before shut-in. Details for each pulse test performed can be found in Tab. 3.5.

Tab. 3.5. Details of pulse tests performed in the intervals in CB2.

Interval	Production Time [s]	Amount of Produced Water [l]	Volume Test Section [m^3]	Initial Pressure [bar]	Pressure Minimum [bar]	Pressure Drop [bar]	Pressure Drop in Percentage of Initial Pressure [%]
1	12	0.1687	0.18	38.25	22.35	15.90	41.6
2	8	0.0847	0.014	38.95	6.15	32.80	84.2
3	12.2	0.1860	0.11	38.63	36.90	1.73	4.5
4	10.3	0.1537	0.057	38.25	27.79	10.46	27.3
5&6	12	0.1977	0.14	38.64	38.47	0.17	0.4
7	~ 12	0.2082	0.09	35.25	32.63	2.62	7.4

3.2.3 Constant Rate Test

From the pulse tests, transmissivity and wellbore storage values for each interval were derived (Chapter 3.3.1). From these values, the constant rate test were designed by defining the flow rates with the Cooper and Jacob (1946) solution the way that the final pressure decrease in the system is nearly 10 bar. A pressure decrease of more than 10 bar would cause geophysical effects (Rutqvist, 1996). During the constant rate tests, it turned out that the calculated test design (flow rates) was not always suitable. For Intervals 1, 3, 4 and 5&6, the calculated flow rate was too small, for Interval 2 too high. The consequence was a too large (>10 bar) or a too small pressure drop (<1 bar), respectively. In these cases, a higher or lower flow rate was applied after the system had stabilized again. Since no pulse tests could be performed for CB1 and CB3, the flow rate of the constant rate test in CB1 and CB3 was chosen slightly higher than

the highest flow rate determined by the pulse tests in the intervals. These rates were needed to be adjusted after the first attempt showed that the chosen flow rates were too low.

In CB1, CB3 and the Intervals 1, 2, 3 and 5&6 one constant rate test each was performed successfully. Three tests in the Interval 4 and two tests in Interval 7 were performed successfully. In order to distinguish the tests in the Intervals 4 and 7, they are numbered consecutively based on the performed tests' dates (e.g. "Interval 4-2" refers to the second constant rate test in Interval 4). Details about the flow rates, production times and recovery phases can be seen in Tab. 3.6.

Tab. 3.6. Details of all successfully performed and analyzed constant rate tests in chronological order.

Interval / Borehole	**Production Phase [Date, hh:min]**	**Production Duration [hh:min]**	**Analyzed Recovery Phase [Date, hh:min]**	**Analyzed Recovery Duration [hh:min]**	**Flow Rate [l/h]**
7-1	03. – 04.03.2020 19:33 – 05:59	10:26	04. – 05.03.2020 05:59 – 17:09	11:10	30
3	05. – 06.03.2020 23:27 – 04:34	04:57	06.03.2020 04:34 – 09:18	04:44	1.02
7-2	06.03.2020 14:48 – 15:50	01:02	06. – 07.2020 15:50 – 11:40	19:50	30
1	07. – 08.03.2020 12:00 – 22:54	34:54	08. – 11.03.2020 22:54 – 10:59	60:05	0.102
4-1	09.03.2020 13:30 – 21:55	08:25	09. – 10.03.2020 21:55 – 12:34	14:39	6
5&6	11.03.2020 02:13 – 05:13	03:00	11.03.2020 05:13 – 14:49	09:36	45
4-2	11. – 12.03.2020 22:01 – 05:38	07:37	12.03.2020 05:38 – 07:18	01:40	4.02
4-3	12.03.2020 07:18 – 13:13	05:55	12. – 13.03.2020 13:13 – 13:22	12:09	7.8
2	12. – 13.03.2020 16:41 – 04:38	11:57	13. – 14.03.2020 04:38 – 00:52	21:14	0.0498
CB3	13.03.2020 15:25 – 18:34	03:09	13. – 14.03.2020 18:34 – 15:09	20:35	90
CB1	14. – 15.03.2020 15:33 – 09:33	18:00	15. – 16.03.2020 09:33 – 07:26	21:53	120

3.3 Test Analysis

The main goal of the test analyses was to determine transmissivity and storativity values for CB1, CB3 and the intervals in CB2. Furthermore, values for flow dimension, wellbore storage and skin factor were determined. The analyses was done with the Matlab toolbox hytool by Renard (2017). The aquifer properties were determined by using analytical solutions of different models (Agarwal et al., 1970; Barker, 1988; Neuzil, 1982; Theis, 1935) performing iterative non-linear optimization curve fitting (e.g. Ramey Jr, 1970) (Fig. 3.5).

In addition, to the determination of the hydraulic parameters the complexity of the natural flow system is investigated by creating and interpreting diagnostic plots. The results of the transient pressure test analyses together with the geological and geotechnical core log (Chapter 2.2.2) are used to identify and characterize a possible existing hydronic backbone.

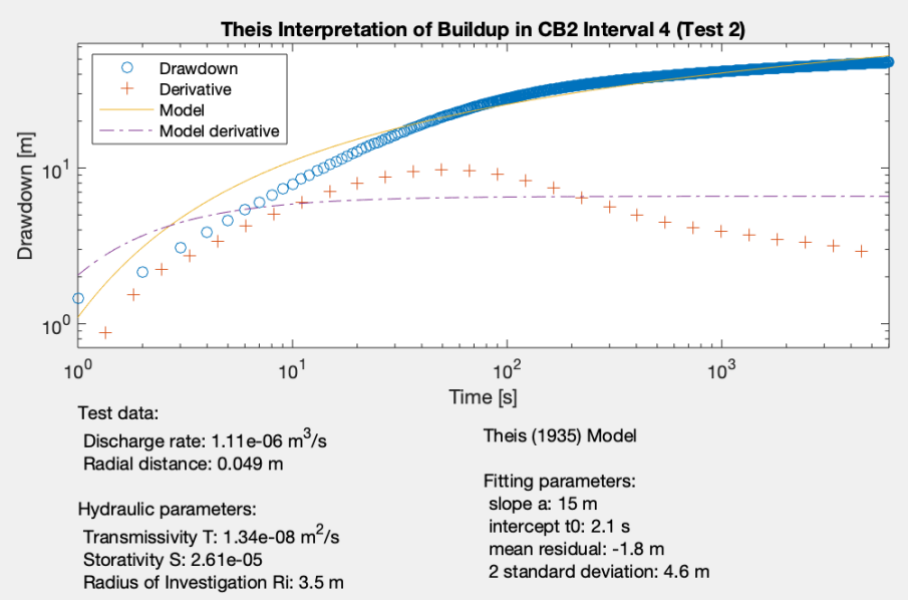

Fig. 3.5. An example for a plot created by hytool reporting the results of the analysis with Theis (1935). Shown is the report of the single well test analysis of the buildup phase of the constant rate test in Interval 4-2.

Which model was applied to which data set is mentioned in the respective subsection. Since pulse tests and constant rate tests (single well and cross-hole responses) are analyzed, possible scale effects can be detected. The results are used for calculations in order to obtain additional properties, such as diffusivity.

With Eq. 3.1 the diffusivity (D) can be calculated from the transmissivity (T) and the storativity (S).

$$D = \frac{T}{S} \qquad \textit{Eq. 3.1}$$

Another way to determine the diffusivity is to plot the characteristic time (Eq. 3.2) against the distance to the active well. In the same graph, trends of normal diffusion for different diffusivity values are plotted ($\sqrt{4Dt}$ vs. t). This way an estimation of the diffusivity values can be made.

$$t_c(r) = \frac{r^2 S}{4T} \qquad \textit{Eq. 3.2}$$

Where,

t_c: Characteristic time [s]

r: Radial distance to active well [m]

S: Storativity [–]

T: Transmissivity [m^2/s]

3.3.1 Pulse Test

The pulse test is analyzed applying the Neuzil (1982) solution, which is based on Jacob (1950), Cooper et al. (1967), Bredehoeft and Papadopulos (1980) and Papadopulos et al. (1973) This analysis provides transmissivity and storativity values. For the analyses following values are assumed:

- Fluid Viscosity: $8.91 \cdot 10^{-4}$ Pa·s

- Fluid Density (Water): 1000 kg/m^3

- Gravitational Constant: 9.81 m/s^2

- Effective Compressibility (Water): $4.4 \cdot 10^{-10}$ [Pa^{-1}]

3.3.2 Constant Rate Test

The constant rate test data was basically evaluated in two ways. First, the tests were evaluated as single well tests, second, as cross-hole tests. In the single well test analysis, the pressure changes in the interval in which the withdrawal takes place is analyzed. In the cross-hole response analysis the pressure response to the withdrawal in another borehole is analyzed. For reasons of simplicity, in the following, when writing about single well test data, only e.g. “drawdown/buildup in Interval 4-2” is written (it is not mentioned that the withdrawal took place in the same interval). In case of cross-hole response data, it is mentioned in which borehole the withdrawal took place (e.g. “cross-hole response in Interval 4 to drawdown/buildup in CB1”).

As a first step of the analysis, diagnostic plots (Fig. 3.6) of the drawdown and buildup phases were created for the single well test data as well as for the cross-hole responses. In a diagnostic plot the pressure data and its derivative is plotted versus time in a log-log plot. one Diagnostic plots help to find a suitable conceptual model for further analyses (Renard et al., 2009). Further, with the help of diagnostic plots statements about the occurring flow regimes can be made (e.g. wellbore storage, infinite acting, constant head boundary, no flow boundary).

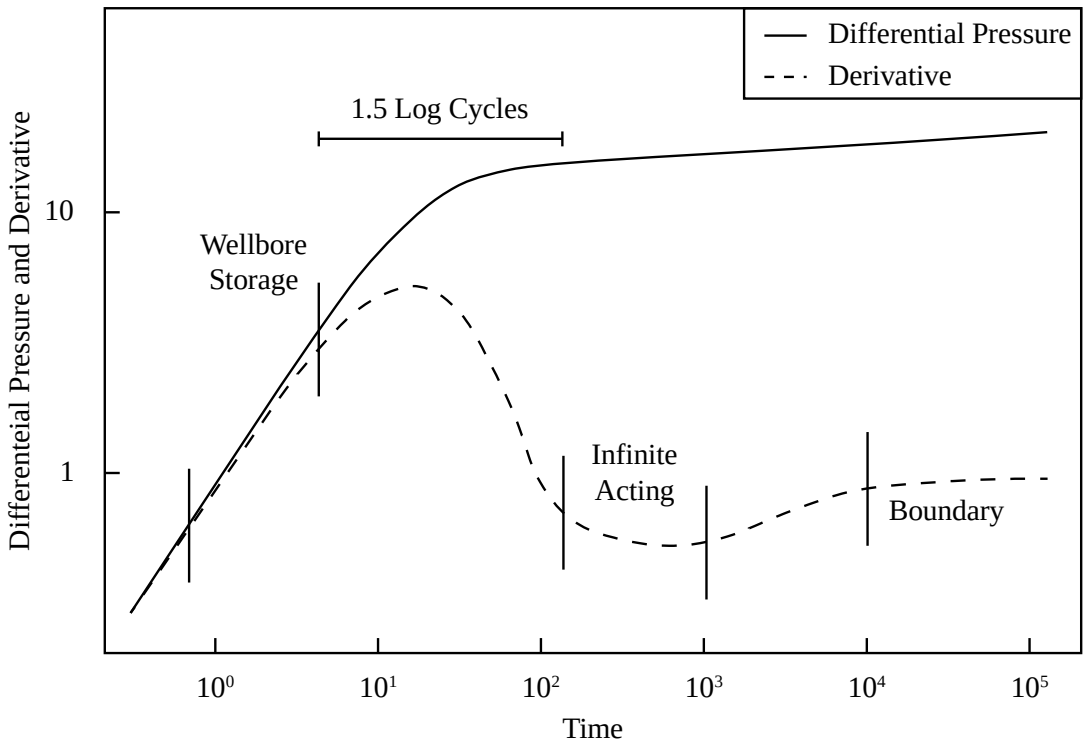

Fig. 3.6. Diagnostic plot showing different indicative sections (wellbore storage, infinite acting and boundary), as well as the critical 1.5 log cycles (modified after Horne, 1990).

3.3.3 Constant Rate Test: Single Well Test Analysis

The single well test analyses are conducted for the drawdown and buildup phases of the performed constant rate tests, applying two conceptual models: Theis (1935) and Generalized Radial Flow (GRF) Model (Barker, 1988). Since the applied hytool Matlab scripts for the analysis with the Theis and GRF models are developed for the analysis of injection tests, the buildup data can directly be analyzed with hytool (under the assumption the pressure is stable at shut-in, thus no superposition effects occur). This does not apply to, the drawdown data which needs to be flipped with Eq. 3.3 before the analysis with hytool. By flipping, the drawdown data, it is treated as buildup data for the analysis.

$$s_{flipped} = s_0 - s_{original} \quad \textit{Eq. 3.3}$$

Where,

$s_{flipped}$: Flipped drawdown pressure data, pretending buildup data [m]

s_0: Pressure before start of drawdown [m]

$s_{original}$: Drawdown pressure data [m]

In order to have longer buildup phases available for analysis, successive data sets have been merged. Therefore, in some cases, pressure data from a data set which contains a withdrawal is used for the evaluation of the buildup in another interval. E.g. Pressure data from the data set which contains the withdrawal of Interval 2 is used in for the prolongation of the buildup phase for Interval 4-2. However, a careful consideration of whether the intervals have responded to each other was made prior to the merging of data sets from of two different constant rate tests.

Single Well Test Analysis: Horner (1951) Plots

Horner (1951) plots for all the buildup phases of the constant rate tests performed in CB1, CB3 and the intervals in CB2 have been created and linear fitting was performed on it to get the initial pressures. For Horner plots the time is plotted at log scale on the x-axis and the pressure at linear scale on the y-axis. The straight line was fitted manually to the latest data points where a linear trend could be detected. Following assumptions are made when the initial pressure is determined by linear fitting on a Horner plot:

- Radial flow in confined aquifer
- Homogenous, isotropic, horizontal aquifer with infinite extension
- Darcy's law is obeyed
- Stable initial conditions
- Constant flow rate throughout the test
- Fluid density follows an exponential type law (see Horner (1951))
- Gravitational forces are neglected

Single Well Test Analysis: Theis (1935) Solution

The analysis applying the Theis (1935) model provides values for transmissivity (T), storativity (S) and radius of investigation (R_i). Following assumptions are made when a test is analyzed using the Theis (1935) solution:

- Radial flow in confined aquifer
- Homogenous, isotropic horizontal aquifer with infinite extension
- Darcy's law is obeyed
- Stable initial conditions
- Constant flow rate throughout the test
- Gravitational forces are neglected

Single Well Test Analysis: GRF Model (Barker, 1988)

The analysis with the GRF model provides values for transmissivity (T), storativity (S) and flow dimension (n). The advantage of the GRF model is that the flow dimension can be determined. While the flow dimension in most models (e.g. Theis, 1935) is defined as a radial

2D flow, the flow dimension in the GRF model can vary between 1D and 3D. The flow dimension is helpful for the characterization of the tested aquifer and allows a statement about the reliability of the analysis with Theis (1935). Fig. 3.7 shows a graphical representation of the subradial (n<2D) and radial (n=2D) flow.

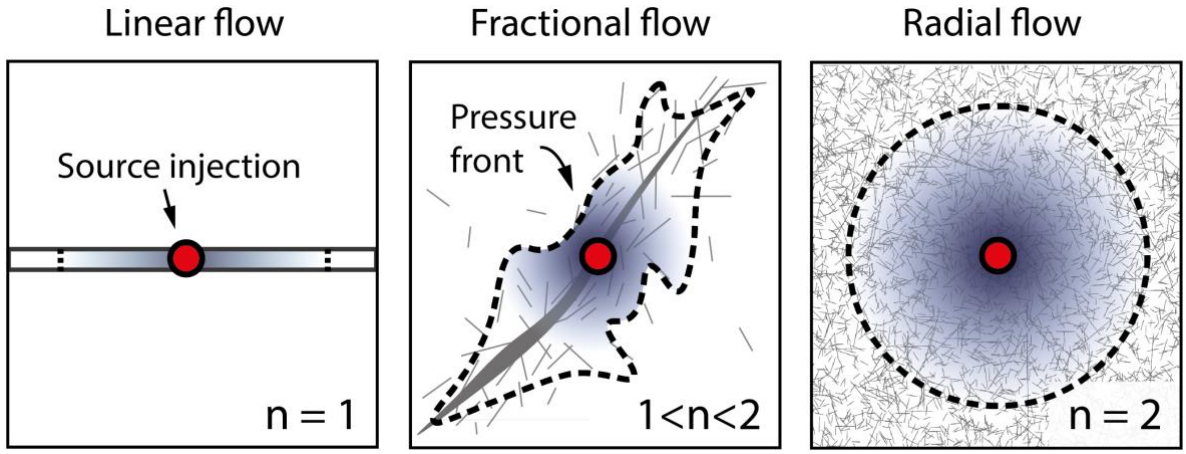

Fig. 3.7. Graphical representation of subradial and radial flow in a fractured media. The red dots indicate pumping/injection locations (Brixel et al., 2020b).

For the evaluation of the constant rate test with the GRF model (Barker, 1988) following assumptions are made (Barker, 1988):

- n-dimensional flow in confined aquifer
- Homogenous, isotropic aquifer with infinite extension
- Darcy's law is obeyed
- Stable initial conditions
- Constant flow rate throughout the test
- Gravitational forces are neglected
- Infinitesimal skin

3.3.4 Constant Rate Test: Cross-Hole Test Analysis

Cross-hole responses in CB1, CB3 and the intervals in CB2 to the withdrawal and buildup in CB1 and CB3 were analyzed using two models: Theis (1935) and Agarwal et al. (1970). For the cross-hole test analysis the distances between the active borehole (CB1/CB3) and the observation borehole/intervals are required. The shortest possible hydraulic connection in the form of a fracture is looked for, as water flow is expected to occur mainly along fractures.

Therefore, all fractures identified by Krietsch (2019) in the ATV log of CB2 are extrapolated to CB1 and CB3 and the shortest connection is determined (Tab. 3.7).

Tab. 3.7. Shortest connection between the intervals and CB1 and CB3, respectively

	Shortest Connection to	
	CB1 [m]	**CB3 [m]**
Interval 1	23.8	60.4
Interval 2	23.4	59.9
Interval 3	21.4	50.7
Interval 4	23.6	45.4
Interval 5&6	18.1	39.1
Interval 7	17.1	30.3

From the shortest hydraulic connection (fracture) between CB1 and CB3 the fractures mapped in CB1 were extrapolated to CB3. Then, shortest hydraulic connection (fracture) in the section borehole meter (BM) 100 to BM 222 of CB2 was identified. The reason for only considering BM 100 to BM 222 is that no structure where significant water flow is expected to occur was found in connection with the core logging of CB1 in the section BM 0 to BM 100. The shortest connection between CB1 and CB3 in the BM 100 to BM 222 resulted to be 29.7 m.

In addition to the quantitative evaluation with the Theis (1935) and Agarwal et al. (1970) solution, a qualitative evaluation is carried out. For this purpose, the pressure response times to the withdrawal in CB1 and CB3 are determined for all intervals as well as for CB3 and CB1, respectively. The response times regarding the start of withdrawal as well as the shut in was determined. The response time was defined as the first notable change in pressure after the start of withdrawal resp. after the shut in.

Cross-Hole Test Analysis: Theis (1935)

The analysis of cross-hole tests with the Theis (1935) solution provides values for transmissivity (T), storativity (S) and radius of investigation (R_i). The same assumptions are made for the analyses of cross-hole tests with the Theis (1935) solution as for the analysis of single well tests with the Theis (1935) solution (Chapter 3.3.3).

Cross-Hole Test Analysis: Agarwal et al. (1970)

The analysis of cross-hole tests with the Agarwal et al. (1970) solution provides values for transmissivity (T), storativity (S), wellbore storage (C_D) and skin factor (S_g). For the evaluation of the constant rate test with the Agarwal et al. (1970) solution following assumptions are made (Agarwal et al., 1970):

- Radial flow in confined aquifer
- Homogenous, isotropic, horizontal aquifer with infinite extension
- Darcy's law is obeyed
- Stable initial conditions
- Constant flow rate throughout the test
- Constant compressibility and constant viscosity of fluid
- Gravitational forces are neglected
- Infinitesimal skin

4 TRANSIENT PRESSURE TESTING RESULTS

4.1 Pulse Test

The pulse test analysis resulted in values for transmissivity and wellbore storage (Tab. 4.1). The curve fits resulted from the analyses of the pulse tests can be seen in Appendix J. Interval 2 shows with 10^{-11} m^2/s the lowest resulted transmissivity, Interval 7 with 10^{-8} m^2/s the highest. Intervals 1, 2 and 3 show all about the same transmissivity values of about 10^{-10} m^2/s. The analyses of the pulse test in Interval 4 resulted in a transmissivity which is about one order of magnitude lower than the one in Interval 7. The transmissivity values were then used for the estimation of the flow rate during constant rate tests (Tab. 4.1).

Tab. 4.1. Results of the pulse tests performed in the intervals in CB2 analyzed with the Neuzil (1982) solution and the proposed flow rate for the constant rate tests.

Interval	Transmissivity (T) [m^2/s]	Wellbore Storage (Sw) [m^2]	Mean Residual of Fit [–]	Standard Deviation of Mean residual [–]	Proposed Flow Rate for Constant Rate Test [l/h]	Production in First Constant Rate Test [l/h]
1	$1.3 \cdot 10^{-10}$	$7.8 \cdot 10^{-7}$	-0.0001	0.0045	0.06	
2	$9.3 \cdot 10^{-12}$	$6.3 \cdot 10^{-8}$	-0.013	0.022	0.006	0.1
3	$2.9 \cdot 10^{-10}$	$4.7 \cdot 10^{-7}$	-0.00027	0.017	0.12	1.5
4	$3.7 \cdot 10^{-9}$	$2.4 \cdot 10^{-7}$	0.00065	0.0049	1.2	2.5
5&6	$2.7 \cdot 10^{-10}$	$6.2 \cdot 10^{-7}$	0.0092	0.053	0.12	0.1
7	$1.1 \cdot 10^{-8}$	$3.9 \cdot 10^{-7}$	0.0019	0.013	3	30

4.2 Constant Rate Test: Single Well

The pressure and flow rate vs. time plots for all analyzed constant rate tests can be found in Appendix K. The quantitative analyses of the single well test result in values for initial pressure, transmissivity, storativity and flow dimension. All results of the single well test analyses inclusive the mean residual of the curve fits and its standard deviation can be seen in the Appendix L. In the following the results are described and presented graphically. Besides the quantitative analyses, qualitative observations of the pressure curve were made.

4.2.1 Qualitative Observations

In order to have longer buildup phases available for analysis, successive data sets have been merged. This is the explanation for the data gaps showing up in the analyzed data. The merging is also the reason for the pressure drops in other intervals/boreholes which can often be observed in the second part of the recovery phase. The pressure decreases are due to pulse tests or constant rate tests in other intervals/boreholes. The extended datasets were only used for analysis if the later tests do not have a visible effect on the pressure in the analyzed intervals/boreholes.

The pressure curve of CB1 shows a certain scattering of the measurements around the general trend, which is always clearly visible. The scattering around the general trend is mostly about ±0.025 bar (sometimes only ±0.0025 bar, which is comparable to the other intervals, rarely up to ±0.1 bar). The drawdown curve of the constant rate test in CB3 shows a short anomaly in one point, which is due to an irregularity in the flow rate. During withdrawal in Interval 3, the pressure is observed to increase slightly after the initial pressure decrease before it decreases again before shut-in. The flow rate during this test was very stable. The drawdown curves of the first and third test in Interval 4 both show strong irregularities. These are due to not fully stable flow during the withdrawal. The drawdown curve of the second test in Interval 4 shows a similar shape to the one in Interval 3 (initial drawdown to a minimum, slight increase in pressure, followed by a decrease in pressure before shut-in). Also during this test, the flow rate was almost constant.

The drawdown in Interval 5&6 is characterized by an oscillating pressure (Fig. 4.1). The oscillating pressure during the drawdown in Interval 5&6 is explained by the unstable (cyclic) flow during the test, which is caused by the automatic valve of the flow controller used in the current study (Fig. 4.2). The cycles are very regular with an amplitude of ~42 l/h (max: 85 l/h; min: 1 l/h) and a period of 10 seconds. However, the average flow rate was 30 l/h and the oscillation show a low magnitude, therefore, the data was analyzed assuming stable flow of 30 l/h.

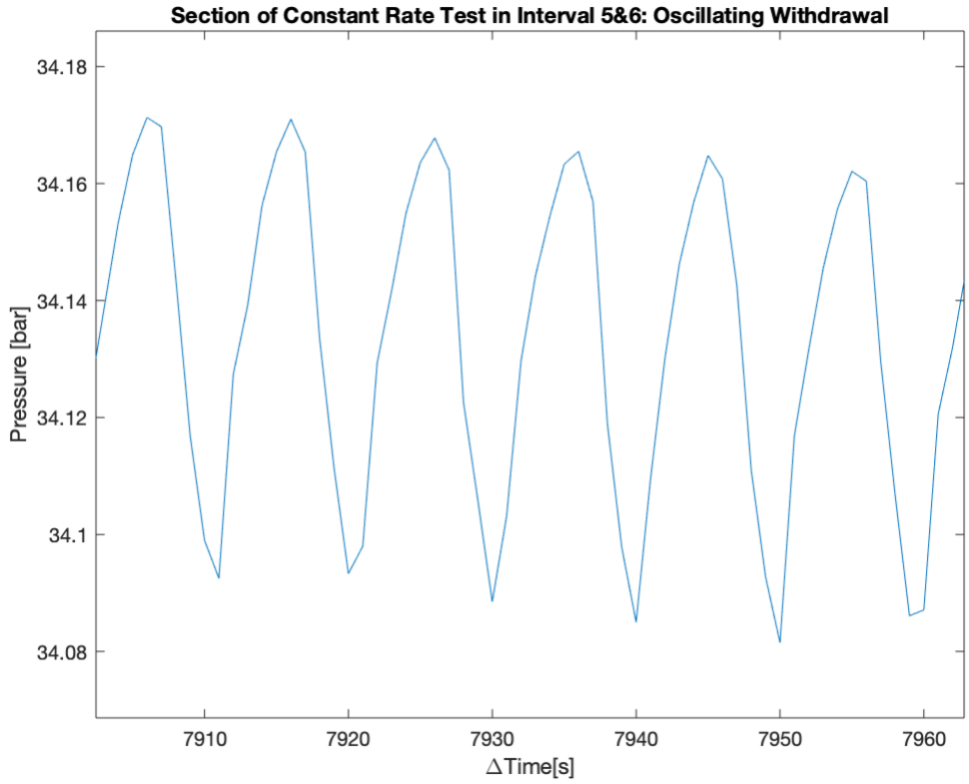

Fig. 4.1. Oscillating pressure in Interval 5&6 during the drawdown phase of the constant rate test.

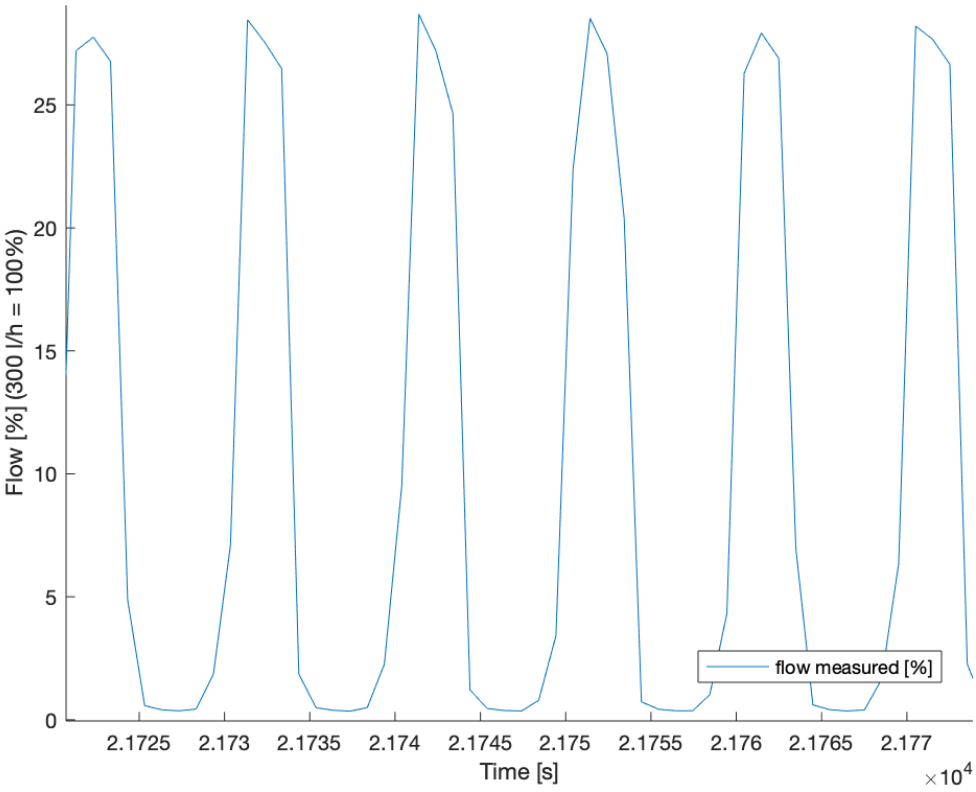

Fig. 4.2. Oscillating flow rate during the constant rate test in Interval 5&6, shown by a section of the flow measurements during the test.

While viewing the pressure data of Interval 2, it was found that its pressure is oscillating (Fig. 4.3). It can be seen that the oscillation does not occur at every point in time (e.g. 10^5 – 10^7 s). The oscillation has a wavelength of about 1800 s and an amplitude of about 0.0015 bar. Period and amplitude were determined from the data from the measurements during the constant rate test in CB1.

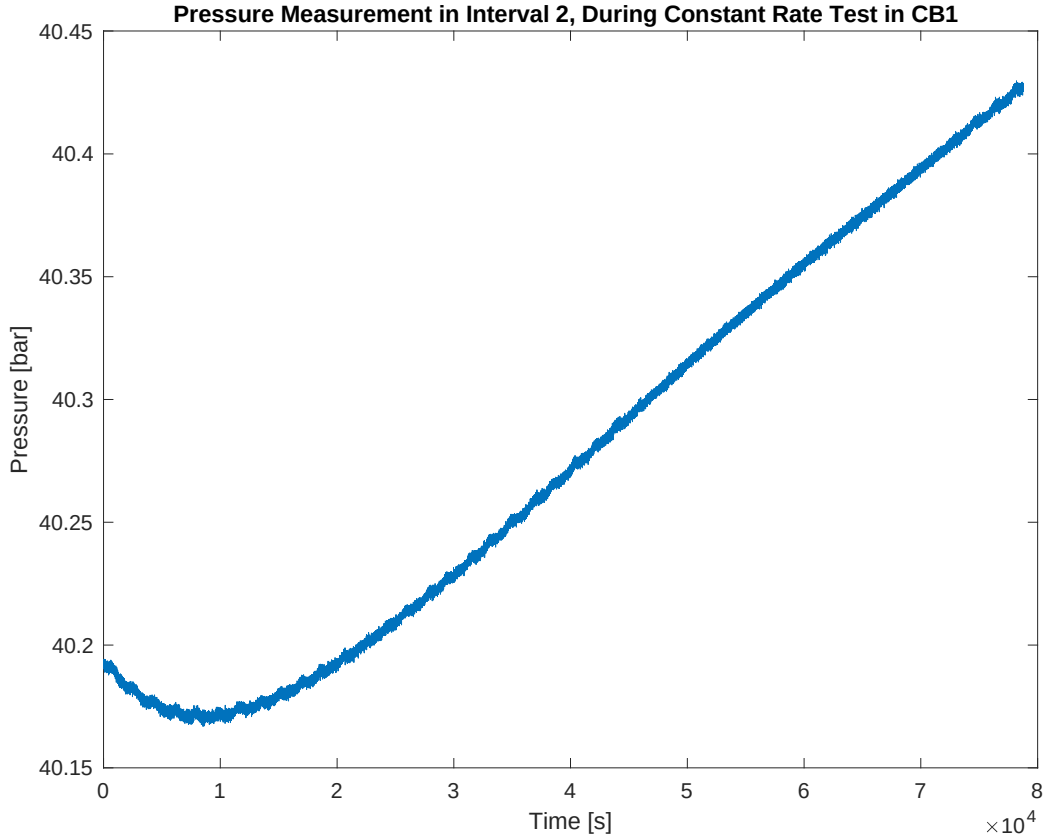

Fig. 4.3. A section of the pressure curve in Interval 2 during the buildup in CB1 as an example for the oscillating pressure in Interval 2.

4.2.2 Initial Pressure

The initial pressures (or static formation pressure) determined with the help of Horner (1951) plot and straight line fitting can be seen in Tab. 4.2.The Horner plots and the manual fitting can be seen in Appendix M. The initial pressures derived from the intervals where more than one constant rate test was performed in are quite consistent (±0.25 bar). Nevertheless, a certain trend was observed in the intervals in which more than one test was performed in, whereby the tests that were carried out later in time resulted in higher initial pressures (see results for Interval 4 and 7 in Tab. 4.2)

Tab. 4.2. Initial pressures derived from the straight line fitting in the Horner plots of the buildup data from the constant rate tests.

Interval / Borehole	Order of Testing	Interval Center [BM]	Initial Pressure [bar]
CB1	11	–	40.2
CB3	10	–	40.5
Interval 1	4	210.645	40.4
Interval 2	7	197.525	40.6
Interval 3	2	182.265	39.0
Interval 4-1	5	171.27	39.4
Interval 4-2	8	171.27	39.7
Interval 4-3	9	171.27	39.8
Interval 5&6	6	153.5	39.9
Interval 7-1	1	132.68	36.2
Interval 7-2	3	132.68	36.7

4.2.3 Diagnostic Plots

For the analyzed constant rate tests in CB1, CB3 and the intervals in CB2 diagnostic plots of the drawdown (Appendix N) and the buildup phases (Appendix O) were created.

It has been found that wellbore storage and skin effects (unit slope plus a hump in diagnostic plot) of varying duration (a few seconds in CB1, CB3 and Intervals 4 and 7 and up to 1000 seconds in Intervals 1, 2, 3 and 5&6). However, in all cases – except for drawdown and buildup in Interval 3 and buildup in Interval 5&6 – the unit slope section is followed by at least 1.5 log cycles of data. The reason why Interval 3 and 5&6 do not fulfill the 1.5 log cycles rule is that the production phase of the constant rate tests in Interval 3 and 5&6 did not last long enough to overcome wellbore storage effect significantly. Another interpretation of the diagnostic plot of Interval 3 and 5&6 is an infinite conductive fracture. However, the 1.5 log cycle rule by Horne (1990) is fulfilled in most cases.

Despite the use of automatic flow meters, the withdrawal was in many cases not stable enough to generate smooth derivative curves. Attempts to smooth the curves with resampling tools in Matlab did not lead to satisfying results. In contrast, the curves of the buildup phases are smooth in most cases (without the need for resampling). Therefore, for the identification of suitable conceptual models for further analysis, the diagnostic plots of the buildup phases were focused on. Nevertheless, the diagnostic plot of the buildup phase should be treated with caution, because superposition effects from the drawdown phase may affect the buildup phase. Furthermore, the buildup phase only contains information about the reservoir if the wellbore storage and skin effects were overcome during the drawdown phase.

The derivative curves in the diagnostic plots of the buildup phases of the Intervals 1, 2, 3 and 5&6 show the same picture: First a section with wellbore storage and then the curve shows a negative slope. The buildup phases of the mentioned intervals are too short to show IARF or even boundary conditions. The derivatives of the three tests in Interval 4 also show negative slopes after the wellbore storage section, but the slopes become less steep about 1.5 log cycle after the end of the wellbore storage for the duration of about one log cycle before the negative slopes become steeper again. The diagnostic plots of CB1 and both tests in Interval 7 in CB2 show a wellbore storage section and a subsequent negative slope of the derivative, which is followed by a positive slope of the derivative. The derivative curve of CB3 is characterized by a borehole storage section, followed by an almost horizontal section (slightly ascending), at the end the curve shows a negative slope. In the diagnostic plots of the buildup phases in CB1, Interval 4-1, 4-3, 7-1 and 7-2, changes in the slope of the derivative curve (becoming negative (CB1), short flattening (Interval 4), becoming positive (Interval 7)) were observed at ~10^4 seconds in all cases.

The examination of the diagnostic plots of the drawdown and buildup phases of CB1, CB3 and the intervals in CB2 lead to the following conclusions:

The drawdown phase of the constant rate tests in CB1, CB3 and the interval 1, 2, 4, 7 were definitely long enough (see 1.5 log cycle rule) so that the buildup phase contains information about the reservoir. The diagnostic plots of the drawdown phase of the Intervals 3 and 5&6 are either interpreted as infinite conductive fracture or as a withdrawal phase which did not overcome the wellbore storage effect significantly. The buildup phases in the Intervals 1 and 2 were too short to make clear statements about the flow regime that would follow the wellbore

storage affected section. CB3 and Interval 4 show signs of constant pressure boundaries. The buildup phase of the Intervals 3 and 5&6 both show signs of infinite conductive fracture. The diagnostic plot of the tests in Interval 7 show derivative curves indicating either a closed boundary or double porosity.

Based on these observations and in discussion with Nathan Dutler, it was decided to analyze the tests with the Theis (1935) and GRF (Barker, 1988) models.

4.2.4 Transmissivity

The transmissivity values resulted from the single well test analyses with Theis (1935) and the GRF (Barker, 1988) model are shown graphically in Fig. 4.4. Tables with the transmissivity values resulted from the single well test analyses can be seen in Appendix L.

Regardless of whether the test data was analyzed with Theis (1935) or the GRF model, the results do not differ by more than one order of magnitude. Regardless of whether the drawdown or buildup phase of a constant rate test was analyzed, the results do not differ by more than one order of magnitude. The single well tests analysis of the drawdown and buildup data of the constant rate tests show transmissivity values between $10^{-11} – 3 \cdot 10^{-6}$ m^2/s. For the intervals where more than one test was performed in (Interval 4 and 7) the results are consistent. The boreholes CB1 and CB3 show the highest transmissivity values ($3.7 \cdot 10^{-7} – 2.8 \cdot 10^{-6}$ m^2/s). The intervals in CB2 can be grouped in three. First, Intervals 1 and 2 with transmissivities of $1.2 \cdot 10^{-11} – 1.4 \cdot 10^{-10}$ m^2/s, second, Intervals 3 and 4 with transmissivities of $1.5 \cdot 10^{-9} – 1.7 \cdot 10^{-8}$ m^2/s and third, Interval 5&6 and 7 with transmissivities of $2.7 \cdot 10^{-8} – 2.1 \cdot 10^{-7}$ m^2/s.

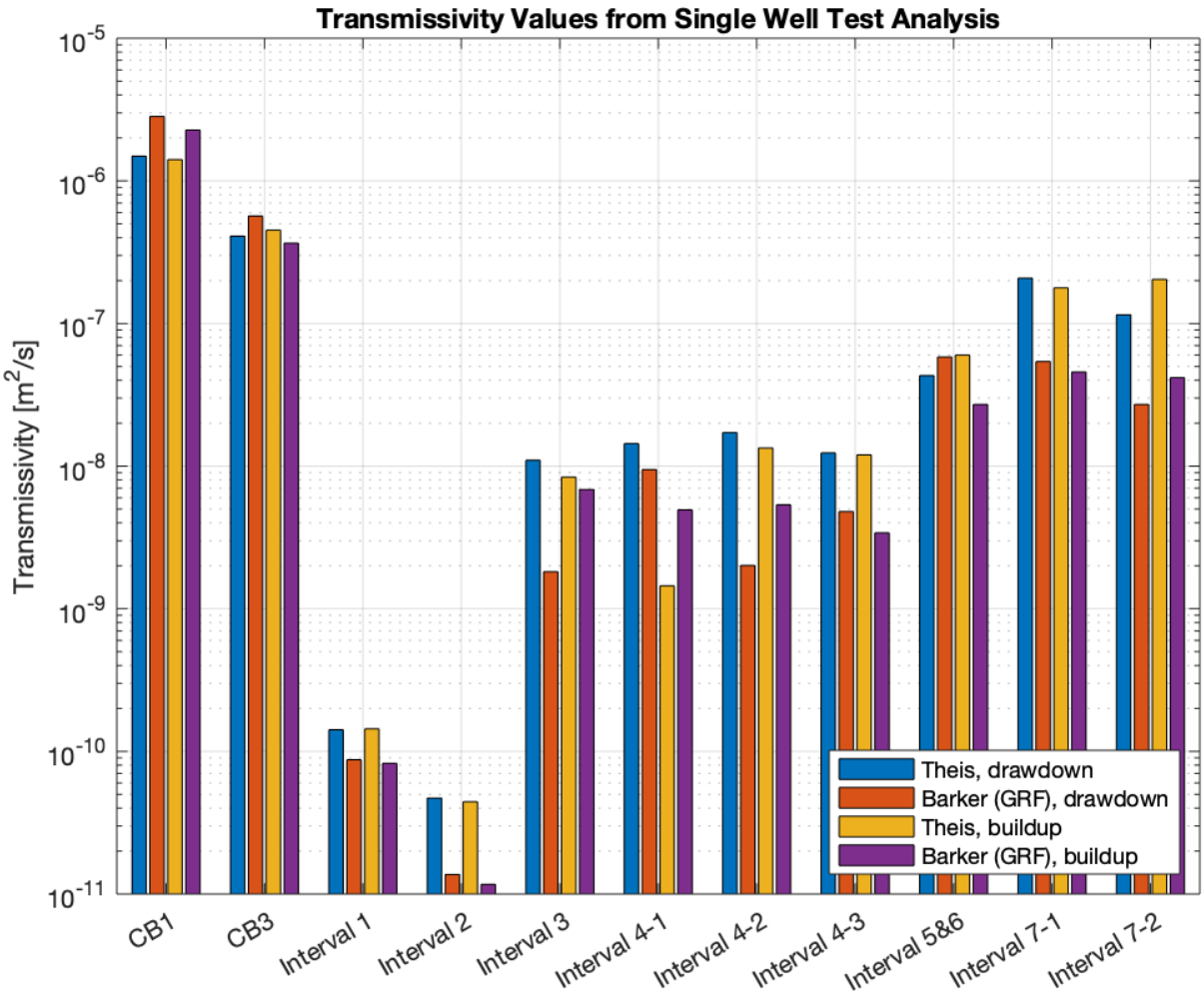

Fig. 4.4. Compilation of transmissivity values resulted from the single well analysis of the constant rate tests on log scale.

4.2.5 Storativity

The storativity values resulted from the single well test analyses with Theis (1935) and the GRF (Barker, 1988) model are shown graphically in Fig. 4.4. Tables with the storativity values resulted from the single well test analyses can be seen in Appendix L. The storativity values resulted from the single well test analyses show values in different orders of magnitude ($4 \cdot 10^{-6}$ – $4 \cdot 10^{-2}$). Considering the results of CB1, CB3, Intervals 1, 2, 3 and 5&6 separately for each interval/borehole, they are consistent regardless of whether drawdown or buildup data was analyzed with Theis or the GRF model (i.e. the results in the respective boreholes/intervals do not differ by more than one order of magnitude). In contrast, the Intervals 4 and 7 (i.e. the results in the respective intervals differ by more than one order of magnitude).

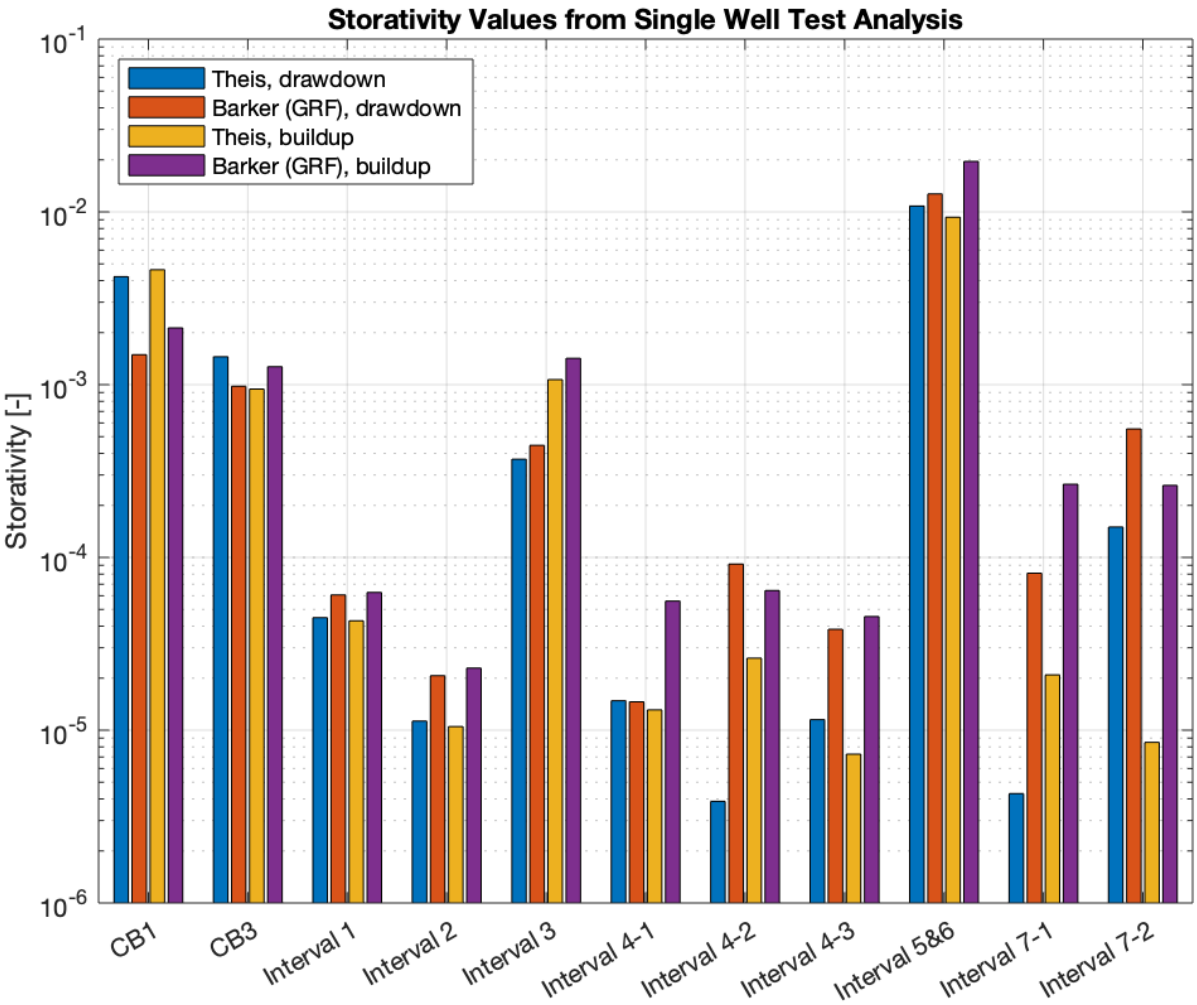

Fig. 4.5. Compilation of storativity values resulted from the single well analysis of the constant rate tests.

4.2.6 Flow Dimension

The flow dimension values resulted from the single well test analyses of the constant rate tests with the GRF model are shown graphically in Fig. 4.6. Tables with the flow dimension values resulted from the single well test analyses can be seen in Appendix I. The Intervals 1, 2, 4 and 7 show flow dimensions over 2 (2.2 to 2.8). Two analyses of drawdown data (Intervals 4-2 and 7-2) resulted in unrealistically high values of over 3. CB1 and CB3 show values of just below two. The Intervals 3 and 5&6 show large differences between the value obtained from the drawdown data and the value obtained from the buildup data. The analysis of the buildup in Interval 5&6 resulted in a flow dimension similar to CB1 and CB3 (i.e. ~1.8). From the analysis of the buildup in Interval 3 the lowest flow dimension (~1.5) resulted.

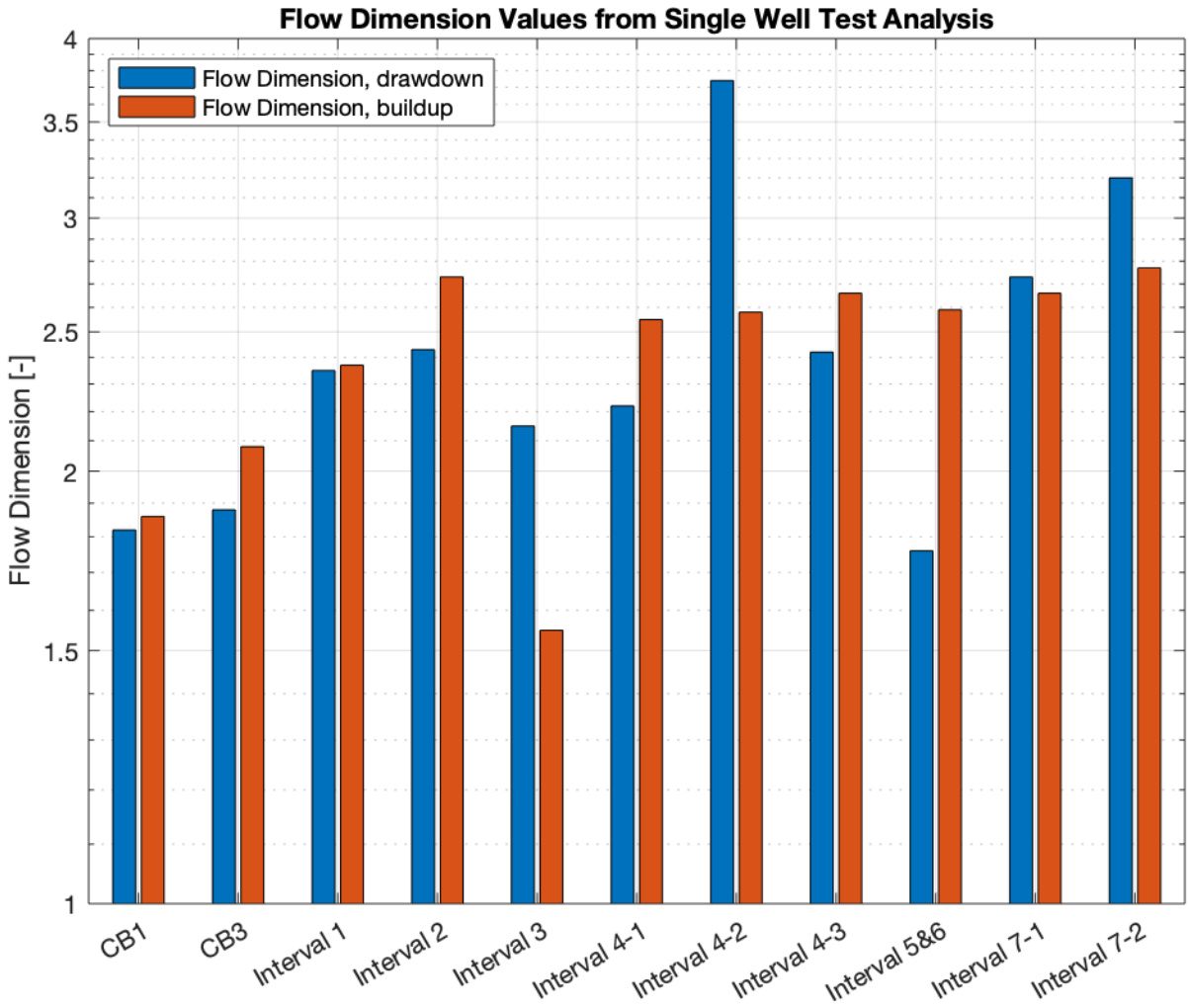

Fig. 4.6. Compilation of flow dimension values resulted from the single well analyses of the constant rate tests applying the GRF model.

4.3 Constant Rate Test: Cross-Hole

During the constant rate tests in CB1, CB3 and the intervals in CB2, the passive boreholes and intervals served as observation boreholes and intervals, respectively. Pressure responses to the constant rate tests were observed in the passive borehole(s)/intervals. Plots of all constant rate tests in which the pressure curves of the passive borehole(s) and intervals are plotted beside the pressure curve of the active borehole/well can be seen in Appendix P. The responses to the constant rate tests in CB1 (Fig. 4.6) and CB3 (Fig. 4.7) were examined in more detail and later analyzed.

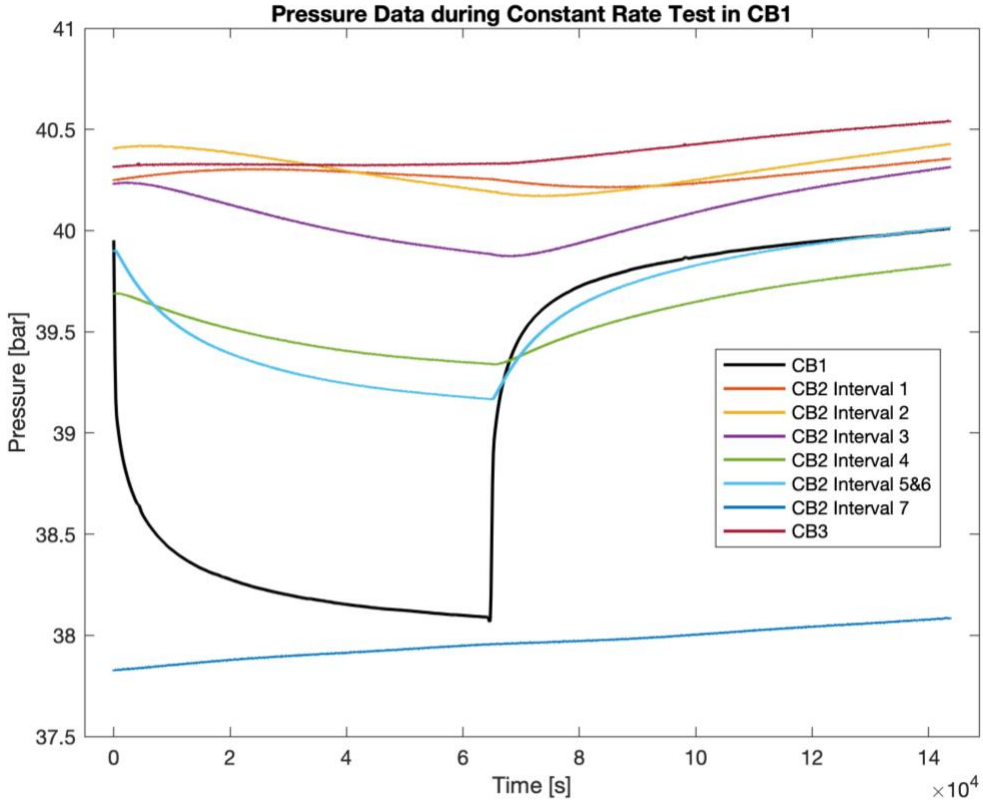

Fig. 4.7. Pressure data during the constant rate test in CB1 (smoothed pressure curve for CB1).

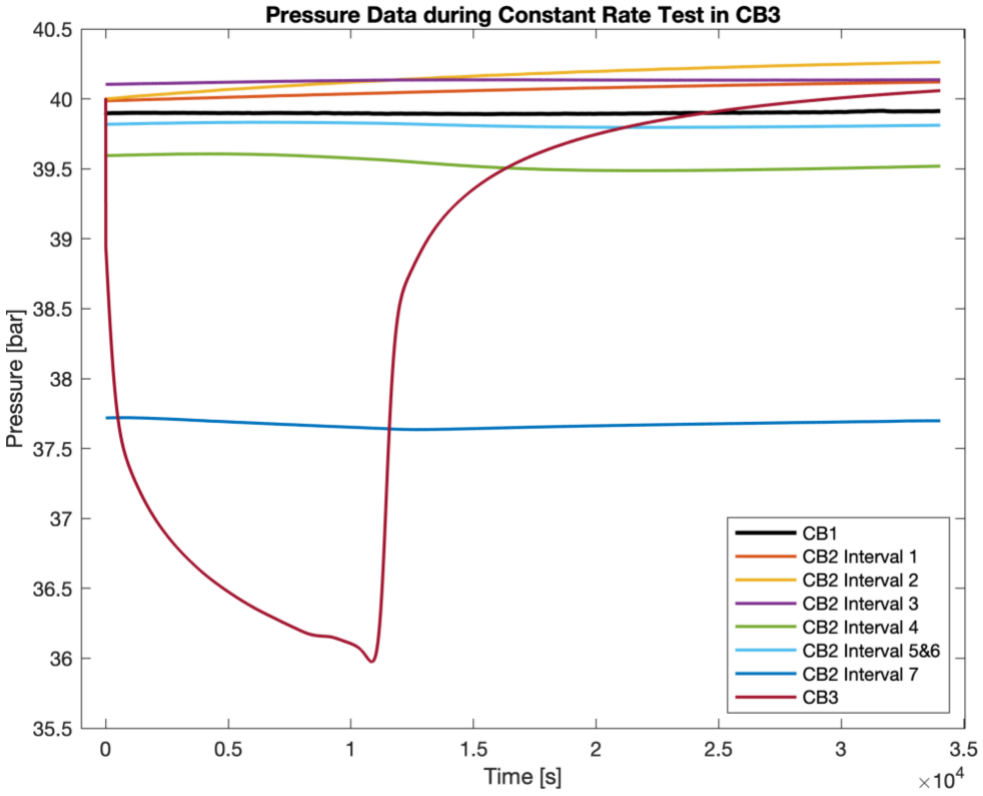

Fig. 4.8. Pressure data during the constant rate test in CB3 (smoothed pressure curve for CB3).

4.3.1 Qualitative Observations

The borehole(s)/interval(s) that have responded to a specific constant rate test can be seen in Tab. 4.3. The responses to the constant rate test in CB and CB3 were considered qualitative first, before a quantitative analysis was conducted. In Fig. 4.6 can be seen that during the constant rate test in CB1, all intervals as well as CB3 show a response. Some intervals respond more strongly and with a smaller time delay (e.g. Interval 5), other intervals show a smaller pressure response and a larger time delay (e.g. Interval 2). The responses during the constant rate test in CB3 (Fig. 4.7) are generally weaker than the ones during the test in CB1, although the shorter duration of the test compared to the constant rate test in CB1 must be taken into account. CB1 and all intervals except intervals 1 and 2 responded to the constant rate test in CB3.

Tab. 4.3. Indicating which interval/borehole responded to each other's constant rate tests responses

	CB3	**Int 1**	**Int 2**	**Int 3**	**Int 4**	**Int 5&6**	**Int 7**
CB1	Yes	Yes	Yes	Yes	Yes	Yes	(Yes)
CB3	–	No	No	Yes	Yes	Yes	Yes
Int 1	–	–	Yes	No	No	No	No
Int 2	–	–	–	No	No	No	No
Int 3	–	–	–	–	Yes	Yes	No
Int 4	–	–	–	–	–	Yes	No
Int 5&6	–	–	–	–	–	–	No

No: no response, *Yes*: clear response, *(Yes)*: minor response

In some cases reverse water level fluctuations also known as Noordbergum effect (Verruijt, 1969) were observed (Fig. 4.9). This is a poroelastic effect where a sharp pressure changes in the observation well/interval almost immediately after the start of the withdrawal or shut-in is observed. A Noordbergum effect was observed in the Intervals 1, 2, 4 and 5&6 after CB1 was shut-in and in Interval 7 after CB3 was shut-in. No detailed investigation about this effect has been conducted and there may be more tests where it shows up. The Noordbergum effect will not be further analyzed and discussed in this thesis.

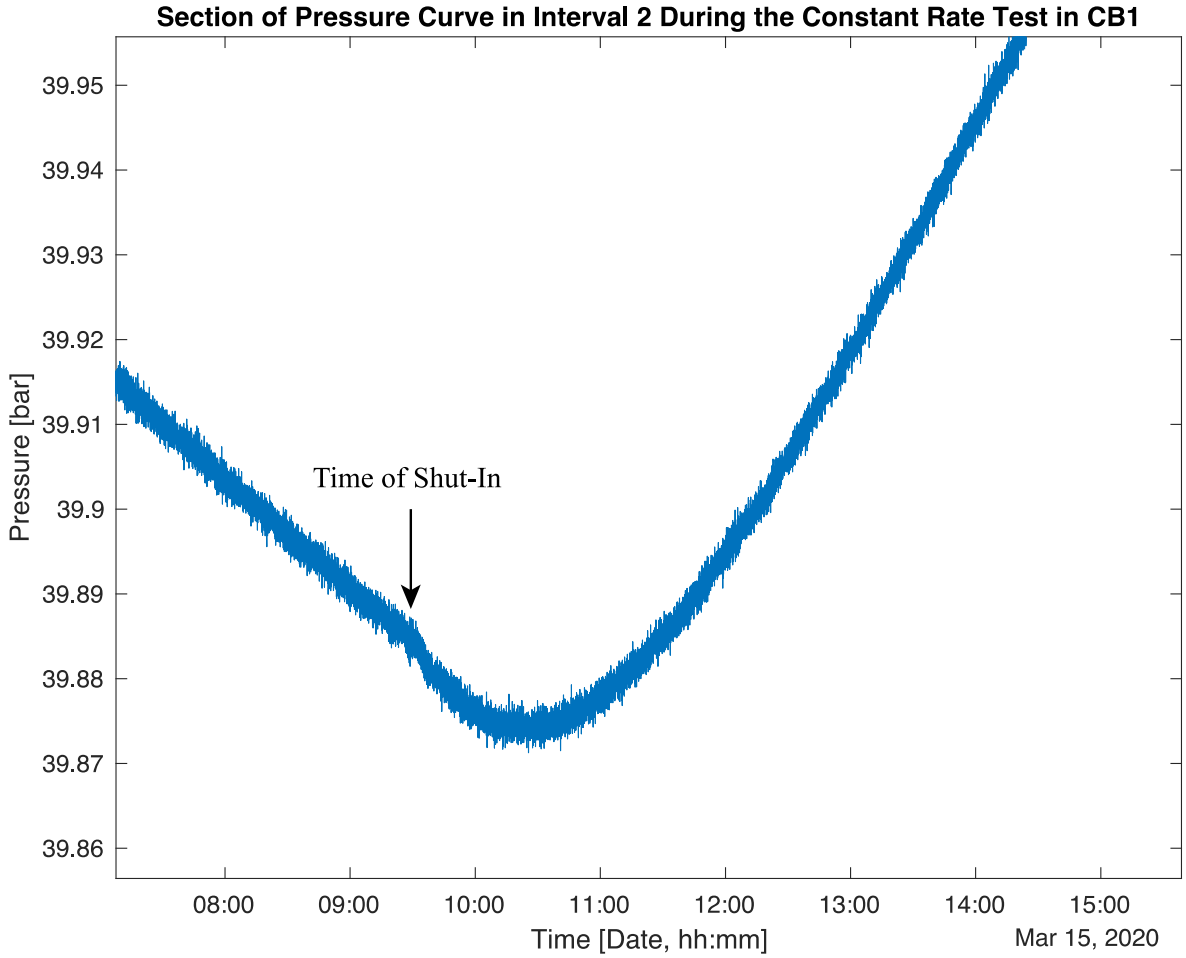

Fig. 4.9. Example for the apparency of the Noordbergum effect in Interval 2 caused by the shut-in in CB1.

4.3.2 Response Times

The absolute response times to the withdrawals in CB1 and CB3 are shown in Tab. 4.4. Clear differences in the response times can be seen. The shortest detected response time shows Interval 5&6 to the withdrawal in CB1 (115 s), with 420 s Interval 4 also response relatively quickly as well. The longest response time shows Interval 7 to the withdrawal in CB1 (19000 s). In contrast, Interval 7 responded fastest to the withdrawal in CB3. Interval 3 responds the slowest to the withdrawal in CB3, which has the third shortest response time to the withdrawal in CB1. CB1 reacted faster (2700 s) to the withdrawal in CB3 than vice versa (3400 s).

Tab. 4.4. Response times regarding the start of the withdrawals in CB1 and CB3. With color code indicating the relative speed of the response (green: fast, red: slow, sperate color code for the two columns).

	Response Time [s]	
	Withdrawal in CB1	**Withdrawal in CB3**
CB1	–	2700
CB3	3400	–
Interval 7	19000	400
Interval 5&6	115	3100
Interval 4	420	3050
Interval 3	1600	7700
Interval 2	4500	n. r.
Interval 1	6100	n. r.

n. r.: no response observed

For a qualitative representation and the comparison of the responses, normalized pressure response plots were created for the responses to the drawdown in CB1 (Fig. 4.10) and CB3 (Fig. 4.11). Due to the normalization, pressure decreases appear as curves with positive slope and vice versa. In a normalized pressure response plot all pressure curves collapse when in a homogenous reservoir (in terms of transmissivity and flow dimension) is tested and pressure moves along straight connection lines. In Appendix Q normalized plots for the buildup phase in CB1 and CB3 can be seen as well as plots were the time is not normalized by the squared distance (but only the pressure by the production rate).

In Fig. 4.10 it can be seen that Interval 5&6 responds fastest relative to its distance to CB1. The reason for the negative slope of the pressure curve in Interval 7 at late time is that the response to the drawdown in CB1 is so weak that it cannot overcome the recovery effect of the not yet completely stabilized system. The response in CB3 is weaker than in the intervals (Interval 7 excluded), but just noticeable. In Interval 1, the recovery effect of the whole system predominates up to a certain time, after which the drawdown response is visible (positive slope).

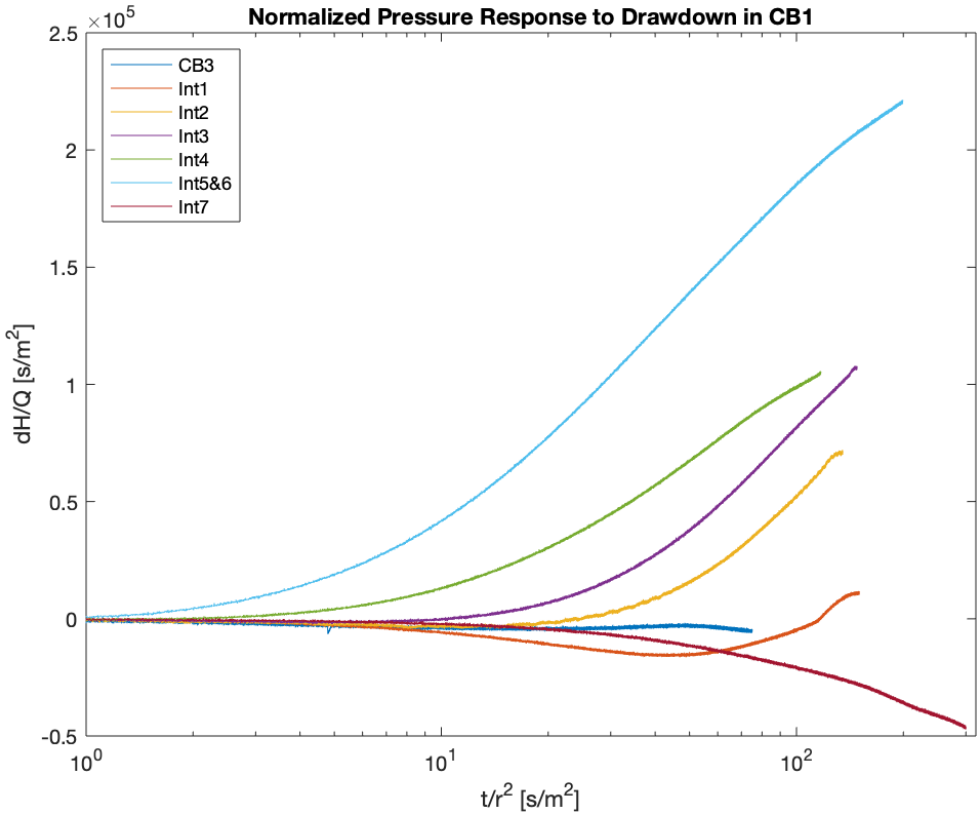

Fig. 4.10. Normalized pressure responses in all intervals and CB3 to the withdrawal in CB1.

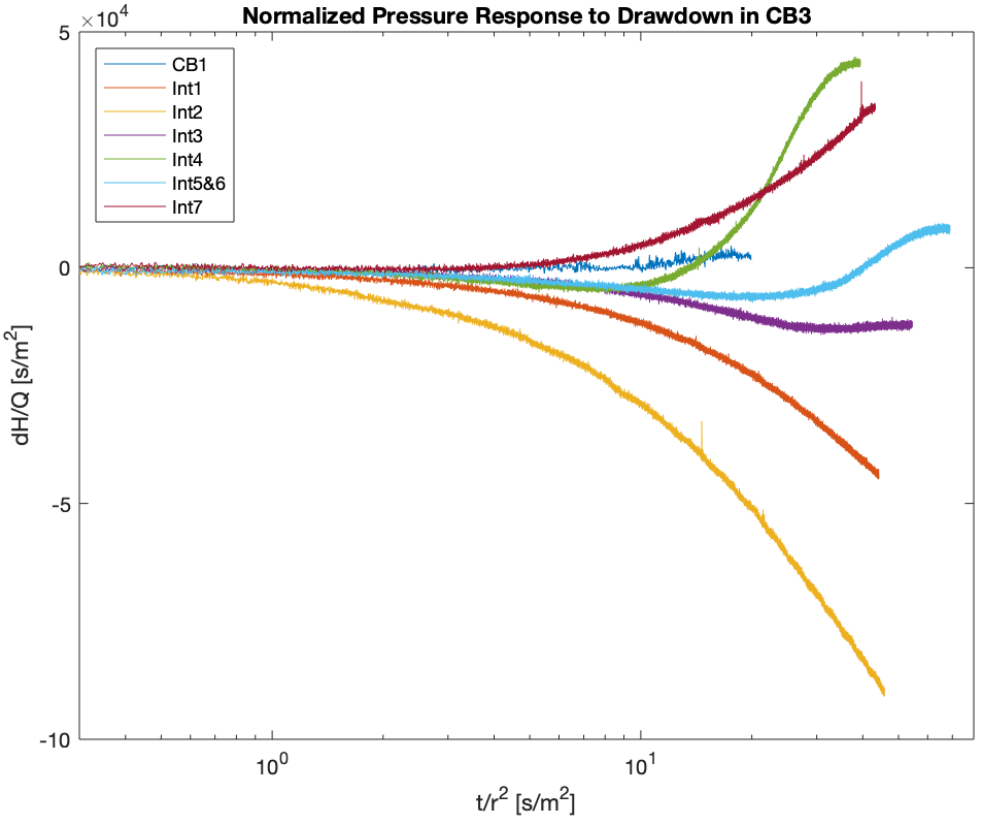

Fig. 4.11. Normalized pressure responses in all intervals and CB1 to the recovery in CB3.

In Fig. 4.11 it can be seen that CB1 responds fastest to the withdrawal in CB3 relative to distance the pressure signal needs to travel. It can be clearly seen that Intervals 1 and 2 do not react to the withdrawal in CB3 and only show the recovery effect in the entire system (negative slope). In the Intervals 3, 4 and 5&6 the recovery effect can also be seen in the beginning, but at a certain time it is followed by the drawdown effect (positive slope) from CB3.

4.3.3 Diagnostic Plots

Diagnostic plots of the analyzed cross-hole responses can be seen in Appendix R, Appendix S, Appendix T and Appendix U. In the diagnostic plots of the cross-hole responses in CB3, Interval 1, 2, 3, and 7 to withdrawal and recovery in CB1, only unit slopes are observed. For the pressure data of interval 7 during withdrawal in CB1 it was not possible to create a diagnostic plot, because no response was observed. In the Intervals 4 and 5&6, the derivative curve deviates slightly from the unit slope towards the end and flattens (both in the response to withdrawal and in the response to recovery). Also, only unit slopes are observed in the diagnostic plots of cross-hole responses in CB1 and all intervals to withdrawal and recovery in CB3.

Based on these observations coupled with the observations made during the single well test analyses, it was decided to analyze the tests with the models of Theis (1935) and Agarwal et al (1970).

4.3.4 Transmissivity

Cross-hole responses in CB1, CB3 and the intervals in CB2 to the recovery in CB1 and CB3 respectively were analyzed. Since the qualitative analysis showed that even the longer lasting buildup data is too short, the analysis of the drawdown data was skipped. To check whether the drawdown data would result in transmissivity data in other orders of magnitude, the responses in Intervals 4 and 5&6 to the withdrawal in CB1 were analyzed (because their diagnostic plots look most promising). The qualitative analysis showed that in Interval 1 and 2 no response to the withdrawal and recovery in CB3 was observed. Therefore, no results are available for those Intervals and the respective test. The models from Theis (1935) and Agarwal et al. (1970) were applied to all analyzed data (Fig. 4.12). The numbers on which Fig. 4.12 is based on can be seen in Appendix V. The transmissivity values resulted from the analyses are in the range of $0.8 \cdot 10^{-6}$ to $6 \cdot 10^{-6}$ m^2/s. The resulted transmissivity value for CB1 ($\sim 5.9 \cdot 10^{-6}$ m^2/s) is the only result that is clearly above $3 \cdot 10^{-6}$ m^2/s.

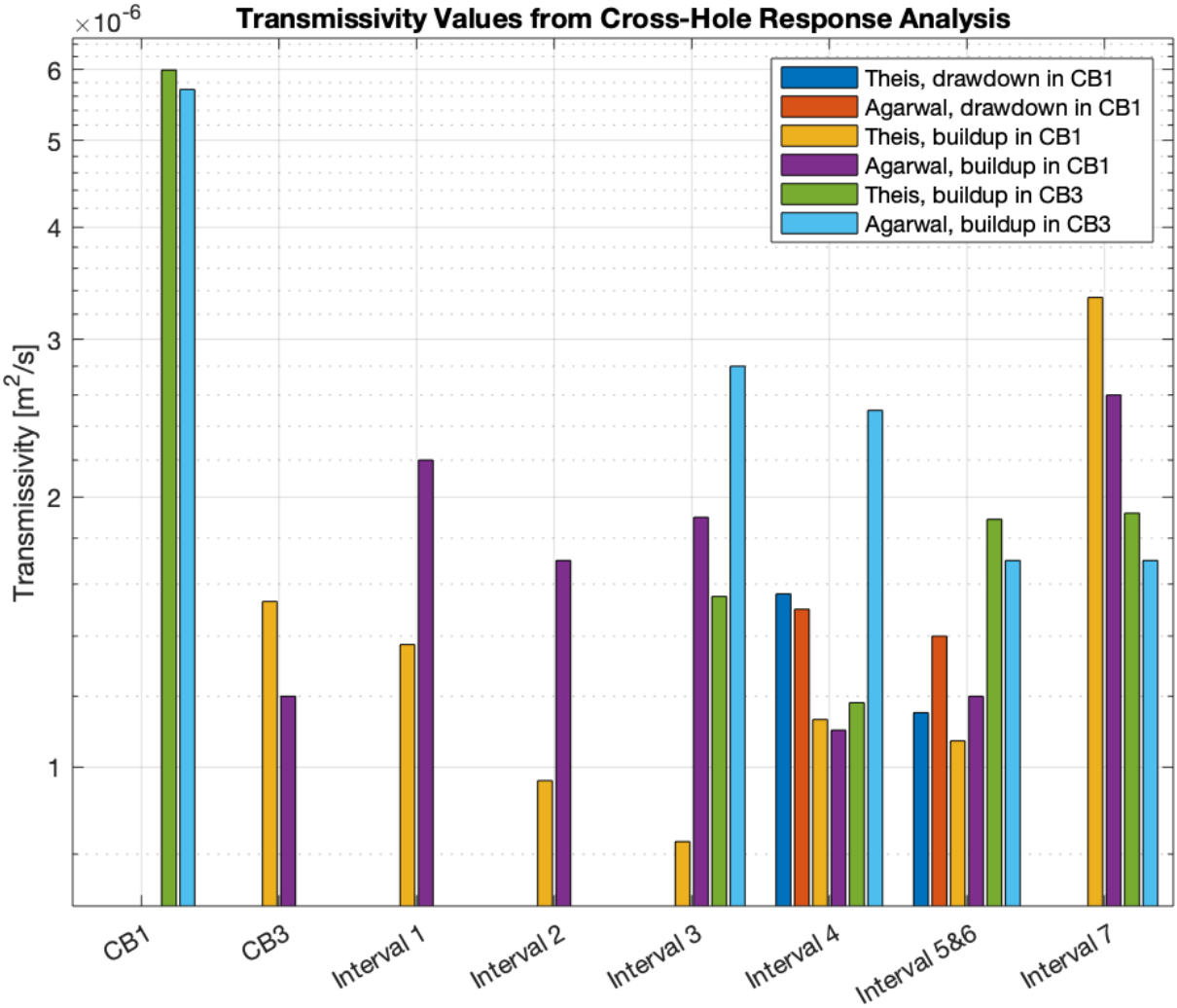

Fig. 4.12. Compilation of transmissivity values resulted from the cross-hole response analysis of the constant rate tests in CB1 and CB3.

4.3.5 Storativity

The storativity values resulted from the cross-hole response analyses (Fig. 4.13) show values in different orders of magnitude ($8 \cdot 10^{-6}$ – $6 \cdot 10^{-4}$). The numbers on which Fig. 4.13 is based on can be seen in Appendix V. The analysis of the response in Interval 7 to the buildup in CB1 is the only one that results in a value above $2.3 \cdot 10^{-4}$ (namely $5.7 \cdot 10^{-4}$). For Intervals 1 and 2 no results are given for the analysis of the responses to the tests in CB3, because no response was observed to it. The results of the analysis of the responses in the Intervals 4 and 5&6 on the drawdown in CB1, show that the values are consistent with the results of the analysis of the responses to the buildup in CB1. Intervals 4, 5&6 and 7 show clear differences in the

results depending on whether the response to the test was analyzed in CB1 or CB3. In Interval 4 and 7 the resulted storativity value is about one order of magnitude higher, when the constant rate test took place in CB1. In the Interval 5&6 the resulted storativity value is slightly higher (0.5 orders of magnitude) for the case where the constant rate test took place in CB3. The results for CB1 and CB3 when the constant rate test was performed in the other borehole show similar values (CB1: $2.3 \cdot 10^{-4}$, CB3: $1.2 \cdot 10^{-4}$). Interval 1, 2 and 3 shows varying different storativities depending on which model was used for the analyzed. In the other cases, the values resulted from the analyses with the two different models are consistent.

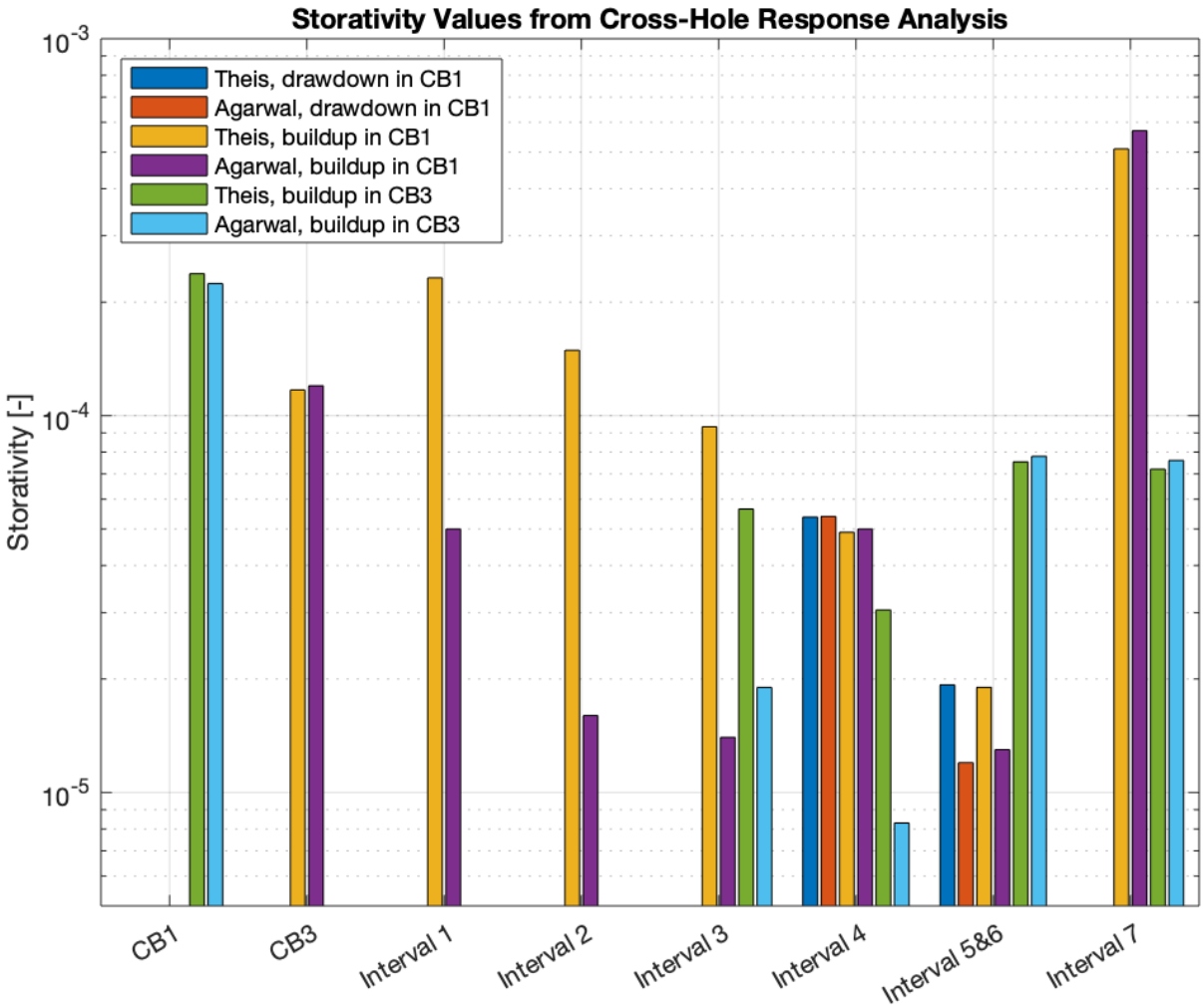

Fig. 4.13. Compilation of storativity values resulted from the cross-hole response analysis of the constant rate tests in CB1 and CB3.

4.3.1 Skin Effect

The analysis of the cross-hole responses in CB1, CB3 and the Intervals 5&6 and 7 resulted in negative skin effect values in the range of -4.4 to -13.0. The analyses of the cross-hole responses in Interval 4 resulted in negative values for analysis of the response to the drawdown and buildup in CB1 (-6.3 resp. -6.4), and in a positive value from the analysis of the cross-hole response to the buildup in CB3 in a value of 38. For the Intervals 1, 2 and 3, skin effect values between 44 and 100 resulted.

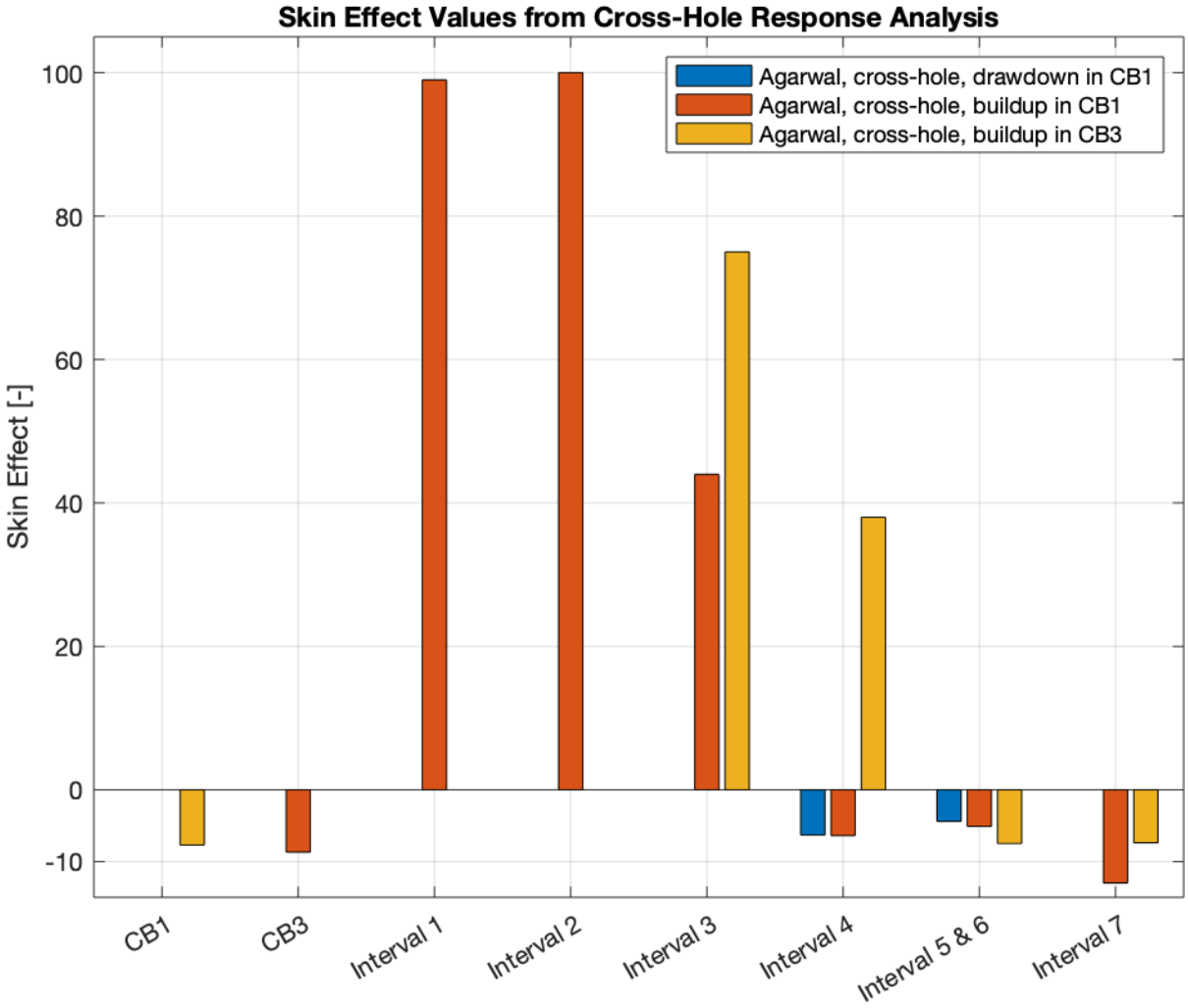

Fig. 4.14. Compilation of wellbore skin effect values resulted from the analysis of cross-hole responses to the constant rate tests in CB1 and CB3.

4.4 Comparison: Single Well Test and Cross-Hole Response Analysis

4.4.1 Transmissivity

The values shown in Fig. 4.15 are the mean of the resulted values from single well tests and cross-hole analyses for each interval/borehole. For the calculation of the average the results of the analyses with all applied models of both the drawdown and the buildup phases were used. It can be seen that the mean values resulted from the single well analysis differ by several orders of magnitude, while the results from the cross-hole analyses are all in the same order of magnitude. Further it can be seen that the transmissivities resulted from the pulse tests are lower than those from the single well test analyses, except in Interval 1 where the value of the pulse test is slightly higher.

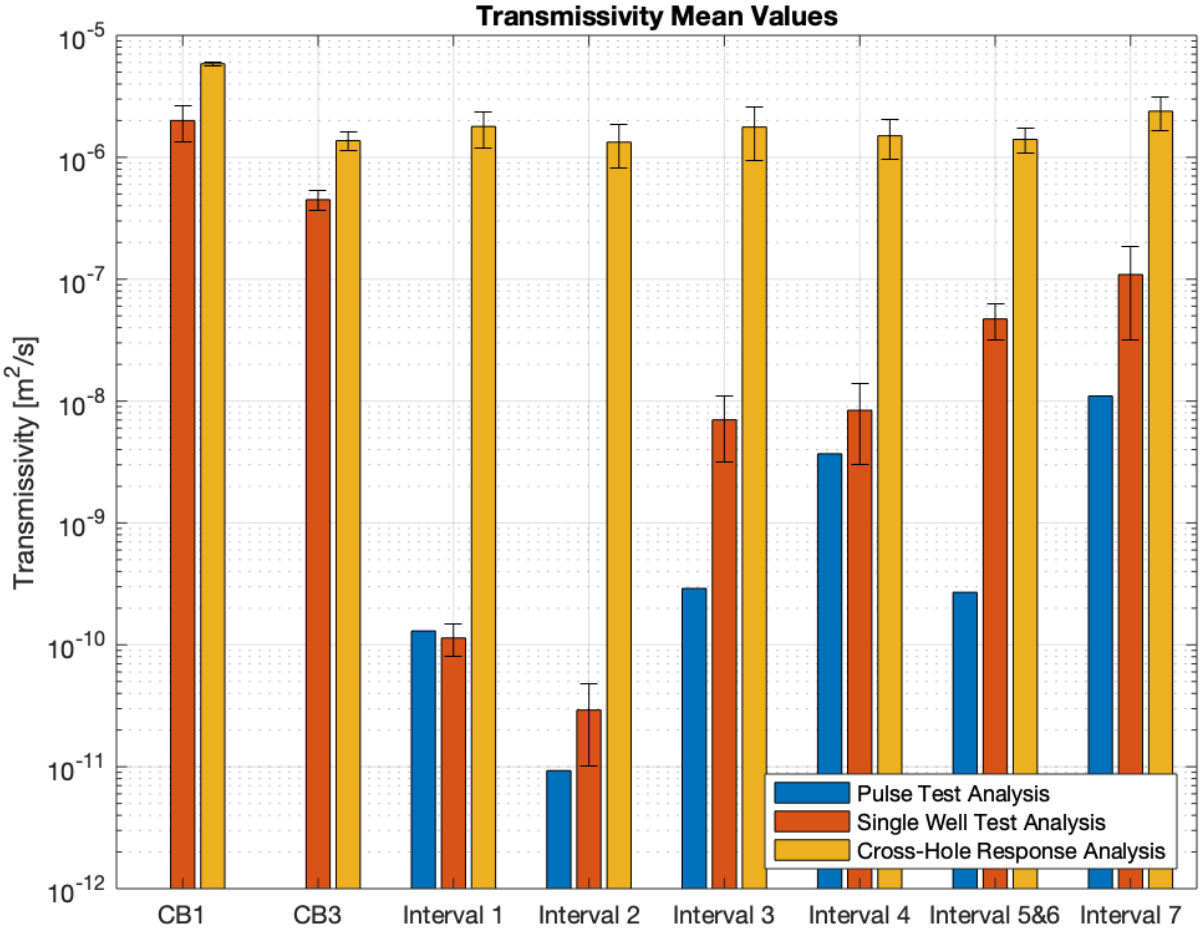

Fig. 4.15. Compilation of transmissivity mean values (with standard deviation) resulted from pulse test, single well test and cross-hole response analysis.

4.4.2 Storativity

Storativity mean values in the range of 10^{-5} to $2 \cdot 10^{-2}$ are observed (Fig. 4.16). For CB1, CB3, Interval 3 and 5&6, the values from the single well tests analyses are higher than those from the cross-hole response analyses. In contrast, for Interval 1, 2, 4 and 7, the mean values from the cross-hole response analyses are higher. Interval 5&6 (single well test analysis) shows the highest storativity value. Whereas the storativity value for Interval 5&6 resulted from the cross-hole response analysis show a low value which is comparable to the lowest values obtained (Interval 1 and 2).

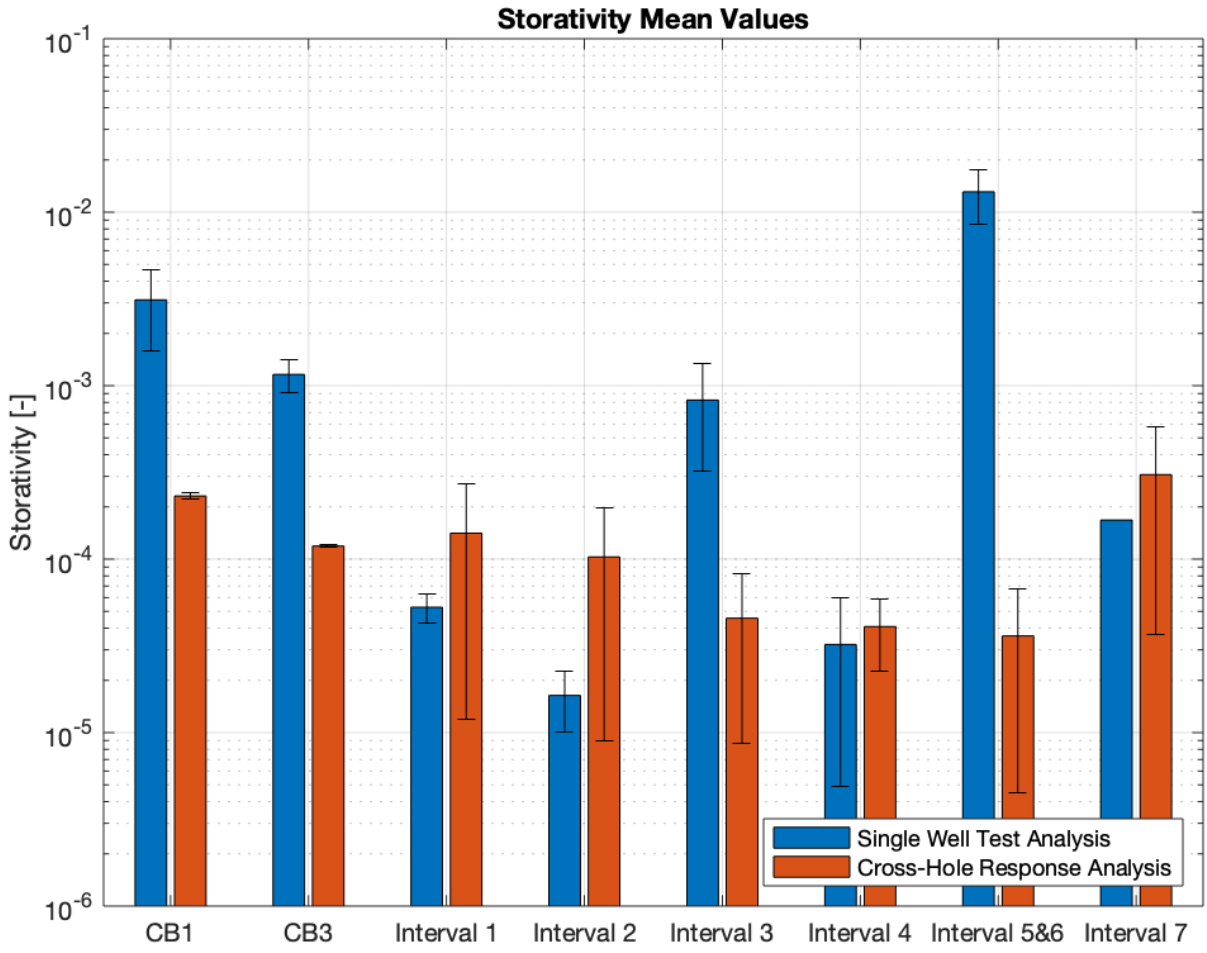

Fig. 4.16. Compilation of storativity mean values (with standard deviation) resulted from the single well and cross-hole response analysis. No standard deviation is reported for the values resulted from the analyses of the cross-hole responses in Intervals 2 and 3, and for the value resulted from the single well test analysis of Interval 7, as the standard deviations are greater than the corresponding mean values, which cannot be represented on a log scale plot.

4.4.3 Diffusivity

The characteristic times (Horner times) were plotted against the distances to the active well (Fig. 4.17). The distances between the borehole(s) and the intervals (Tab. 3.7) was determined by looking for the fractures which represents the shortest connection between them. To estimate diffusivity values between intervals, CB1 and CB3, normal diffusion for varying diffusivity values were plotted with in the same graph. The values read from the diffusion plot are plotted in Fig. 4.18 and can be found in Appendix W. From the diffusion plot it can be seen that all diffusivity values – except the one from the response in Interval 7 to the buildup in CB1 – are between 10^{-1} and 10^{-2} m^2/s. Furthermore, all intervals – except Interval 7 – show consistent values regardless of whether the response to the drawdown in CB1 or CB3 is plotted in the diffusion plot.

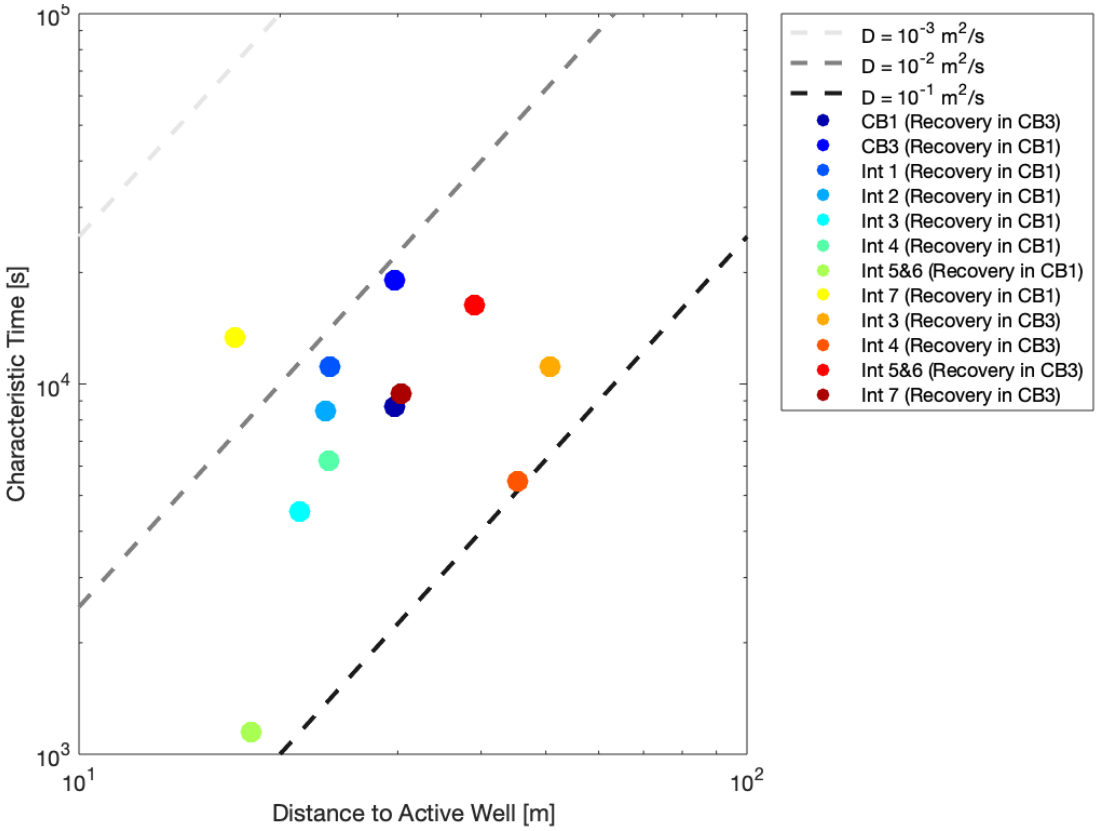

Fig. 4.17. Plotted are the response times vs. distances to the active well (colored dots) at log-log scale and the normal diffusion for varying diffusivity values (dashed lines).

In Fig. 4.18 all the diffusivity values resulted from the single well test analyses, the cross-hole response analyses and the readings from the diffusion plot (Fig. 4.17) are compiled at a log scale plot.

The diffusivity values resulted from the single well test analyses are generally lower than the resulted values from the cross-hole response analyses, except for the diffusivity values for Interval 7originating from the analysis with Theis. For CB1, CB3 and Interval 4 the difference of the diffusivity values resulted from the single well test analysis and the cross-hole test analysis is about one order of magnitude; for the Intervals 1, 2, 3, and 5&6 between three and four orders of magnitude.

The diffusivities obtained from the diffusion plot reading are in most cases consistent with the diffusivities resulted from the cross-hole response analyses.

For CB1, Interval 1, 2, 4 and 7 the diffusivity values resulted from the single well test analyses show differences whether the data was analyzed with Theis or the GRF model. For all of the above mentioned – except CB1 – the diffusivity value resulted from the analysis with Theis is higher in comparison to the diffusivity resulted from the analysis with the GRF model.

For the Intervals 1, 2, and 3 the diffusivity values from the analyses of the cross-hole response to the buildup in CB1 show large differences (> one order of magnitude) depending on whether the response was analyzed with the Theis or Agarwal model. For the mentioned intervals the diffusivities resulted from the analysis with Agarwal are higher than the ones from the analysis with Theis

The diffusivity values for the Intervals 4 and 7 resulted from the analysis of the cross-hole response to the buildup in CB3 are higher than the values resulted from the analysis of the cross-hole response to the buildup in CB1. The diffusivity values for the Interval 5&6 resulted from the analysis of the cross-hole response to the buildup in CB3 are lower than the values resulted from the analysis of the cross-hole response to the buildup in CB1.

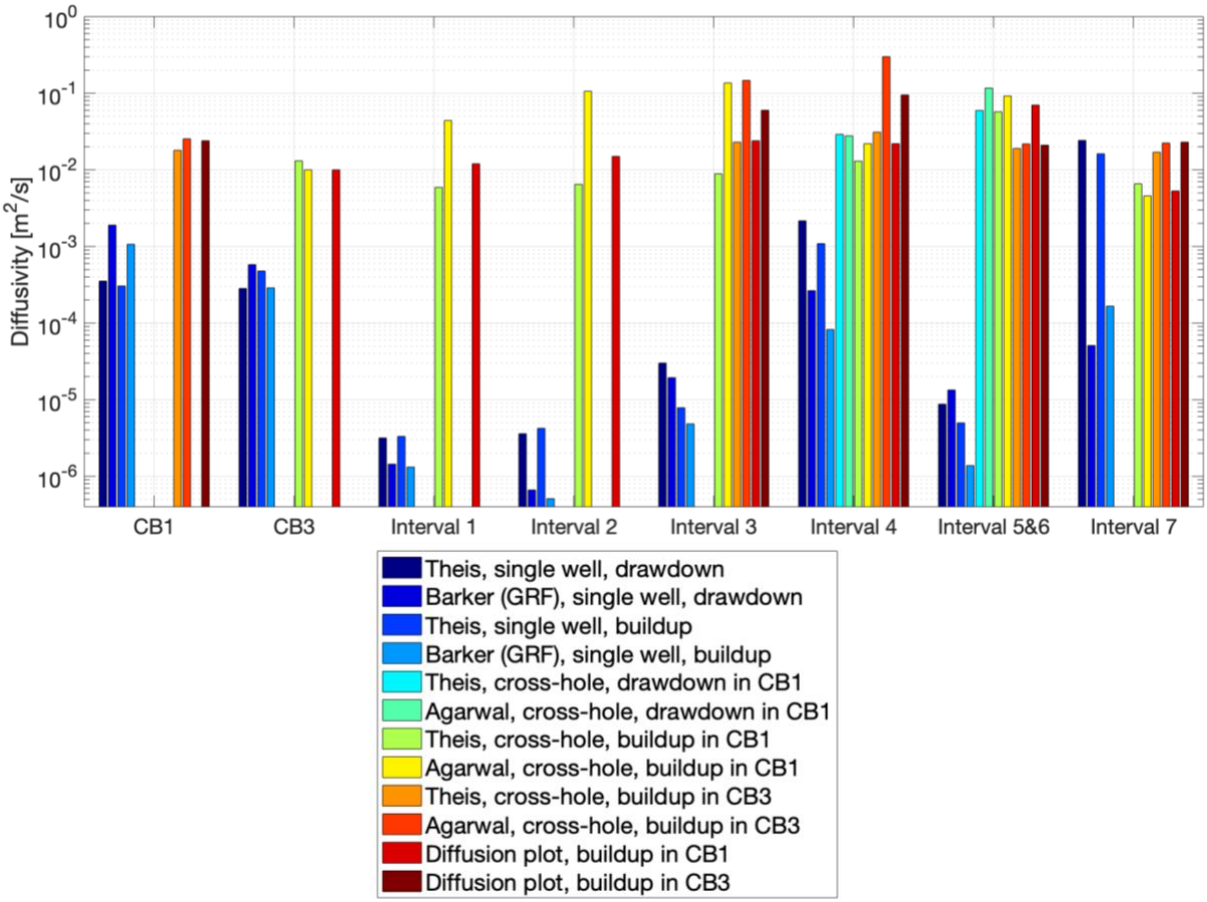

Fig. 4.18. Compilation of the diffusivity values resulted from single well test analyses and cross-hole response analyses as well as the values obtained from the diffusion plot.

5 INTERPRETATION AND DISCUSSION

5.1 Single Well Test Analysis

5.1.1 Qualitative Observations

The scattering of the pressure data in CB1 is because the pressure sensor was attached to a metal line. This made the measurement susceptible to vibrations.

The oscillating pressure in CB2 Interval 2 (Fig. 4.3) indicates that the transmissivity in this interval is low and is most probably a poroelastic effect.

The general increase in pressure across the entire system is attributed to the fact that prior to testing the boreholes stayed repeatedly open in order to conduct tests and logs on them. The opened state of the boreholes lowered the hydraulic head in the system. Despite the shut-in of the boreholes two weeks before the first test (Tab. 3.3), the pressure could not recover completely. Therefore, a general recovery trend was going on during the tests. It was found (Chapter 5.2.4), that the overall system recovery has no influence on the results of the cross-hole response analyses. Single well test analysis generally deals with larger pressure changes, therefore, it is can be stated that the observed overall system recovery does not influence them either.

5.1.2 Initial Pressure

The resulting initial pressures in the intervals in which more than one test was performed (Intervals 4 and 7) showed an increasing trend for the tests performed later (Tab. 4.2). This could be due to the fact that the whole system is not in a completely stabilized state. It should also be noted that infinite acting radial flow (IARF) is assumed for the straight line fitting, but this was practically never achieved during constant rate tests. Meier (2020) took measurements of the pressure in CB1 during its drilling. The highest measured pressure was 48.4 bar in CB1 on the 25.09.2020 (just before its completion). After the completion of the borehole they experienced several periods of open state, which prevent the pressure from stabilize completely. The pressure values from measurements during drilling are probably closer to the real static formation pressure than the initial pressures derived from the Horner plots.

The generally lower initial pressure in intervals closer to the tunnel is explained by the fact that the tunnel acts as a drainage of the aquifer. Interval 7 has the lowest initial pressure

(i.e. ~36.5 bar which is ~3 bar lower compared to the second lowest initial pressure, i.e. Interval 3 with 39.0. The reason for this could be that Interval 7 is the uppermost interval of the multipacker system and therefore an indirect connection to the upper, open part of CB2 is possible. Due to this connection the pressure in Interval 7 cannot recover as fast as the other intervals.

With initial pressures between 36 and 41 bar, the groundwater level is about 400 meter above the tunnel level.

5.1.3 Diagnostic Plots

The diagnostic plots of the buildup in CB3 show signs of a constant head boundary. The diagnostic plot of the drawdown in CB3 shows a rather clear IARF section, so it can be assumed that CB3 has indeed a constant head boundary and it is not a superposition effect from of the drawdown (Horne, 1990). For CB3 the constant head boundary is most likely the tunnel (i.e. several fault zones TM 1940 – 1990 (Jordan, 2019)). The derivative curve of both the drawdown and the buildup in Interval 4-3 also show signs of a constant head boundary (Intervals 4-1 and 4-2 had too irregular flow rates to show a clear derivative curve). As the boundary effect can be seen as well in the drawdown curve of Interval 4, it can be assumed that it has a real constant head boundary. For Interval 4, either the high transmissive structure intersecting Interval 5&6 or Interval 7 (see Chapter 2.2.2 and 5.2.4) are suspected to represent the observed constant head boundary. In Interval 7 signs for a closed boundary or double porosity are observed (steeply increasing derivative curve at late time). To be able to confirm one of the two possibilities a longer data set would be necessary. This would show whether the derivative curve flattens out again or whether it continues to rise with the same slope. A flattening would then imply double porosity. A further rise would imply closed boundary. From looking at the pressure responses (Chapter 5.2.2), it can be seen that Interval 7 is not well connected to other intervals. From this it was concluded that the structures intersecting Interval 7 are laterally limited. Therefore, closed boundary seems to be more justifiable than double porosity. The constant rate tests in CB1 and the Intervals 1, 2, 3 and 5&6 did not reach boundaries.

As already mentioned in Chapter 4.2.3, no diagnostic plot (except the one from CB3) shows extended periods of infinite acting flow (IAF). This means that neither the Theis model nor the GRF model are perfectly fitting models. Nevertheless, an estimation of the order of magnitude of transmissivity is possible (Dutler, personal communication, May, 2020).

5.1.4 Transmissivity

Transmissivity values in the range of 10^{-11} to 10^{-7} m^2/s were obtained from the constant rate test in the Intervals 1 to 7. Transmissivity values of $5 \cdot 10^{-7}$ and 10^{-6} m^2/s were obtained for CB1 and CB3, respectively. This is largely consistent with the transmissivity values determined with transient pressure pulse tests in the Grimsel Tests Site (GTS) by Brixel et al. (2020a). In the GTS – located in granitic rock of the Aar Massif – single fractures were tested, and transmissivity values of 10^{-12} to 10^{-6} m^2/s resulted. The fact that CB1 and CB3 show the highest transmissivity values is most likely due to the fact that the high transmissive structures intersecting the intervals in CB2 also intersect the other two boreholes. Therefore, CB1 and CB3 are showing a superposition of several transmissivities from different structures. Nevertheless, the results for CB1 and CB3 must be treated with caution, as a changing hydraulic head along the boreholes and a superposition of several conductive structures is present. Both does not correspond to the assumptions made for the Theis and GRF models. CB1 shows a slightly higher transmissivity, presumable due to the fact that CB1 is 110 m longer than CB3. As a result, CB1 is intersected by a conductive structure (at BM 277), which most probably is intersecting neither CB2 nor CB3. This conclusion is drawn for the following reason. Flow measurements during drilling in CB1 showed 11 l/min before BM 277 and 26 l/min after BM 227 (see Fig. 3.2). In CB2 and CB3 the highest measured flow rates were just below 10 l/min.

The transmissivity values resulting from the single well test analyses of the constant rate tests (Appendix L) are qualitatively consistent with the observations made during core logging and the definition of zones of interest. Appendix F shows the ATV sections and core photos of the BM in which the presumably most conductive structures are located. A description of the geology and the presumably most structures for each interval can be found in Chapter 3.1.3.

Interval 2 shows the lowest transmissivity values. This was expected because Interval 2 is the shortest and located in Intact Granite (Type 2). Further, this interval is not intersected by any fractures but only by one discontinuity characterized by a series of open pores, which may have been created by pressure solution or by hydrothermal flow. Interval 1 shows the second lowest transmissivity values. Interval 1 is also located in Intact Granite (Type 2) and is not intersected by fractures but only two discontinuities with the same properties as the one in Interval 2. Therefore, a low transmissivity is expected too. In addition to the porosity along the

described discontinuity, a disperse porosity was observed in the Intact Granite (Type 2). The observed transmissivity values in Interval 1 and 2 are approximately one order of magnitude higher than the transmissivity values determined by Brixel et al. (2020a) for intact crystalline rock. The porous discontinuities are most probably responsible for the slightly increased transmissivity. The disperse porosity plays only a minor role – if any at all– as the isolated pores do not represent a flow path.

The Intervals 3 and 4 show similar transmissivities. Both intervals are located in Foliated Granite (Type 2). Evaluating the travel time ATV log, a fracture zone and about ten single fractures were found in Interval 3 and some fractures in Interval 4. During core logging fractures with vuggy porosity and fractures with newly formed minerals were found in the depth of both intervals. In Interval 4 single fractures with vuggy porosity were found in a healed fracture zone. Interval 3 shows vuggy porosity along single fractures as well as in the mentioned fracture zone. To create vuggy porosity and precipitate new minerals, a considerable flow of water is required. It is therefore expected that these structures are determining the transmissivity value in both intervals.

Interval 5&6 shows a similar transmissivity as Interval 7. This is remarkable because in Interval 7 a 10 m-long fracture zone is located whereas in Interval 5&6 only about six single fractures are located along which vuggy porosity was observed. Therefore, Interval 5&6 was expected to show a similar transmissivity as Intervals 3 and 4. This means that rock with a fairly intact appearance (Foliated Granite (type 2), Interval 5&6) can show a transmissivity similar to the one of a rock that is totally intersected by fractures (Foliated Granite (type 1), Interval 7). This is in conflict with the statement from Brixel et al. (2020a), who found a clearly higher transmissivity for single fractures in fracture zones compared to single fractures in intact rock.

The differences between the results of the analysis with the GRF model and Theis correlate in all cases (except buildup in the Intervals 3 and 5&6) with the flow dimension. In the cases where the flow dimension is greater than two (supra-radial), the transmissivity value resulting from the analysis with the GRF model is smaller than the one resulting from the analysis with Theis. If the value is smaller than two (sub-radial), the transmissivity value resulting from the analysis with the GRF model is higher than the one resulting from the analysis with Theis. Applying the GRF model, the calculation of transmissivity is not directly dependent on the flow dimension. The transmissivity is directly depending on the slope of the straight line fitted to the

late time data. The flow dimension is determined by intercept of the fitted straight line with the horizontal axis for s (drawdown) = 0. This confirms that the GRF model works. Since the results from the application of the Theis and GRF models are usually consistent, no separate interpretation of the two datasets is made.

About the accuracy of the fit it can be said, that for the fit with the GRF model in almost all cases a mean residual closer to zero (Appendix L) was obtained compared with that of the Theis model. Thus, it could be assumed that the values resulting from the GRF analysis provide more reliable estimation, but this is probably not the case: The GRF model would only provide more reliable values if a long period of IAF was available for the analyses, as mentioned above, this was rarely the case. Without the long period of IAF the apparently better fit with GRF model may be along (e.g.) reservoir boundary affected data. From the boundary affected data the GRF model would then define an inaccurate flow dimension, which leads to inaccurate hydraulic parameters even though the fit was good.

5.1.5 Storativity

Storativity values resulting from single well test analyses of constant rate test are often inaccurate (Ludvigson & Hjerne, 2014), as these tests do not reach far into the aquifer. In this work, the single well test analysis resulted in storativities in the range of $10^{-5} – 10^{-2}$. In fractured crystalline rock specific storages around 10^{-7} m^{-1} are expected (Achtziger-Zupancic et al., 2017). To get from the storativity to the specific storage in confined aquifer, the storativity values needs to be divided by the aquifer thickness (more detail about this in Chapter 5.2.5). In this case the interval length can be taken as the aquifer thickness. With interval lengths of about 10 to 22 m – Interval 2 excluded – the resulting specific storages would be about one order of magnitude smaller than the storativities ($\sim 10^{-6} – 10^{-3}$ m^{-1}). These values are still significantly higher than the expected 10^{-7} m^{-1} (Achtziger-Zupancic et al., 2017). Hence, this work confirms that storativity (and specific storage) values the resulting from single well test are not reliable. Therefore, the storativity (and diffusivity) values resulted from the single well test analyses should not be used further.

5.1.6 Flow Dimension

The GRF model used to determine the flow dimensions is only an approximation and the resulted flow dimensions are not very reliable. As mentioned above, the periods of IAF were too short to achieve good fits with the GRF model. Brixel et al. (2020b) as well as Le Borgne

et al. (2004) also determined flow dimensions in crystalline rock. The median of the flow dimensions determined by Brixel et al. (2020b) is 1.3 (N=61). Le Borgne et al. (2004) determined flow dimension in the range of 1.4 – 1.7 . In this thesis flow dimensions in the range of 1.3 – 2.8 with a median of 2.4 (N=22) resulted. Thus, the BULG shows significantly higher flow dimensions compared to the GTS, which indicates a more interconnected reservoir.

Although the GRF model is only an approximation and the results show significant differences to previous studies, the flow dimension determined in this study correlates well with the observed geological structures. The geological correlation to the determined flow dimensions is explained in the following. The analysis of the tests in CB1 and CB3 show flow dimensions slightly below two. From this it can be interpreted that the system is an anisotropic system and several structures define the hydraulic parameters. This corresponds to the observations made during the definition of zones of interest and core logging, namely, several presumably conductive structures were observed.

The Intervals 1 and 2 show values slightly below 2.5. This would suggest that in these two intervals many conductive fractures can be observed and that the system is approximately isotropic. However, the ATV evaluation and core logging showed that only very few discontinuities intersect the two intervals, which implies a low flow dimension. This shows that the GRF did not work well for the single well test analyses of the Intervals 1 and 2. The only explanation for the relatively high flow dimension is that, contrary to expectations, Intact Granite (Type 2) allows a certain amount of water flow through the intact rock. Since the Intact Granite (Type 2) shows a disperse porosity this cannot be completely excluded. Nevertheless, a considerably amount of water flow in intact granite is still unlikely: A total amount of ~3.5 l of water was produced during the constant rate test in Interval 1 (duration of production ~35 hours with production rate of 0.1 l/h) and 0.6 l of water during the constant rate test in Interval 2 (duration of production ~12 hours with production rate of 0.05 l/h).

The high flow dimension (2.25) resulting from the analyses of the drawdown in Interval 3 is almost certainly due to the fact that IAF was never present during the test. The low flow dimension (~1,5) resulting from the analysis of the buildup in Interval 3 suggests that one conductive structure mainly determines the hydrological parameters. This correlates with the observations during core logging, since a fracture zone with vuggy porosity is observed in

Interval 3. As the flow dimension is greater than 1, it is concluded that the few single fractures with vuggy porosity, observed in Interval 3, also do have an impact on the hydraulic parameters.

Most of the analyses of the tests in Interval 4 resulted in a flow dimension of ~2.5. The analysis of the drawdown in Interval 4-2 resulted in a flow dimension of above 3.5 which obviously are not valid. The flow dimension of ~2.5 suggests that the three observed fractures with vuggy porosity all contribute to the flow. If one single fracture was dominating the flow, the flow dimension would be significantly lower. But this may be over-interpreted, as from the diagnostic plots for the tests in Interval 4 it was interpreted that a constant head boundary defines the shape of the pressure curve. Thus, the GRF model – which assumes IAF without boundary – provides inaccurate results even though a good fit is possible.

The flow dimension determined with the analysis of the drawdown in Interval 5&6 shows a very low flow dimension (1.3). This is almost certainly due to the fact that no IAF occurred during the drawdown in Interval 5&6. A flow dimension of 1.9 resulted from the analyses of the buildup in Interval 5&6. This indicates that each of the three observed fractures with vuggy porosity has an influence on the hydrological parameters.

For Interval 7 the flow dimension resulted in values above 2.5 which meets the expectations. As Interval 7 is characterized by a fracture zone which extends over almost the whole length of the interval. Thus, it is realistic that (almost) spherical flow can be achieved.

5.2 Constant Rate Test: Cross-Hole

5.2.1 Qualitative Observation

If an interval/borehole shows a response to the withdrawal in another interval/borehole, it is expected to happen also in the opposite direction. However, this was often not the case. Almost all intervals responded to the withdrawals in CB1 and CB3 but only the withdrawal in Interval 5&6 caused a response in CB1 and CB3. This is probably because the total inflow into the boreholes CB1 and CB3 obscured the pressure anomaly caused by the withdrawals in the intervals. Interestingly, the Intervals 5&6 and 7 do not respond to each other's pressure changes. The two adjacent intervals both show zones (in ATV and core log) along which considerable water flow is suspected. Apparently the two zones do not intersect. It is therefore expected that one zone is laterally limited.

Interval 2 responded to many tests with a minor response. Most of the responses in Interval 2 are likely to be of poroelastic nature as it is a short interval and shows a very low transmissivity. Interval 5&6 did not respond to the withdrawal in Interval 3 (although Interval 3 does respond to the withdrawal in Interval 5&6) presumably because the flow rate during the constant rate test in Interval 3 was too low to cause a response in the high transmissive Interval 5&6. Intervals 1 and 2 – the two bottom intervals in CB2 – do not respond to the withdrawal in CB3, presumably because CB2 is longer than CB3. Thus, the Intervals 1 and 2 are intersected by structures which do not intersect CB3, hence, there is no connection between CB3 and the Intervals 1 and 2.

By noticing the Noordbergum effect it was clear that poroelastic effects occur. Poroelastic effects can influence the test results. An analysis of this effect could be valuable. In this thesis, however, it was not further investigated.

5.2.2 Response Times

The pressure propagation is independent of the pumping rate, therefore, CB1 is expected to show the same response times to the withdrawal in CB3 as vice versa. However, CB1 responded ~12 min faster to the withdrawal in CB3 than CB3 responded to the withdrawal in CB1 (Tab. 4.4) This observation is consistent with the diffusivity values read from the diffusion plot (Fig 4.17). There, the reading of the diffusivity value for CB1 on the response in CB3 results in a higher diffusivity than vice versa (Chapter 4.4.3). A final explanation for this phenomenon was not found, but the following factors might have an influence: 1) The different wellbore storages of CB1 and CB3 and 2) gravitational forces which might have an influence on the pressure propagation velocity along the inclined structure which creates the connection between CB1 and CB3.

The reason for Interval 1 and 2 not responding to the withdrawal in CB3 is explained in Chapter 5.2.1. Interval 2 shows a more pronounced response to the drawdown in CB1 than Interval 1(FIG. 4.10). This is interesting as both intervals are located in Intact Granite (Type 2), and Interval 2 is much shorter than Interval 1. This could mean, that both intervals are equally well connected to CB1, but the response has a stronger influence on the shorter Interval 2, because the storage effects in it are smaller.

Intervals 3, 4 and 5&6 show a faster response to withdrawal in CB1 than to the one in CB3. It should be noted that the distances between the intervals and CB1 are generally smaller than

the distances between the intervals and CB3 (Tab. 3.7). It is noticeable that Interval 3 shows a much stronger response to CB1 than to CB3 (FIG 4.10, FIG. 4.11) This implies a better connection between Interval 3 and CB3 than between Interval 3 and CB1.

A response time to the withdrawal in CB1 of 19'000 s (~5 h 16 min) was found for Interval 7. As it can be seen in Fig. 10 the response in Interval 7 to the withdrawal in CB1 is very weak and never exceeds the overall system recovery trend (the pressure keeps rising at any time). Therefore, it is possible that the determination of the response time in Interval 7 to the withdrawal in CB1 is quite inaccurate. Hence, not too much should be interpreted into this value. In contrast to the late and weak response to the withdrawal in CB1, Interval 7 responded strongly and quickly to the constant rate test in CB3. This indicates that the structure connecting Interval 7 and CB3 is either relatively short (several meters) or shows strong lateral heterogeneity regarding its transmissivity.

Summarizing it can be said that the tested reservoir shows a strong heterogeneity: Interval 5&6 responds fastest and most pronounced to the withdrawal in CB1; Interval 7 responds fastest and Interval 4 most pronounced to the withdrawal in CB3.

Considering the response times to the withdrawal in CB3, it would be possible that the responses do not reach the Intervals 3, 4 and 5&6 directly, but indirectly via CB1. Interval 7 would be the only one to respond to the withdrawal in CB3 directly. However, this possibility was not investigated further.

5.2.3 Diagnostic Plots

It is very important to note that most diagnostic plots show only wellbore storage (Appendix S). The responses in Interval 4 and 5&6 are the only ones that show a clear deviation from the unit slope (wellbore storage effect). However, even there the 1.5 log cycle rule by Horne (1990) is never fulfilled, which means that the hydraulic parameters resulted from the cross-hole response analyses might be affected by wellbore storage effect. Significantly longer production phases during the constant rate tests in CB1 and CB3 would have been necessary to obtain clear aquifer responses (i.e. IAF).

5.2.4 Transmissivity

All transmissivity values resulting from the cross-hole response analyses are in the same order of magnitude. The very similar transmissivity values for CB1, CB3 and all the intervals

indicate, that in the far field they are all connected to the same conductive structure. A transmissivity of about 10^{-6} m^2/s can be estimated for the overall reservoir. It is very important to note that for the cross-hole tests analyses mostly wellbore storage affected pressure data was available. Therefore, the reliability of the results from the cross-hole response analyses is not guaranteed.

The analysis of the responses Interval 4 and 5&6 to the drawdowns in CB1 also resulted in transmissivity values in the same order of magnitude as the analysis of the responses to the buildups in CB1 and CB3. This indicates that the results are representative despite the wellbore storage dominated response signals. The curve fitting with Theis and Agarwal showed very similar mean residuals (APPENDIX V). From this it can be deduced that both models with which the pressure responses were analyzed provide equally reliable results. The main difference between the Theis and the Agarwal model is that the Agarwal model takes into account a possible skin effect. The fact that the curve fitting with two models have very similar mean residuals confirms the assumption that no (significant) skin effect occurs in the tested boreholes.

In order to check whether the overall system recovery had an effect on the results of the cross-hole response analyses, a further evaluation was carried out: A linear fit was applied to the data of the not responding Interval 7 during the constant rate test in CB1. This linear trend was then subtracted from the pressure data in the intervals before the repetitive analysis. The resulting transmissivity values were still in the range of 10^{-6} to 10^{-5} m^2/s. This means that the overall system recovery has no significant effect on the results of the cross-hole responses.

5.2.5 Storativity

The results of the cross-hole response analyses need to be treated with caution as mostly wellbore storage affected pressure data was analyzed. Intervals 4 and 5&6 provide the most reliable storativity values, as they are based on analyses of data that deviate significantly from the unit slope (wellbore storage) in the diagnostic plots. The storativity value for Interval 7 resulting from the analysis of the (late and weak) cross-hole response to the recovery in CB1 shows a higher value than the one resulting from the analysis of the response to the buildup in CB3. The explanation for this might be that Interval 7 only shows weak responses to pressure changes in CB1. Therefore, not a real response was analyzed. Hence, the storativity (and

diffusivity) value resulted from the analysis of the response in Interval 7 to the withdrawal in CB1 is not to be considered further.

Comparing the resulting storativities (Chapter 4.2.5) with other studies is quite challenging. The reasons for this are explained below. Often (e.g. Achtziger-Zupancic et al. (2017), Brixel et al. (2020a)) the storativities values are discussed in less detail than the transmissivities values. Rutqvist (1996) dedicates a paper to the determination of storativities, but only single fractures were tested, which was not the case in this study. In addition, other studies do not always indicate Storativity (S) but Specific Storage (S_s). The storativity of a confined aquifer is defined as the volume of water released from storage per unit surface area of the aquifer per unit decline in hydraulic head (Ferris et al., 1962). Specific storage is the volume of water that a unit volume of aquifer releases from storage under a unit decline in hydraulic head (Ferris et al., 1962). With a given aquifer thickness (b), the storativity (S) can be converted into the specific storage (S_s) with Eq. 5.1.

$$S_s = \frac{S}{b} \qquad \text{Eq. 5.1}$$

The determination of the aquifer thickness in fractured rock is not trivial. Either the length of the interval/borehole or the thickness of the conductive structures can be taken for the aquifer thickness. If the length of the interval/borehole is taken, the resulting specific storage is smaller than the storativity. On the contrary, if the thickness of the conductive structures is taken for the calculation – in this case the opening of the fractures – the result is a considerably larger specific storage than the original storativity. In this case the corresponding interval/borehole lengths were used for the calculation, as the conductive structures are expected to be interconnected with other structures. The specific storage values for the intervals ($5 \cdot 10^{-7}$ – $7 \cdot 10^{-5}$ m^{-1}) are about one order of magnitude smaller than the original storativity values ($8 \cdot 10^{-6}$ – $6 \cdot 10^{-4}$). Except for Interval 2 for which the difference is smaller as the interval has only a length of 2 m. For the boreholes specific storages result ($6 \cdot 10^{-7}$ – $8 \cdot 10^{-7}$ m^{-1}) are about two orders of magnitude smaller than the original storativities (10^{-4} – $2 \cdot 10^{-4}$).

Achtziger-Zupancic et al. (2017) have found a correlation between the depth below surface (mbgl) and specific storage. The correlation is based on many values in depths between 0 and 1000 mbgl and only two values in greater depth (~1.6 km). Remarkably, the two values at the depth of ~1.6 km are showing higher values (~10^{-5} m^{-1}) than the found correlation predicts (less than 10^{-6} m^{-1}). Applying the correlation to the BULG a specific storage of $6 \cdot 10^{-7}$ m^{-1} is

expected. The specific storage values calculated from the storativities by dividing them by the corresponding interval/borehole lengths are significantly higher ($2 \cdot 10^{-6}$ to $7 \cdot 10^{-4}$ m^{-1}). Remarkably, these values fit quite well to the two storativity values in the data set from Achtziger-Zupancic et al. (2017) at the depth of ~1.6 km. This leads to the assumption that the correlation found by Achtziger-Zupancic et al. (2017) is not applicable for greater depths. But to confirm this, a much more detailed analysis with larger data sets is necessary.

Despite the above mentioned uncertainties, in the following an attempt is made to place the resulted storativities in a geological context: The fact that most of the storativity values resulting from the analyses of cross-hole responses are similar to each other, supports the hypothesis (Chapter 5.2.4) that all intervals are connected to the same high transmissive structure (which intersects Interval 5&6).

5.2.6 Skin Effect

The drilling of CB1, CB2 and CB3 was done using water as a drilling liquid – a drilling liquid with mud would cause a positive skin effect. Furthermore, no stimulation was performed in the BM where the intervals in CB2 are located – stimulation would cause a negative skin effect. Hence, no strong skin effects are expected, neither positive nor negative. According to Horne (1990) the skin effect is in general not expected to be below -5 or above 20. This means that the positive skin effect values (in Interval 1, 2, 3, 4) are unrealistically high. Also, the skin effects which show negative values are rather unrealistic as some of them show values below -5. It could be that during or after the drilling process fracture fillings have been flushed from the fracture into the borehole, which would result in a negative skin effect. Nevertheless, the evaluation of the borehole log and core logs did not show any signs of fractures with major infilling, which could have been washed out. This leads to the conclusion that the assumptions for the applied model by Agarwal (e.g. isotropic medium) to determine the skin effect are not valid for the tested reservoir or the data is too strongly affected by wellbore storage effects.

5.3 Comparison Single Well Test and Cross-Hole Response Analysis

5.3.1 Transmissivity

The transmissivity values resulting from single well test analyses are distributed over five orders of magnitude while those resulting from cross-hole response analyses are all in the same order of magnitude. It can be observed that the resulting transmissivities from cross-hole response analyses are in the same order of magnitude as the highest transmissivity values from single well test analysis (CB1). Cross-hole data generally reach further into the formation than single well test data. The most probable interpretation of the cross-hole analysis results is explained in the following. All intervals are directly connected by fractures to one dominating high transmissive structure, otherwise known as the hydraulic backbone of the tested reservoir. Most likely, the backbone is intersecting Interval 5&6. This assumption is mainly based on three observations. First, Interval 5&6 shows a relatively high transmissivity resulting from the single well test analysis. Second, it seems that the high transmissive structure intersecting Interval 5&6 has a wide lateral extension, as Interval 5&6 showed responses to the constant rate tests in both CB1 and CB3. Third, the fastest pressure response was observed in Interval 5&6 (see response in Interval 5&6 to the withdrawal in CB1). The single well test analysis of the constant rate test in Interval 7 also resulted in a high transmissivity value, further, it showed a fast response to the withdrawal in CB3. Nevertheless, the structure intersecting Interval 7 is excluded to be the backbone as Interval 7 showed no or only a weak response to the withdrawal in CB1.

5.3.2 Storativity

As mentioned in the Chapters 5.1.5 the storativity values resulted from the single well test analyses are not very reliable. A clear interpretation of the relationship between the storativity values resulted from the single well test and the cross-hole response analyses would be very speculative, therefore it is not given here.

5.3.3 Diffusivity

The diffusivity values given for the single well tests are not to be considered further, as they are directly depending on the storativity values which are not reliable (see Chapter 5.1.5).

In addition, the diffusivity value resulted from the analysis of the response in Interval 7 to the withdrawal in CB1 is not to be considered either (Chapter 5.2.5).

The most remarkable thing about the diffusivity values is that the values obtained from calculations with the results of the cross-hole response analyses and the one obtained from diffusion plot reading match well. From this one can tell, that normal diffusion takes place.

The diffusivity values obtained are consistent with the those determined by Brixel et al. (2020b) in the GTS. Brixel et al. (2020b) distinguished between fault zone, wall damage zone and linking damage zone. The diffusivity values obtained in the present study correspond to some of the values resulting for the fault zones and damage wall zones in the GTS. Tests on linking damage zones in the GTS resulted in greater diffusivity values than those obtained in this study.

This observation is important because the cross-hole response analyses were mostly performed on wellbore storage affected pressure data, and therefore the reliability of the data was questioned.

6 CONCLUSION

The tested reservoir volume at the Bedretto Underground Lab for Geoenergies shows transmissivity values that range over five orders of magnitude, strong scale effects as well as the evidence of the presence of a hydraulic backbone in the system.

The transmissivity values obtained in this thesis are largely consistent with the results from the Grimsel Test Site (Brixel et al., 2020). At small scale (pulse test, mm – dm) the reservoir shows transmissivities which range over four orders of magnitude, depending on the tested section (interval). For example, from the analysis of the pulse test in Interval 2 a transmissivity of ~$9 \cdot 10^{-11}$ m^2/s, in Interval 3 one of ~$3 \cdot 10^{-10}$ m^2/s and in Interval 7 one of ~$1 \cdot 10^{-8}$ m^2/s resulted. At medium scale (single well test, several meters) the reservoir shows transmissivities in five orders of magnitude, depending on the tested interval. For example, from the single well test analyses of the constant rate test in Interval 2 a transmissivity mean value of ~$3 \cdot 10^{-11}$ m^2/s, in Interval 3 one of ~$7 \cdot 10^{-9}$ m^2/s and in Interval 7 one of ~$1 \cdot 10^{-7}$ m^2/s resulted. The large scale (cross-hole response, tens of meters) transmissivity of the structures connecting the intervals with the boreholes CB1 and CB3 is about 10^{-6} m^2/s for all of them. The large scale transmissivity resulted from the cross-hole response analyses, corresponds approximately to the value resulting from the single well test analysis of the constant rate test in CB1. Furthermore, the cross-hole response analyses showed a similar and relatively high (e.g. Achtziger-Zupancic et al., 2017; Brixel et al., 2020; Rutqvist, 1996) storativity value for all intervals (~10^{-4}). It is concluded that at large scale all intervals are connected to a hydraulic backbone. However, no prove was found that the connection is a natural structure (e.g. open fracture), hence, it is possible that CB1 or CB3 is the connection between the hydraulic backbone and the conductive structures that intersect the intervals. Interval 5&6 is the only interval that shows high transmissivity at medium scale (single well test, several meters) and a fast and pronounced response to either CB1 or CB3 as well as a pronounced response to the other. Therefore, it is assumed that the backbone intersects Interval 5&6. From this it can be concluded that at medium scale the detected backbone has a transmissivity of about 10^{-7} m^2/s (deduced from the transmissivity values resulted from the single well test analysis for Interval 5&6). Furthermore, from the fact that the Intervals 3 and 4 showed pressure responses to the constant rate test in Interval 5&6, the backbone is not an isolated preferential flow channel through the reservoir, but a preferential flow path which is connected to other structures. The backbone is most

probably characterized by the most conductive structure in Interval 5&6, which is located at BM 159 (ATV log as reference) of CB2. Thus, the main structure of the backbone has dip angle and dip direction of 58/329 and is characterized by an 8 cm long hydrothermally altered, fractured section with vuggy porosity (opening <1 cm) and newly formed minerals along their fracture surfaces (Fig. 2.7, F).

The exact intersection depth of CB1 and CB3 with the hydraulic backbone cannot be conclusively determined as no multi packer systems were installed in CB1 and CB3. However, GPR, flow measurements during drilling and observation during the core logging process suggest that the hydraulic backbone intersects CB1 at BM 181 and CB3 at BM 151 (both depths with reference to ATV log).

The assumption that the hydraulic backbone is connected to other structure over large distances, is based on the fact, that the Intervals 3 and 4 responded to the constant rate test in Interval 5&6, which is suspected to be intersected by the hydraulic backbone. The backbone's main structure is located in a healed fracture zone and is accompanied by a few single fractures with vuggy porosity which are located at about 1 m distance to the main structures. From the orientation (tunnel perpendicular) of the presumably most conductive structures in the intervals can be concluded that brittle-ductile shear zones (of Alpine age) are partially hydrothermally altered (and possibly reactivated) which increases the transmissivity significantly. The Alpine structures which underwent the strongest weathering are forming the hydraulic backbone in the reservoir around the BULG.

From the fact that at large scale all intervals showed the same high transmissivity (10^{-7} m^2/s) it was deduced that all the intervals are connected to the hydraulic backbone. From observations during core logging and the evaluation of the ATV log from CB2 a presumably most conductive structure for each interval and its orientation was determined. The presumably most conductive structure in all intervals is represented by the fractures with a similar orientation as the backbone itself. There are three possible scenarios how the backbone parallel conductive structures intersecting the intervals are connected to the hydraulic backbone: 1) The presumably most conductive structures and the hydraulic backbone are directly connected because of a slight differences in the structure's orientations, 2) a conductive structure set with a different orientation represents the connecting structure and 3) CB1 or CB3 represents the connection. In case a natural structure connects the presumably most conductive structures

intersecting the intervals in CB2 with the hydraulic backbone, the N–S striking fracture set is most likely the one which connects them. This is based on the observation from Jordan (2019) that the N-S striking fracture set must be conductive as it causes dripping zones in the tunnel.

7 ACKNOWLEDGEMENT

I would like to thank Prof. Dr. Simon Löw for giving me the opportunity get an insight into this very interesting major project. I am very grateful for the valuable inputs during the core logging process, the support during the development of the test design and the proficient supervision.

I would also like to thank my co-supervisor Dr. Nima Gholizadeh Doonechaly for his essential support during the test design, execution, evaluation and interpretation of the results. I would like to express my appreciation for his mentoring and encouragement. His availability to answer all questions was very valuable during the collaboration.

In collaboration with my fellow student and friend Matthias Meier we developed the core log. I'm thankful for the constructive teamwork during the work and for shortening the many hours of driving between Zürich and Bedretto.

In particular I would like to thank Nathan Dutler for the incredibly competent and warmhearted support. His experience in handling test data contributed a lot to this thesis. A huge thanks goes also to Dr. Bernard Brixel who was a great help in interpreting the results and bringing it into a larger context.

Furthermore, I would like to thank Dr. Peter Guntli (Sieber Cassina + Handke AG) for his support during the core logging, his vast experience was a great enrichment. I am very happy about the immense helpfulness of Francisco Serbeto (Geo-Energie Suisse AG) and Marian Hetrich (SCCER-SoE).

Furthermore, I would like to thank Dr. Alexis Shakas and Dr. Hannes Krietsch for providing and explaining the data they collected in the BULG.

Last but not least, I am grateful to my friends making the many hours of studying at the ETH not feeling as work at all and my family, especially my father, for the inspiration and support during this time.

8 REFERENCES

Agarwal R. G., Al-Hussainy R. & Ramey Jr H. J. (1970). An investigation of wellbore storage and skin effect in unsteady liquid flow: I. analytical treatment. *Society of Petroleum Engineers Journal, 249*, 279-290.

Barker J. A. (1988). A generalized radial flow model for hydraulic tests in fractured rock. *Water Resources Research, 24*(10), 1796-1804.

Bredehoeft J. D. & Papadopulos S. (1980). A method to determine the hydraulic properties of tight formations. *Water Resources Research, 16*, 233-238.

Brixel B., Klepikova M., Jalali R., Lei Q., Roques C., Krietsch H. & Loew S. (2020). *Tracking Fluid Flow in Shallow Crustal Fault Zones: 1. New in situ Permeability Measurements*. ETH Zurich.

Castilla R. & Krietsch H. (2019). Integrated structural logging of CB wells in the Bedretto Lab (unpublished figure: Wells-CB-1_200_200131.pdf). Geo-Energie Suisse AG and ETH Zurich.

Cooper H. H., Bredehoeft J. D. & Papadopulos S. (1967). Response of a finite-diameter well to an instantaneous charge of water. *Water Resources Research, 3*(1), 263-269.

Cooper H. H. & Jacob C. E. . (1946). A generalized graphical method for evaluating formation constants and summarizing well field history. *Transactions Amemrican Geophysical Union, 27*, 526-534.

Deere D.U. & Deere D.W. . (1988). *The Rock Quality Designation (RQD) Index in Practice*. Philadelphia: American Society for Testing Materials. 91–101

Hafner S. (1958). *Petrographie des südwestlichen Gotthardmassivs zwischen St. Gotthardpass und Nufenenpass.* ETH Zurich,

Hoek E. & Brown E. T. (1997). Practical estimates of rock mass strength. . *International Journal of Rock Mechanics and Mining Sciences, 34*(8), 1165-1186.

Horne R. N. (1990). *Modern Well Test Analysis – A Compute-Aided Approach*. Standford University.

Horner D. R. (1951). *Pressure Build-up in Wells*. Paper presented at the 3rd World Petroleum Congress, The Hague, the Netherlands.

Jacob C. E. . (1950). *Engineering Hydraulics: Flow of ground water*. New York: John Wiley and Sons. 321-386

Jordan D. (2019). *Geological Characterization of the Bedretto Underground Laboratory for Geoenergies.* (Master Thesis), ETH Zurich,

Keller AG. (2020). Pressure Transmitters, Serie 33X. Retrieved from https://keller-druck.com/en/products/pressure-transmitters/standard-pressure-transmitters/series-33x. Last Access: 27.09.

Keller F. & Schneider T. R. (1982). Geologie und Geotechnik. *Schweizer Ingenieur und Architekt, 100 (Heft 24)*.

Krietsch H. (2019). *Borehole Logging Data from Characterization Boreholes in Bedretto Underground Lab for Geoenergies*. Retrieved from: http://hdl.handle.net/20.500.11850/443521

Laws S. (2001). *Structural, Geomechanical and Petrophysical Properties of Shear Zones in the Eastern Aar Massif, Switzerland.* (Doctoral Thesis), ETH Zurich,

Lim S. S. & Martin C. D. (2010). Core disking and its relationship with stress magnitude for Lac du Bonnet granite. *International Journal of Rock Mechanics and Mining Sciences, 47*(2), 254–264.

Lützenkirchen V. H. (2002). *Structural geology and hydrogeology of brittle fault zones in the central and eastern Gotthard massif, Switzerland.* ETH Zurich,

Lützenkirchen V. H. & Loew S. (2011). Late Alpine brittle faulting in the Rotondo granite (Switzerland): Deformation mechanisms and fault evolution. *Swiss Journal of Geosciences, 104*.

Marquer D. (1990). Structures et déformation alpine dans les granites hercyniens du massif du Gothard (Alpes centrales suisses). *Eclogae Geologicae Helvetiae, 83*(1), 77-97.

Meier M. (2020). *Heat Dilution Testing in Deep Underground Excavations.* (Master Thesis), ETH Zurich,

Münger A. & Meier M. . (2020). *Geological Corelog of CB1, CB2 and CB3 in the BULG.* (unpulished).

Neuzil C. E. (1982). On conducting the modified 'Slug' test in tight formations. *Water Resources Research, 18*(2), 439-441.

Obert L. & Stephenson D. E. (1965). *Rock Mechanics - Stress Conditions under which Core Discing Occurs*.

Agarwal R. G., Al-Hussainy R. & Ramey Jr H. J. (1970). An investigation of wellbore storage and skin effect in unsteady liquid flow: I. analytical treatment. *Society of Petroleum Engineers Journal, 249*, 279-290.

Barker J. A. (1988). A generalized radial flow model for hydraulic tests in fractured rock. *Water Resources Research, 24*(10), 1796-1804.

Bredehoeft J. D. & Papadopulos S. (1980). A method to determine the hydraulic properties of tight formations. *Water Resources Research, 16*, 233-238.

Brixel B., Klepikova M., Lei Q., Roques C., Jalali R., Krietsch H. & Loew S. (2020). *Tracking Fluid Flow in Shallow Crustal Fault Zones: 2. Insights on Fluid Pressure Diffusion in Damage Zones*. ETH Zurich.

Castilla R. & Krietsch H. (2019). Integrated structural logging of CB wells in the Bedretto Lab (unpublished figure: Wells-CB-1_200_200131.pdf). Geo-Energie Suisse AG and ETH Zurich.

Cooper H. H., Bredehoeft J. D. & Papadopulos S. (1967). Response of a finite-diameter well to an instantaneous charge of water. *Water Resources Research, 3*(1), 263-269.

Cooper H. H. & Jacob C. E. . (1946). A generalized graphical method for evaluating formation constants and summarizing well field history. *Transactions Amemrican Geophysical Union, 27*, 526-534.

Horne R. N. (1990). *Modern Well Test Analysis – A Compute-Aided Approach*. Standford University.

Horner D. R. (1951). *Pressure Build-up in Wells*. Paper presented at the 3rd World Petroleum Congress, The Hague, the Netherlands.

Jacob C. E. . (1950). *Engineering Hydraulics: Flow of ground water*. New York: John Wiley and Sons. 321-386

Jordan D. (2019). *Geological Characterization of the Bedretto Underground Laboratory for Geoenergies.* (Master Thesis), ETH Zurich,

Keller AG. (2020). Pressure Transmitters, Serie 33X. Retrieved from https://keller-druck.com/en/products/pressure-transmitters/standard-pressure-transmitters/series-33x. Last Access: 27.09.

Krietsch H. (2019). *Borehole Logging Data from Characterization Boreholes in Bedretto Underground Lab for Geoenergies*. Retrieved from: http://hdl.handle.net/20.500.11850/443521

Meier M. (2020). *Heat Dilution Testing in Deep Underground Excavations.* (Master Thesis), ETH Zurich,

Münger A. & Meier M. . (2020). *Geological Corelog of CB1, CB2 and CB3 in the BULG.* (unpulished).

Neuzil C. E. (1982). On conducting the modified 'Slug' test in tight formations. *Water Resources Research, 18*(2), 439-441.

Papadopulos Stavros S., Bredehoeft John D. & Cooper Hilton H. (1973). On the analysis of 'slug test' data. *Water Resources Research, 9*(4), 1087-1089.

Ramey Jr H. J. (1970). Short-time well test data interpretation in the presence of skin effect and wellbore storage. *Journal of Petroleum Technology, 249*, 97 - 104.

Renard Ph. (2017). Hytool: an open source matlab toolbox for the interpretation of hydraulic tests using analytical solutions. *The Journal of Open Source Software, 2(19)*, 441.

Renard Ph., Glenz D. & Mejias M. (2009). Understanding diagnostic plots for well-test interpretation. *Hydrogeology Journal, 17*(17), 589-600.

Rutqvist J. (1996). Hydraulic pulse testing of single fractures in porous and deformable hard rocks. *Quarterly Journal of Engineering Geology and Hydrogeology, 29*(2), 181-192.

Sergeev S. A., Meier M. & Steiger R. H. (1995). Improving the resolution of single-grain U/Pb dating by use of zircon extracted from feldspar: application to the Variscan magmatic cycle in the central Alps. *Earth and Planetary Science Letters, 134*(1-2), 37-51.

SFOE Swiss Federal Office of Energy (2018). Energy Strategy 2050 once the new energy act is in force.

Shakas Alexis. (2020). *Post-proces*sed GPR data for CB boreholes. https://doi.org/10.3929/ethz-b-000441162

SSCER-SoE Swiss Competence Center for Energy Research – Supply of Electricity. (2020). sccer-soe.ch. Last Access: 30. January 2020.

Steiger R. H. (1962). *Petrographie und Geologie des südlichen Gotthardmassivs zwischen St. Gotthard-und Lukmanierpass.* ETH Zurich.

Theis C. V. (1935). The relation between the lowering of the Piezometric surface and the rate and duration of discharge of a well using ground-water storage. *Transactions, American Geophysical Union, 16*(2), 519.

Wenning Q. C., Madonna C., Haller A. D. & Burg J.-P. (2018). Permeability and seismic velocity anisotropy across a ductile-brittlefault zone in crystalline rock. . *Solid Earth Discuss.*

9 DECLARATION OF ORIGINALITY

Eidgenössische Technische Hochschule Zürich
Swiss Federal Institute of Technology Zurich

Declaration of originality

The signed declaration of originality is a component of every semester paper, Bachelor's thesis, Master's thesis and any other degree paper undertaken during the course of studies, including the respective electronic versions.

Lecturers may also require a declaration of originality for other written papers compiled for their courses.

I hereby confirm that I am the sole author of the written work here enclosed and that I have compiled it in my own words. Parts excepted are corrections of form and content by the supervisor.

Title of work (in block letters):

Hydraulic Backbone of CB1 to CB3 Boreholes in the Bedretto Underground Lab

Authored by (in block letters):

For papers written by groups the names of all authors are required.

Name(s):	**First name(s):**
Münger	Andri

With my signature I confirm that

- I have committed none of the forms of plagiarism described in the 'Citation etiquette' information sheet.
- I have documented all methods, data and processes truthfully.
- I have not manipulated any data.
- I have mentioned all persons who were significant facilitators of the work.

I am aware that the work may be screened electronically for plagiarism.

Place, date	**Signature(s)**
Zurich, 03.10.2020	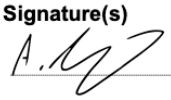

For papers written by groups the names of all authors are required. Their signatures collectively guarantee the entire content of the written paper.

10 APPENDIX

Appendix A: Geological Core Log of CB1, CB2 and CB3 in the BULG I

Appendix B: Discontinuity terminology from Jordan (2019), after Laws (2001) and Lützenkirchen (2002). IV

Appendix C: Examples for types of borehole wall defects V

Appendix D: Graphs indicating borehole wall defects in boreholes CB1, CB2, CB3 VI

Appendix E: Possible packer installation sections in CB1, CB2 and CB3 VII

Appendix F: ATV log and core photos with Intervals' most conductive structures VIII

Appendix G: Stereoplot indicating structures in ATV for CB1, CB2 and CB3 XIV

Appendix H: Protocol of events in CB1, CB3, and Interval in CB2 XV

Appendix I: Flow Board XVIII

Appendix J: Pulse Test, Curve Fitting, Results XIX

Appendix K: Constant rate test pressure curves, drawdown (with flow rate) and buildup XX

Appendix L: Results of single well test analyses of the constant rate tests XXIV

Appendix M: Horner plots, with manual linear fit on late time data XXVI

Appendix N: Diagnostic plots, single well test, drawdown XXX

Appendix O: Diagnostic plots, single well test, buildup XXXII

Appendix P: Pressure Responses to constant rate tests XXXIV

Appendix Q: Diagnostic plots, cross-hole responses to drawdown in CB1 XXXVI

Appendix R: Diagnostic plots, cross-hole responses to drawdown in CB1 XXXVIII

Appendix S: Diagnostic plots, cross-hole responses to buildup in CB1 XL

Appendix T: Diagnostic plots, cross-hole responses to drawdown in CB3 XLII

Appendix U: Diagnostic plots, cross-hole responses to buildup in CB3 XLIII

Appendix V: Transmissivity and storativity values from cross-hole responses analyses XLIV

Appendix W: Diffusivity values from single well test and cross-hole response analyses XLVI

Appendix A: Geological Core Log of CB1, CB2 and CB3 in the BULG

Geological Core Log 1:1000 of CB1 (BULG)

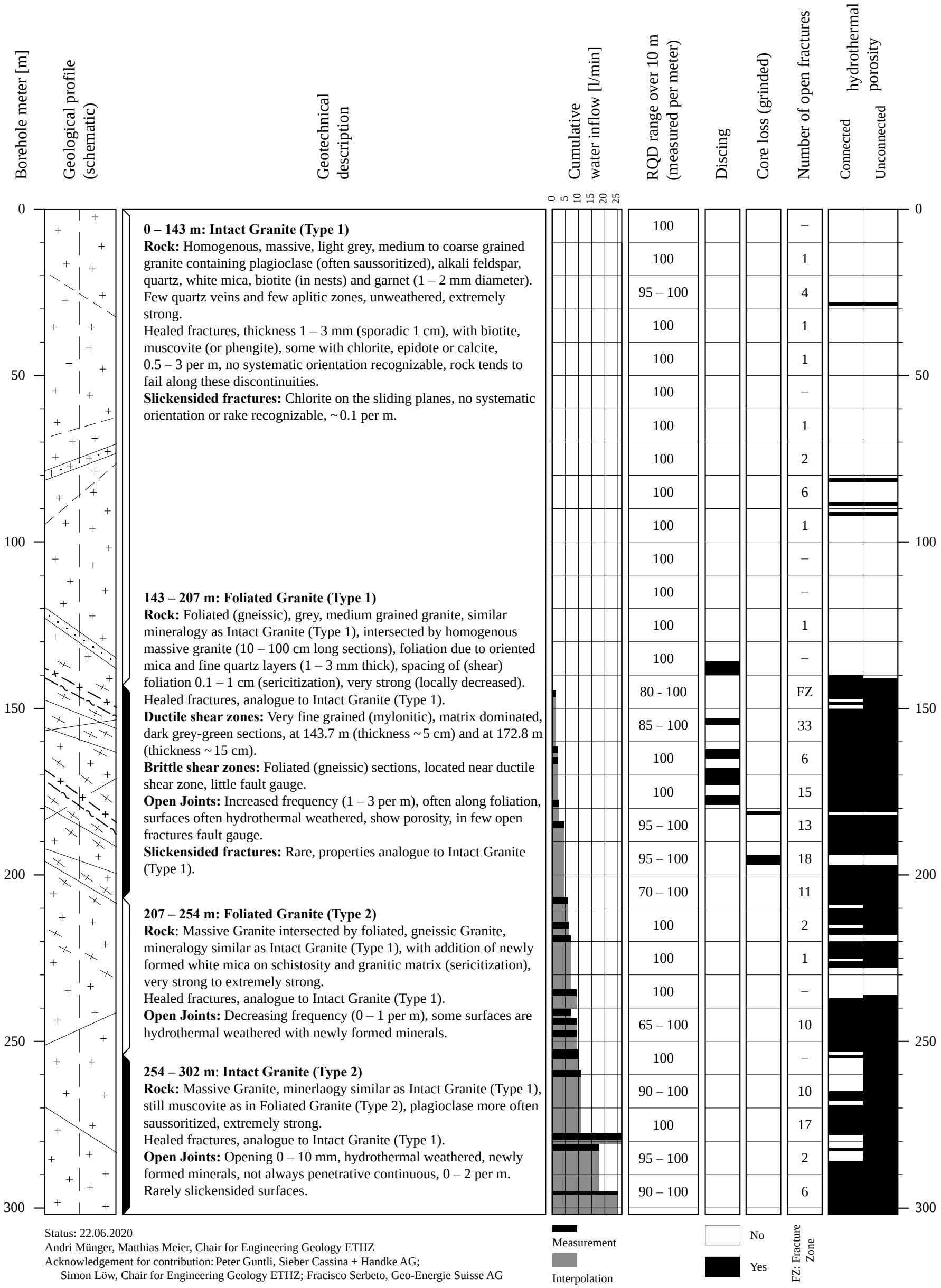

Status: 22.06.2020
Andri Münger, Matthias Meier, Chair for Engineering Geology ETHZ
Acknowledgement for contribution: Peter Guntli, Sieber Cassina + Handke AG;
Simon Löw, Chair for Engineering Geology ETHZ; Fracisco Serbeto, Geo-Energie Suisse AG

Fig. 10.1. Geological Core Log of CB1 in the BULG

Geological Core Log 1:1000 of CB2 (BULG)

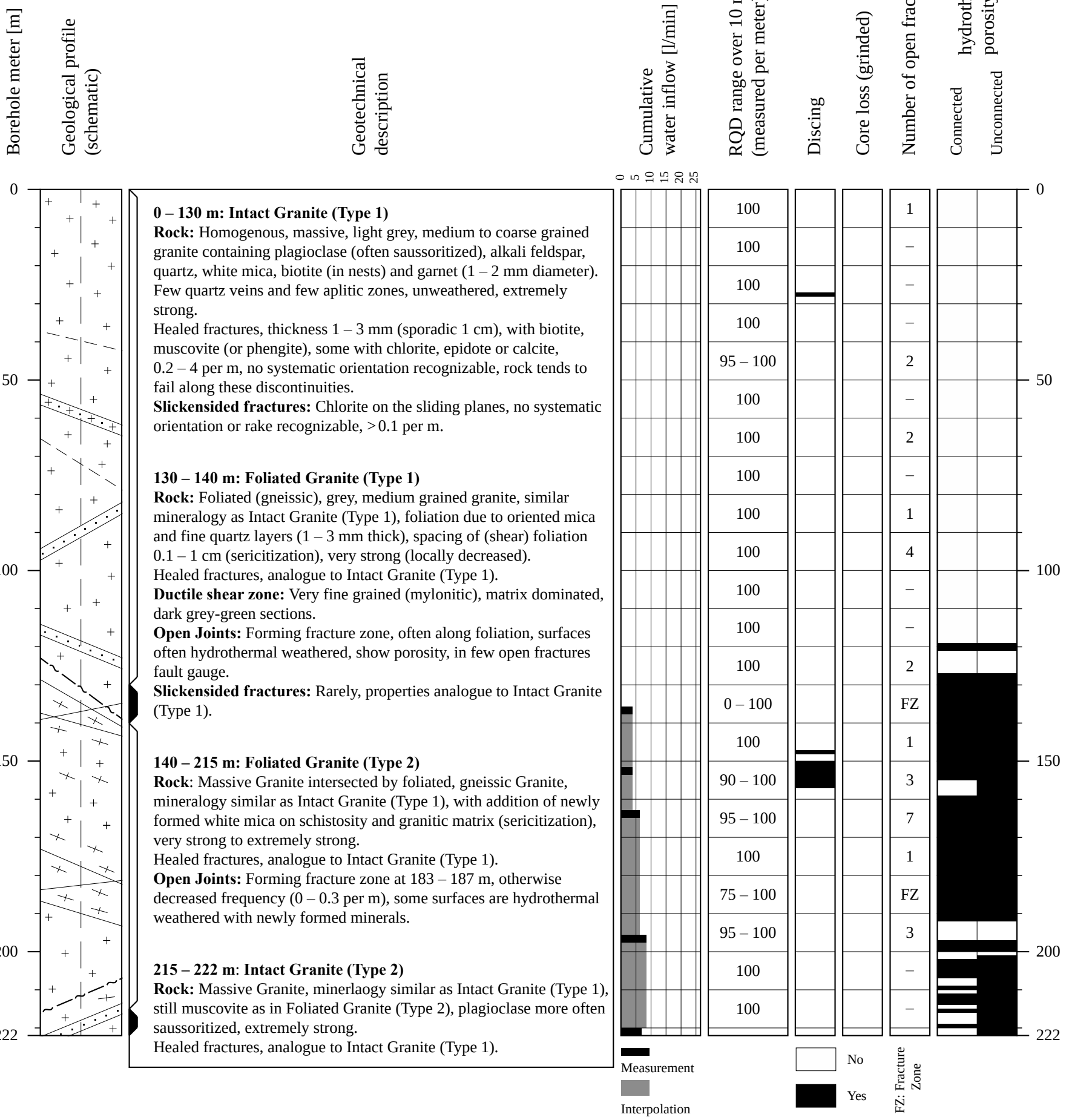

Status: 22.06.2020
Andri Münger, Matthias Meier, Chair for Engineering Geology ETHZ
Acknowledgement for contribution: Peter Guntli, Sieber Cassina + Handke AG;
Simon Löw, Chair for Engineering Geology ETHZ; Fracisco Serbeto, Geo-Energie Suisse AG

Fig. 10.2. Geological Core Log of CB2 in the BULG

Geological Core Log 1:1000 of CB3 (BULG)

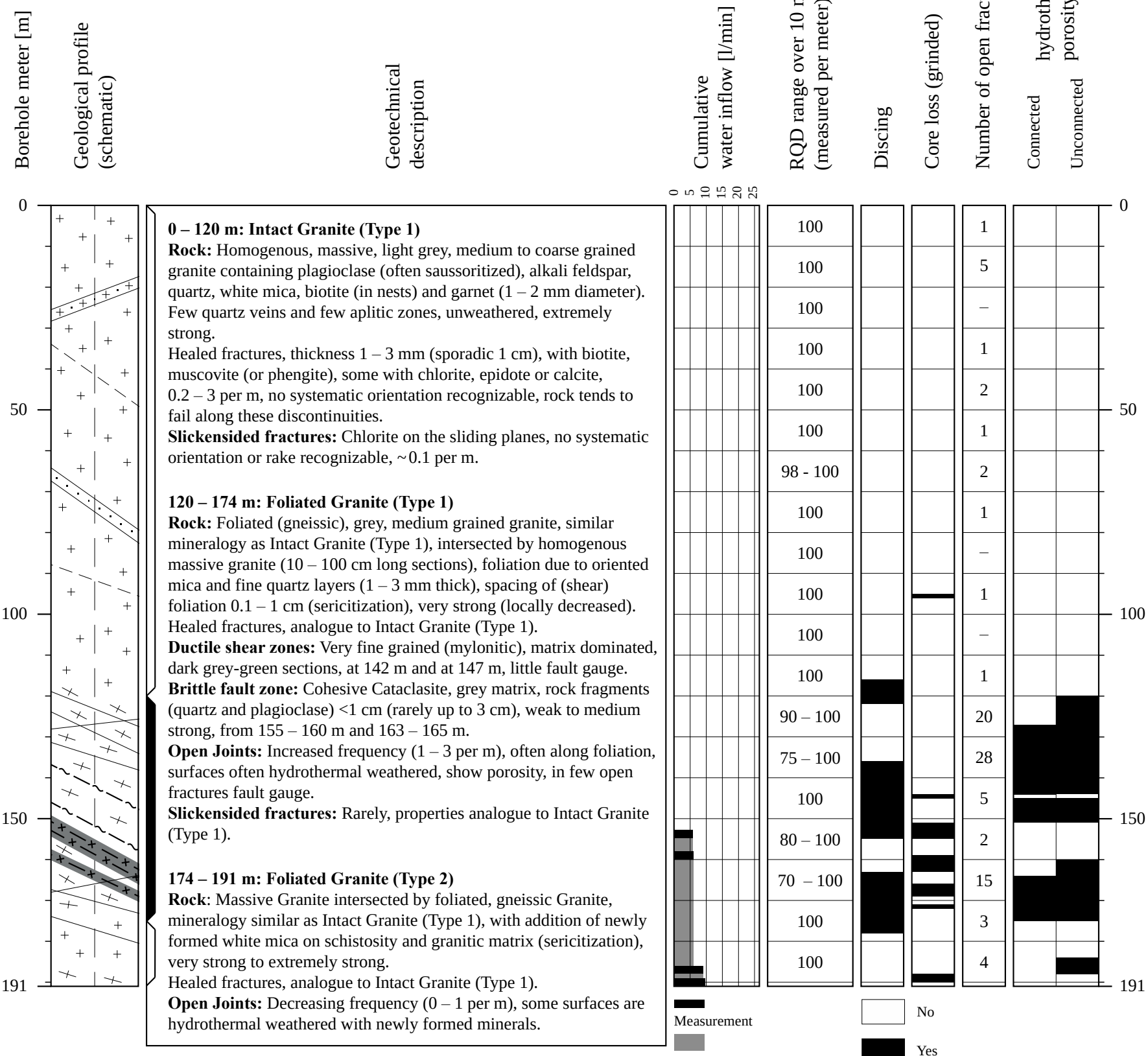

Status: 22.06.2020
Andri Münger, Matthias Meier, Chair for Engineering Geology ETHZ
Acknowledgement for contribution: Peter Guntli, Sieber Cassina + Handke AG;
Simon Löw, Chair for Engineering Geology ETHZ; Fracisco Serbeto, Geo-Energie Suisse AG

Fig. 10.3. Geological Core Log of CB3 in the BULG

Appendix B: Discontinuity terminology from Jordan (2019), after Laws (2001) and Lützenkirchen (2002).

Discontinuity: General term denoting any mechanical defects, flaws, or planes of weakness in a rock mass without consideration of their origins. It is the collective term for most types of joints, weak bedding planes, weak schistosity planes, weakness zones, and faults (ISRM, 1978).

Fracture: Discrete break along where loss of cohesion occurred (Griggs, 1960; Logan, 1979). It is by definition a result of a brittle process. Shear fracture are commonly (curvi-) planar features and are by definition associated with a discreate shear displacement.

Fractures zone: Location where fractures spacing is much closer than in the average rock mass.

Joint: Discontinuities where no displacement features are visible, the term joint is used.

Shear fracture: Can be used as alternative to fault to describe small fractures where shear displacement occurred. Lützenkirchen (2002) defines a shear fractures as a single planar feature as opposed to a fault zone that represents an intensely fractured zone of considerable width.

Fault: Planar or zonal structures (meter-scale or larger) across which visible shear displacement discontinuities occurred.

Fault zone: Tabular region that contains many parallel or anastomosing fault surfaces. There is not agreement minimum thickness of fault core from which on it is considered as fault zone.

Ductile shear zone: Shear zones where displacement occurs without development of fractures on grain scale. Deformation is mainly achieved by crystal plasticity and may comprise only a minor amount of fracturing. Ductile deformation mechanisms become dominant at greater depth when temperature and confining pressure become higher. For a quatzo-feldspathic crystalline rock like granite, the transition between brittle and ductile deformation behaviour occurs in the interval 10–15 km for a normal geothermal gradient (Sibson, 1977).

Fault zone characterization: (Lützenkirchen, 2002)

- Fault core: Zone of intensely crushed or smeared rock
- Damage zone: Zone around the core with a network of subsidiary fractures veins and small faults
- Protolith: Hardly any brittle deformation except joints

Fault core rocks: (Laws 2001; Lützenkirchen 2002)

- Fault gauge
- Fault breccia (>30% rock fragments)
- Cataclasite (cohesive <30% rock fragments)

Exfoliation joints: Also known as sheet joints or unloading joints, are joints developed subparallel to a free surface topography due to a reduction in stress normal to the free surface. Exfoliation can produce new fractures sub-parallel to the present-day rock surface, but it can also propagate, open or enlarge favorably oriented pre-existing discontinuities.

Lützenkirchen (2002) and van der Pluijm & Marshack (2004), suggest to only use the term shear zone for ductile deformation zones.

Appendix C: Examples for types of borehole wall defects

Section of Acoustic (ATV) and Optical (OPTV) Televiewer data set from CB1

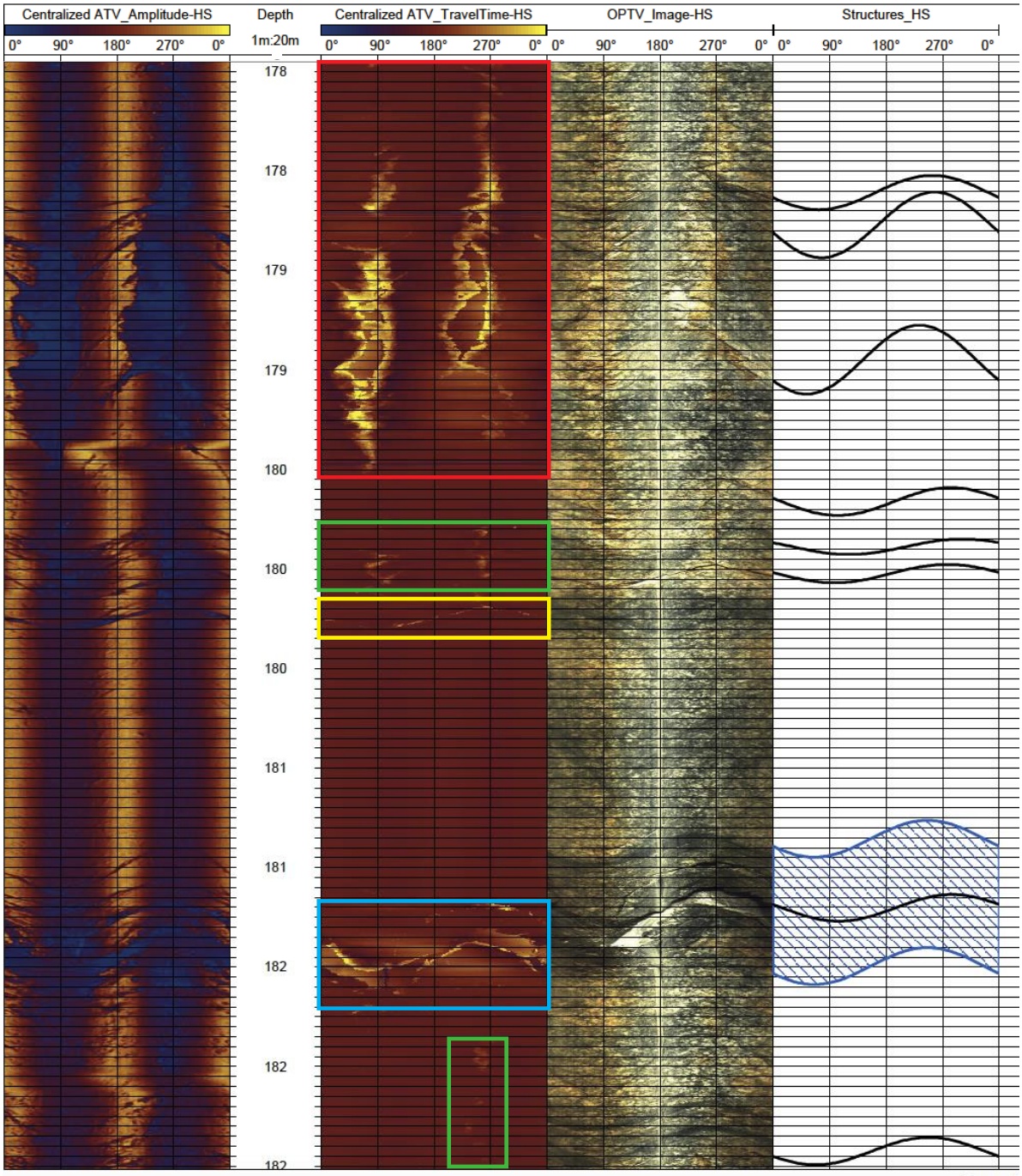

Fig. 10.4. Examples for types of borehole wall defects.
Category 1: Small Anomaly (green)
Category 2: Single Fracture (yellow) or Fault Zone (blue)
Category 3: Borehole Breakout (red)

Appendix D: Graphs indicating borehole wall defects in boreholes CB1, CB2, CB3

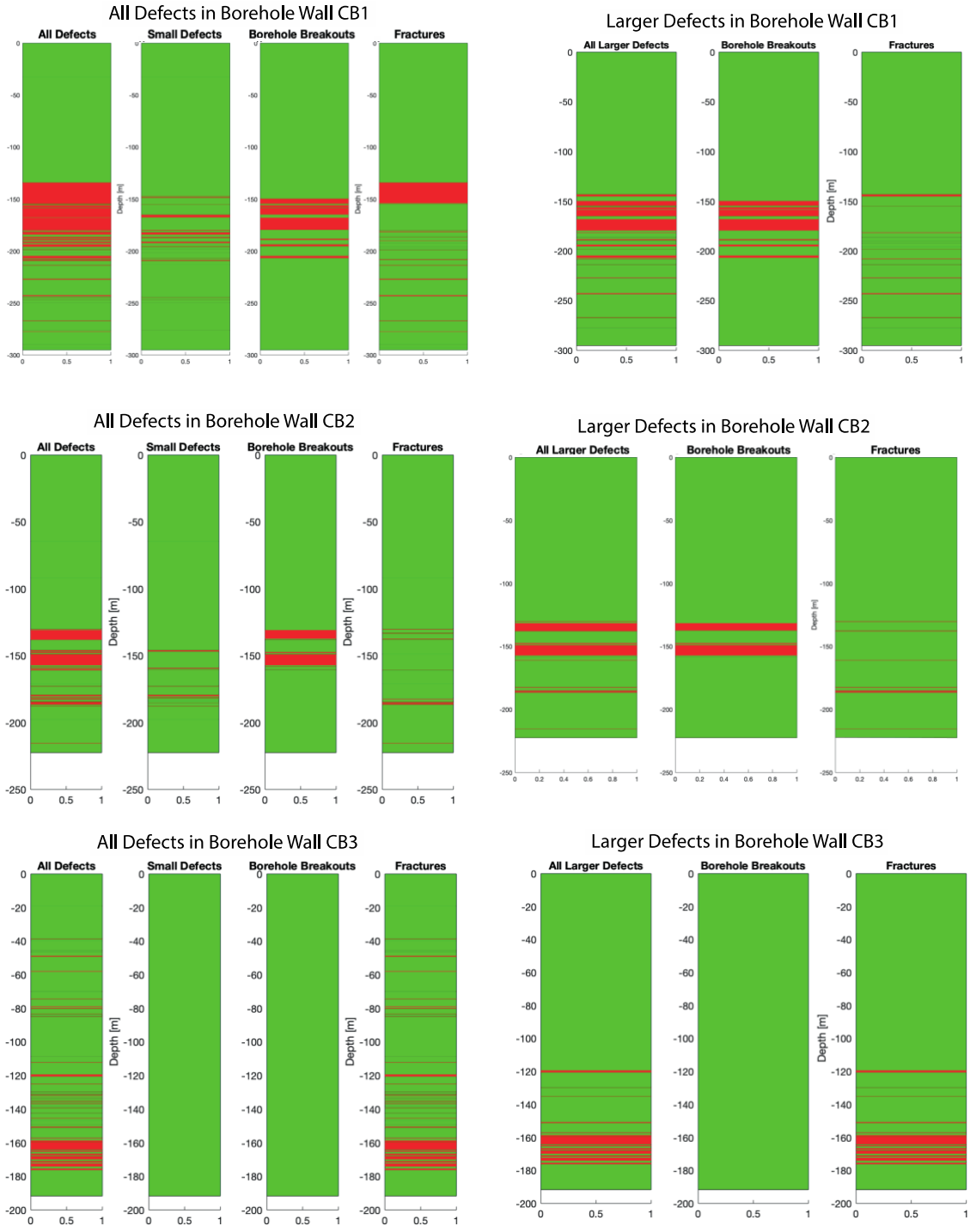

Fig. 10.5. Graphs indicating the identified defects in the borehole wall of CB1, CB2, CB3.

Seven graphs per borehole are shown. In the four graphs on the left all intervals in which defects were found are shown in red, whereat the most left one the three categories are plotted in one column. In the three graphs on the right, only those intervals are shown in red where "large defects" were found, whereat the most left one the two categories are plotted in one column. Borehole breakouts, fault zones and fracture zones are classified as "large defects", whereas the category "small defects" and single fractures are not included in the category "large defects".

Appendix E: Possible packer installation sections in CB1, CB2 and CB3

Tab. 10.1. Possible packer installation locations per borehole.

CB1 possible locations (all defects)	**CB1 possible locations (large defects only)**	**CB2 possible locations (all defects)**	**CB2 possible locations (large defects only)**	**CB3 possible locations (all defects)**	**CB3 possible locations (larger defects only)**
14.0 – 32.4	14.9 – 143.0	16.0 – 64.4	16.0 – 130.4	17.0 – 19.0	17.0 – 119.3
32.5 – 143.0	145.0 – 149.6	64.5 – 91.8	137.9 - 147.3	19.1 – 38.5	120.6 – 129.5
145.1 – 147.4	165.0 – 167.9	91.9 – 130.1	158.3 – 160.7	39.6 – 45.5	129.8 – 134.9
184.1 – 186.1	181.7 – 186.1	138.2 – 145.7	161.0 – 182.2	46.4 – 48.7	135.1 – 150.5
199.5 – 201.4	190.1 – 192.2	161.0 – 171.0	182.7 – 184.7	49.2 – 57.8	151.1 – 156.9
201.6 – 204.5	196.0 – 198.2	173.0 – 179.3	186.6 – 215.3	58.1 – 69.9	176.3 – 191.7
209.4 – 213.2	198.5 – 204.5	187.9 – 197.6	215.6 – 222.5	70.1 – 74.3	
214.0 – 226.7	208.5 – 213.5	197.7 – 215.3		74.6 – 78.8	
227.6 – 242.4	213.9 – 226.7	215.6 – 222.5		80.2 – 83.1	
246.9 – 249.6	227.6 – 242.4			85.0 – 108.4	
249.8 – 266.8	243.6 – 266.8			108.5 – 111.9	
267.4 – 276.4	267.4 – 277.4			112.2 – 119.3	
277.8 – 289.7	277.8 – 295.2			120.6 – 124.7	
290.0 – 292.4				125.0 – 129.5	
292.6 – 295.2				139.4 – 142.3	
				142.5 – 145.3	
				146.7 – 149.3	
				151.1 – 156.9	
				176.3 – 191.7	

Appendix F: ATV log and core photos with Intervals' most conductive structures

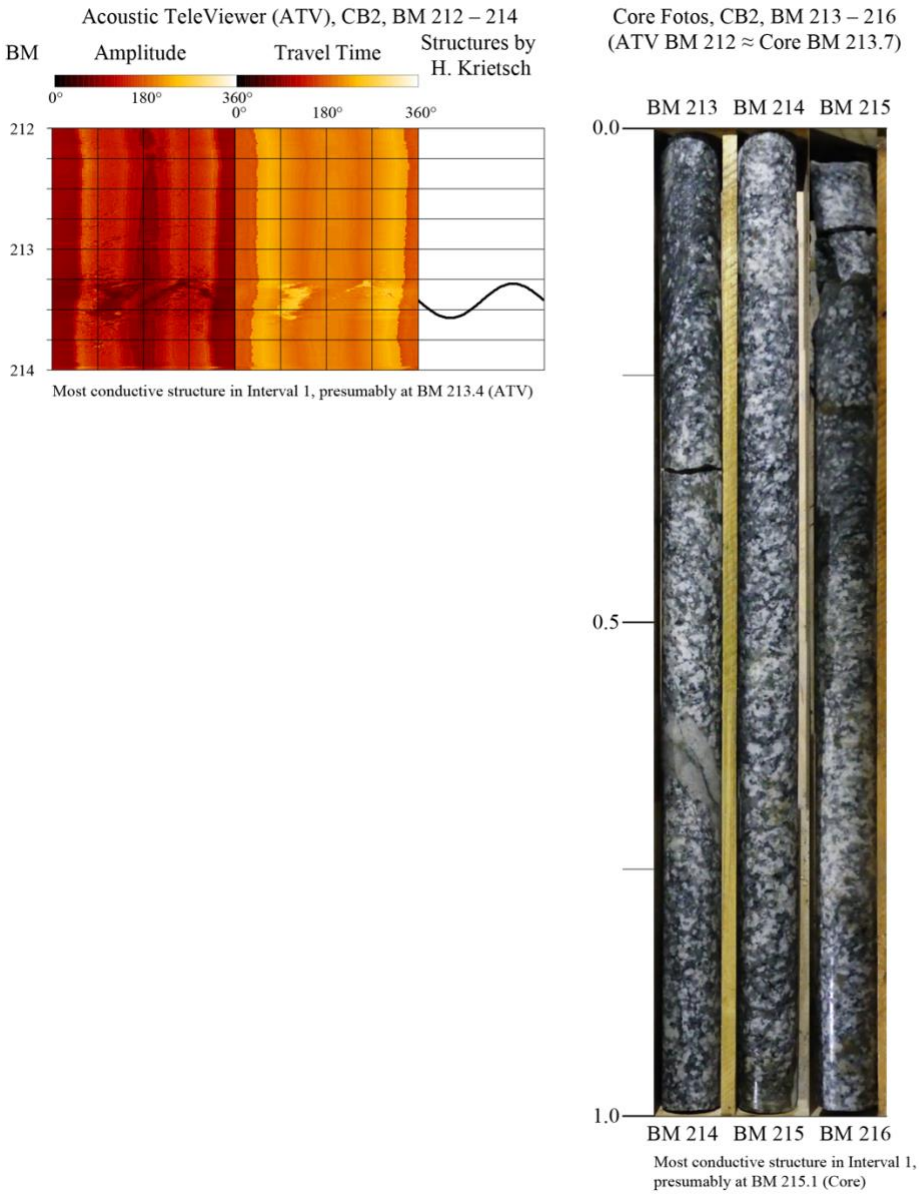

Fig. 10.6. ATV log section and core photos showing the presumably most conductive structure in Interval 1.

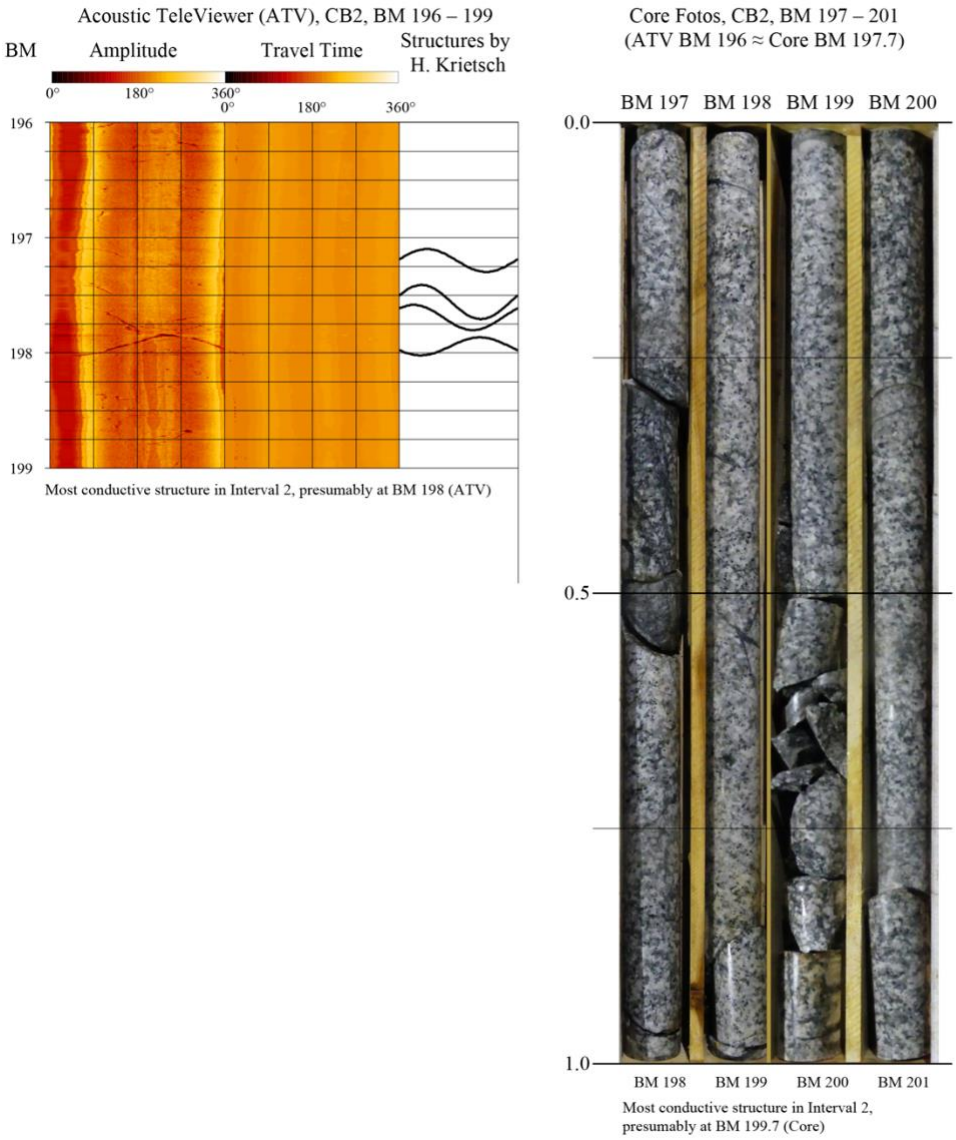

Fig. 10.7. ATV log section and core photos showing the presumably most conductive structure in Interval 2.

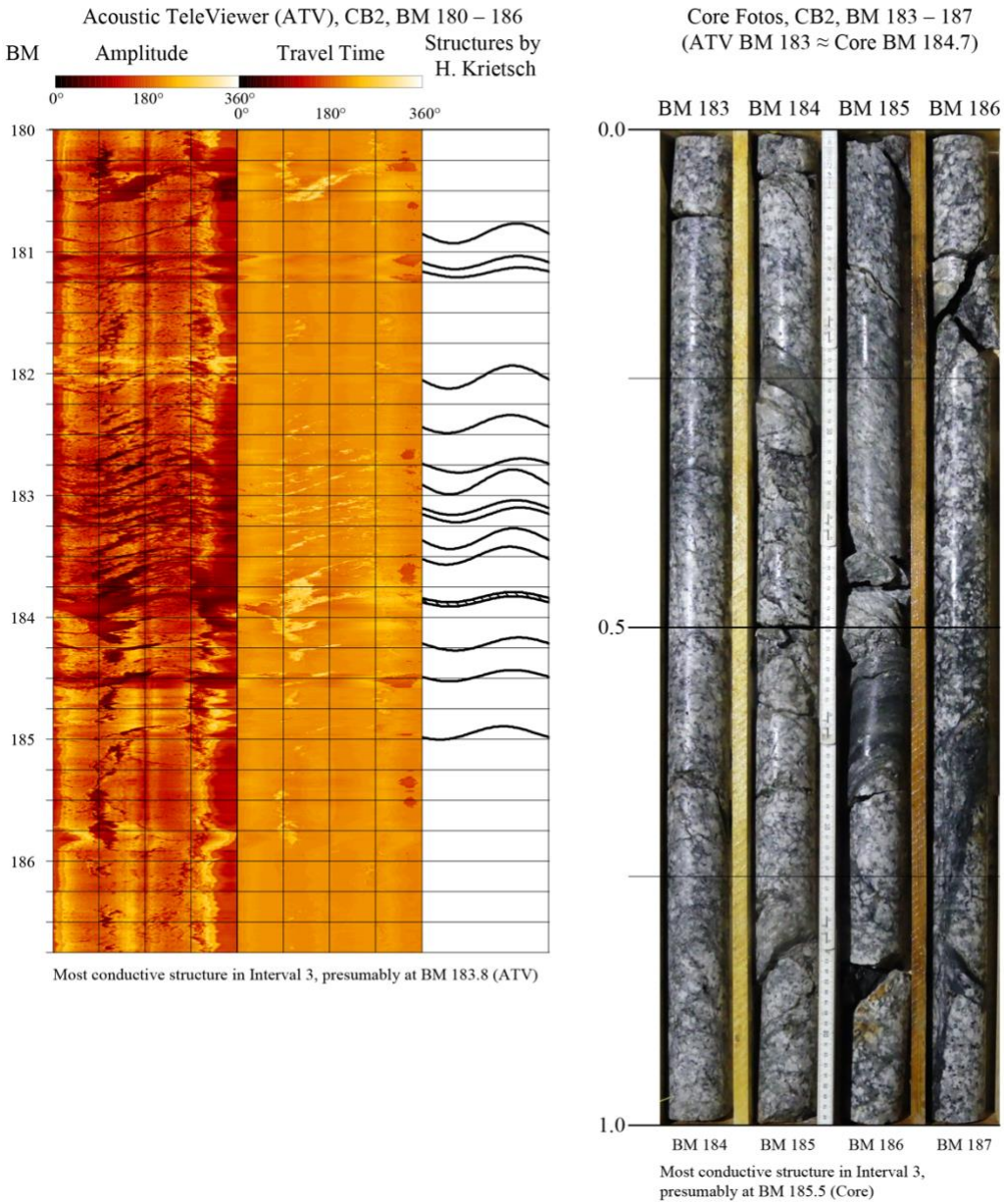

Fig. 10.8. ATV log section and core photos showing the presumably most conductive structure in Interval 3.

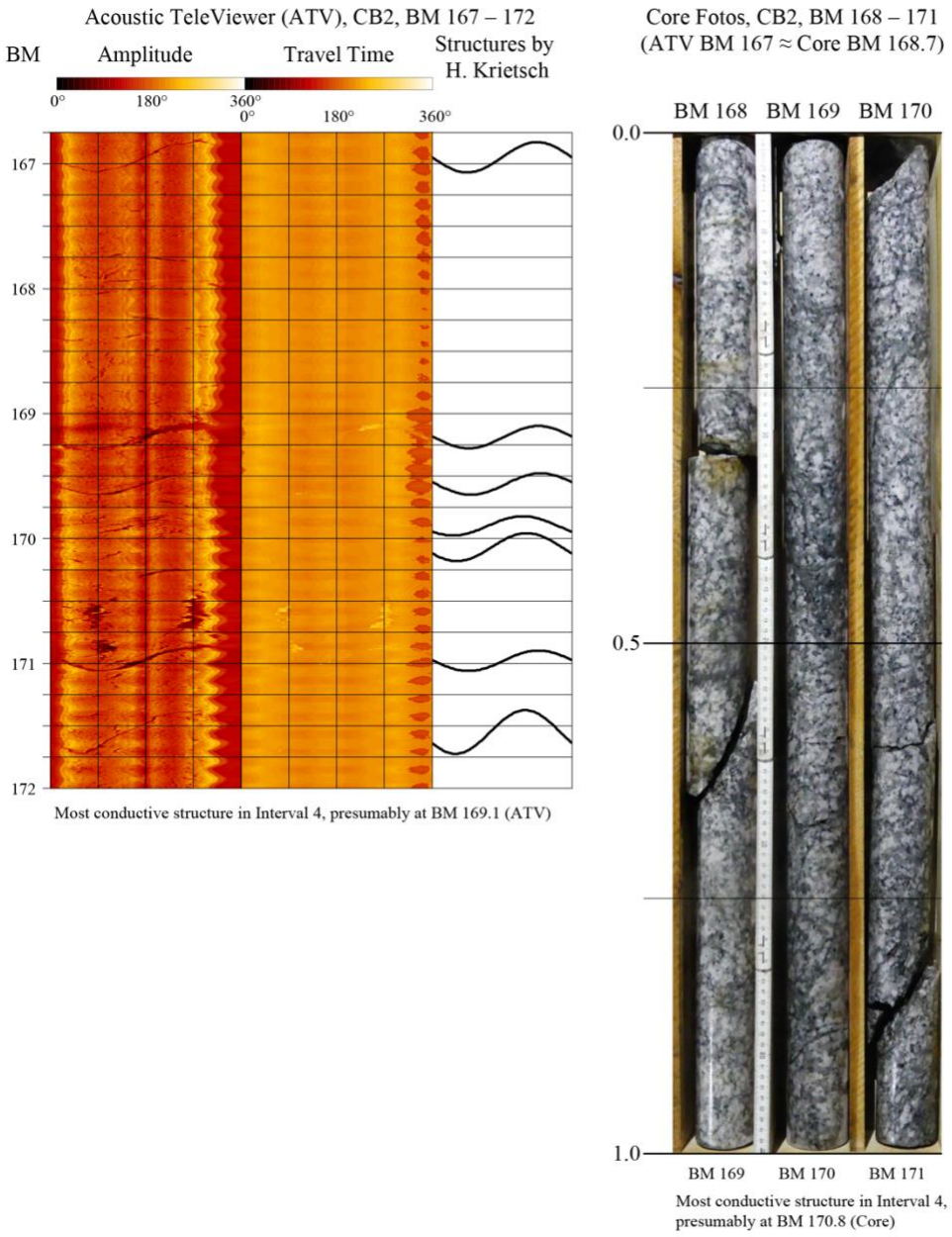

Fig. 10.9. ATV log section and core photos showing the presumably most conductive structure in Interval 4.

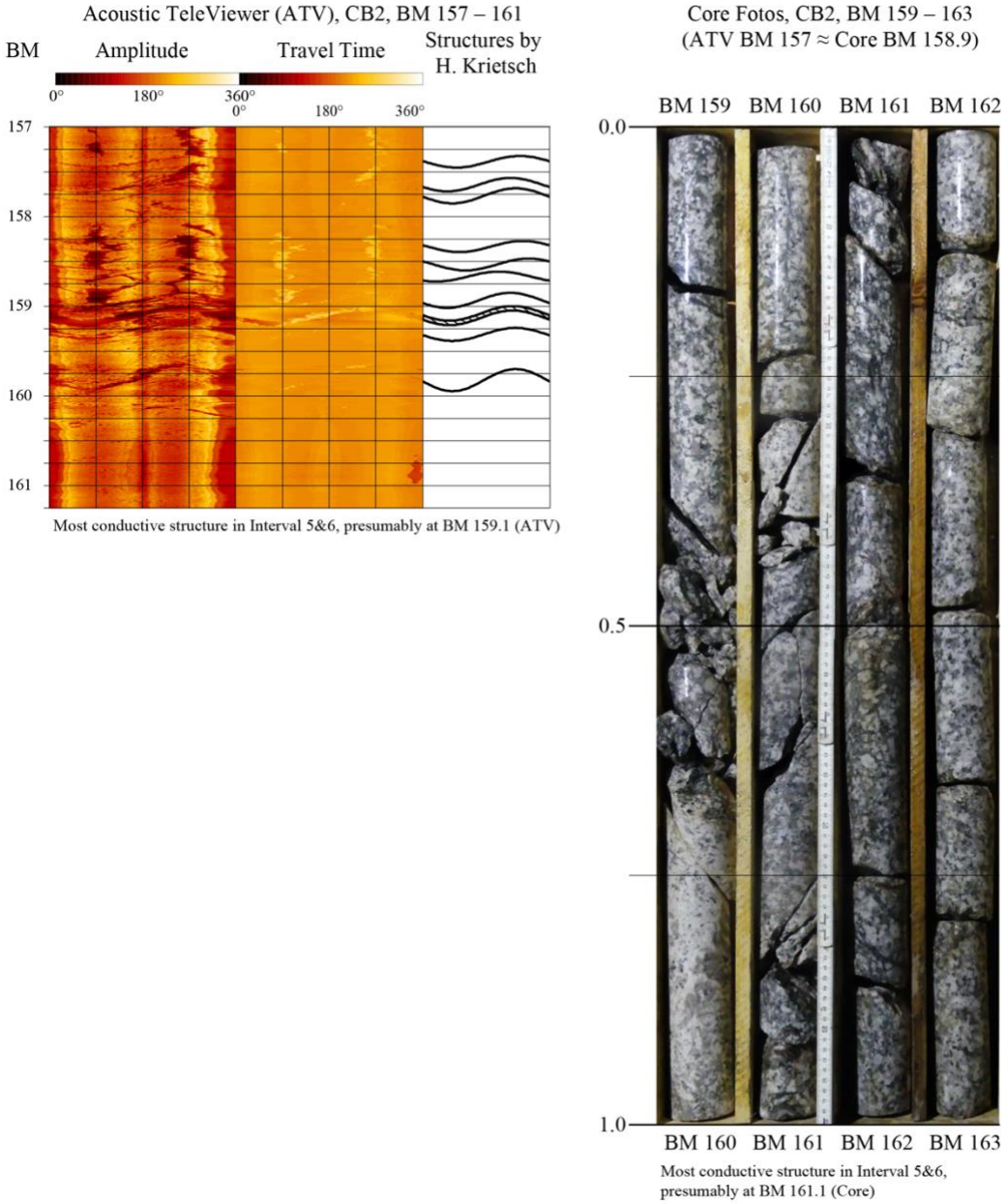

Fig. 10.10. ATV log section and core photos showing the presumably most conductive structure in Interval 5&6.

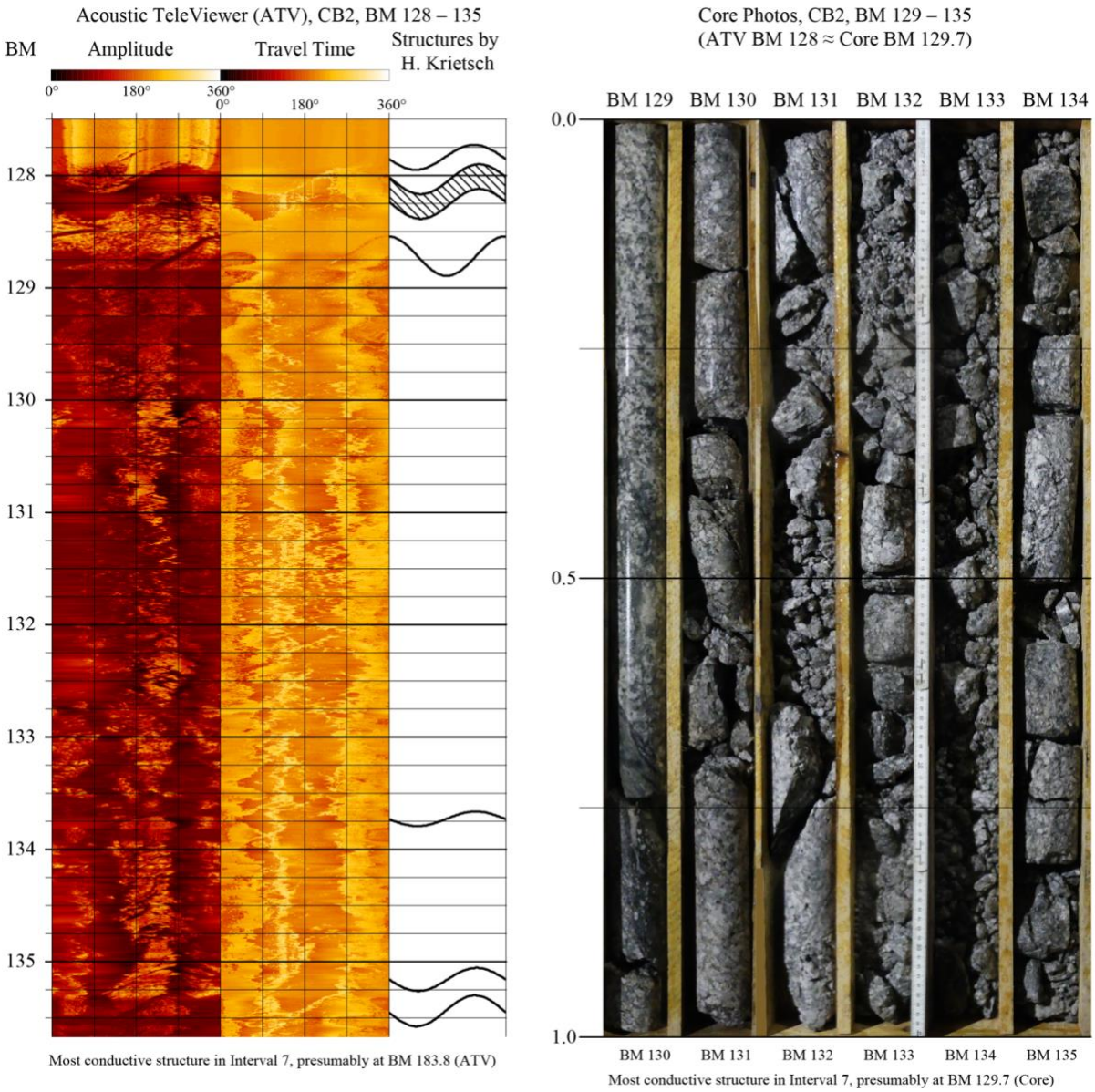

Fig. 10.11. ATV log section and core photos showing the presumably most conductive structure in Interval 7.

Appendix G: Stereoplot indicating structures in ATV for CB1, CB2 and CB3

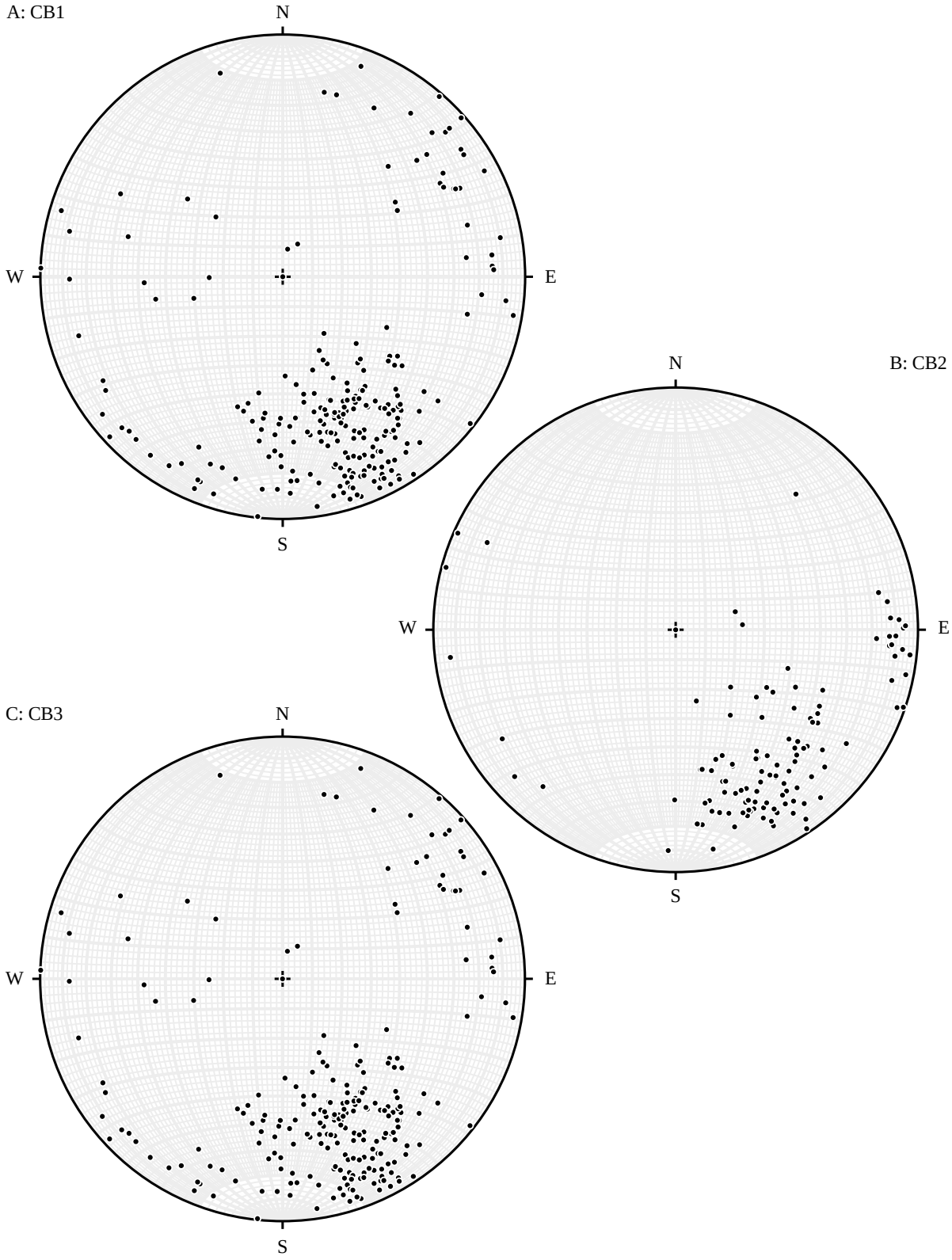

Fig. 10.12. Stereoplot indicating the poles of all structures mapped in ATV logs by H. Krietsch for the boreholes CB1 (A), CB2 (B) and CB3 (C).

Appendix H: Protocol of events in CB1, CB3, and Interval in CB2

Tab. 10.2. Protocol of events in CB1, CB3, and Interval in CB2 (Part I)

Test Period [Date, hh:mm]	Test Type	Interval / Borehole	Comment	Flow Rate Setting	Duration of Recovery before Test [hh:mm:ss]
18.02. – 03.03.2020	Shut-In of CB1, CB3 and all Intervals: Start Pressure Stabilization				
03.03.2020 10:46	Pulse	Interval 7			14 days
03.03.2020 13:39	Pulse	Interval 3			02:53:00
03.03.2020 13:55 – 14:20	Constant Rate	Interval 3	unstable flow, repeated later	1.5	
03. – 04.03.2020 19:33 – 05:59	Constant Rate	Interval 7		30	05:13:00
05.03.2020 10:00	Pulse	Interval 3			04:01:00
05.03.2020 12:52 – 13:18	Constant Rate	Interval 3	unstable flow, repeated later	1	
05.03.2020 13:20 – 13:26	Constant Rate	Interval 3	flow rate too low to achieve targeted drawdown, repeated later	0.3	
05.03.2020 14:32 – 14:47	Constant Rate	Interval 3	unstable flow, repeated later	24	
05.03.2020 17:12 – 17:43	Constant Rate	Interval 3	too high flow rate probably a drawdown of >10 bar would have resulted	24	
05. – 06.03.2020 23:27 – 04:34	Constant Rate	Interval 3		1	05:44:00
06.03.2020 08:55	Pulse	Interval 6			04:21:00
06.03.2020 09:09	Pulse	Interval 2			00:14:00
06.03.2020 09:19	Pulse	Interval 3			00:10:00
06.03.2020 09:23	Pulse	Interval 4			00:04:00
06.03.2020 09:26	Pulse	Interval 1			00:03:00
06.03.2020 14:48 – 15:50	Constant Rate	Interval 7		30	04:22:00
06.03.2020 18:00 – ??:??	Constant Rate	Interval 1	unstable flow, repeated later	?	

Tab. 10.3. Protocol of events in CB1, CB3, and Interval in CB2 (Part II)

Test Period [Date, hh:mm]	Test Type	Interval / Borehole	Comment	Flow Rate Setting	Duration of Recovery before Test [hh:mm:ss]
07. – 08.03.2020 12:00 – 22:54	Constant Rate	Interval 1		0.1	~17:00
09.03.2020 10:24 – 11:43	Constant Rate	Interval 4	too high flow rate probably a drawdown of >10 bar would have resulted	2.5	
09.03.2020 13:30 – 21:55	Constant Rate	Interval 4		6	01:47:00
10.03.2020 12:00 – 12:12	Constant Rate	Interval 5&6	flow rate too low to achieve targeted drawdown, repeated later	0.1	
10.03.2020 12:35 – 12:37	Constant Rate	Interval 5&6	flow rate too low to achieve targeted drawdown, repeated later	10	
10.03.2020 21:05 – 21:47	Constant Rate	Interval 5&6	too high flow rate probably a drawdown of >10 bar would have resulted	75	
11.03.2020 02:13 – 05:13	Constant Rate	Interval 5&6		30	04:26:00
11.03.2020 11:56 – 12:14	Constant Rate	Interval 2	unstable flow, repeated later	0.1	
11.03.2020 14:20 – 14:22	Constant Rate	Interval 4	flow rate too low to achieve targeted drawdown, repeated later	1	
11.03.2020 14:59 – 15:00	Constant Rate	Interval 4	wrong settings	90	
11.03.2020 15:23 – 15:51	Several Constant Rate	Interval 4	trying to find suitable flow rate	90, 45, 225, 30, 15	
11. – 12.03.2020 22:01 – 05:38	Constant Rate	Interval 4		4	06:10:00
12.03.2020 07:18 – 13:13	Constant Rate	Interval 4		8	01:40:00
12. – 13.03.2020 16:41 – 04:38	Constant Rate	Interval 2		0.05	03:28:00
13.03.2020 14:04 – 14:05	Constant Rate	CB3	flow rate too low to achieve targeted drawdown, repeated later	40	
13.03.2020 14:11 – 14:11	Constant Rate	CB3	predefined flow rate not reachd, repeated later	200	
13.03.2020 14:27 – 14:27	Constant Rate	CB3	predefined flow rate not reachd, repeated later	200	

Tab. 10.4. Protocol of events in CB1, CB3, and Interval in CB2 (Part III)

Test Period [Date, hh:mm]	Test Type	Interval / Borehole	Comment	Flow Rate Setting	Duration of Recovery before Test [hh:mm:ss]
13.03.2020 14:39 – 14:41	Constant Rate	CB3	unstable flow, repeated later	80	
13.03.2020 14:53 – 15:00	Constant Rate	CB3	flow rate too low to achieve targeted drawdown, repeated later	80	
13.03.2020 15:13 – 15:13	Constant Rate	CB3	predefined flow rate not reachd, repeated later	200	
13.03.2020 15:17 – 15:18	Constant Rate	CB3	predefined flow rate not reachd, repeated later	200	
13.03.2020 15:18 – 15:18	Constant Rate	CB3	too high flow rate, probably a drawdown of >10 bar would have resulted repeated later	200	
13.03.2020 15:25 – 18:34	Constant Rate	CB3		90	00:07:00
14.03.2020 06:10 – 06:10	Constant Rate	CB1	flow rate too low to achieve the targeted drawdown, repeated later	90	
14.03.2020 07:39 – 07:39	Constant Rate	CB1	unstable flow, repeated later	120	
14.03.2020 07:52 – 07:53	Constant Rate	CB1	unstable flow, repeated later	120	
14. – 15.03.2020 15:33 – 09:33	Constant Rate	CB1		120	07:40:00

Appendix I: Flow Board

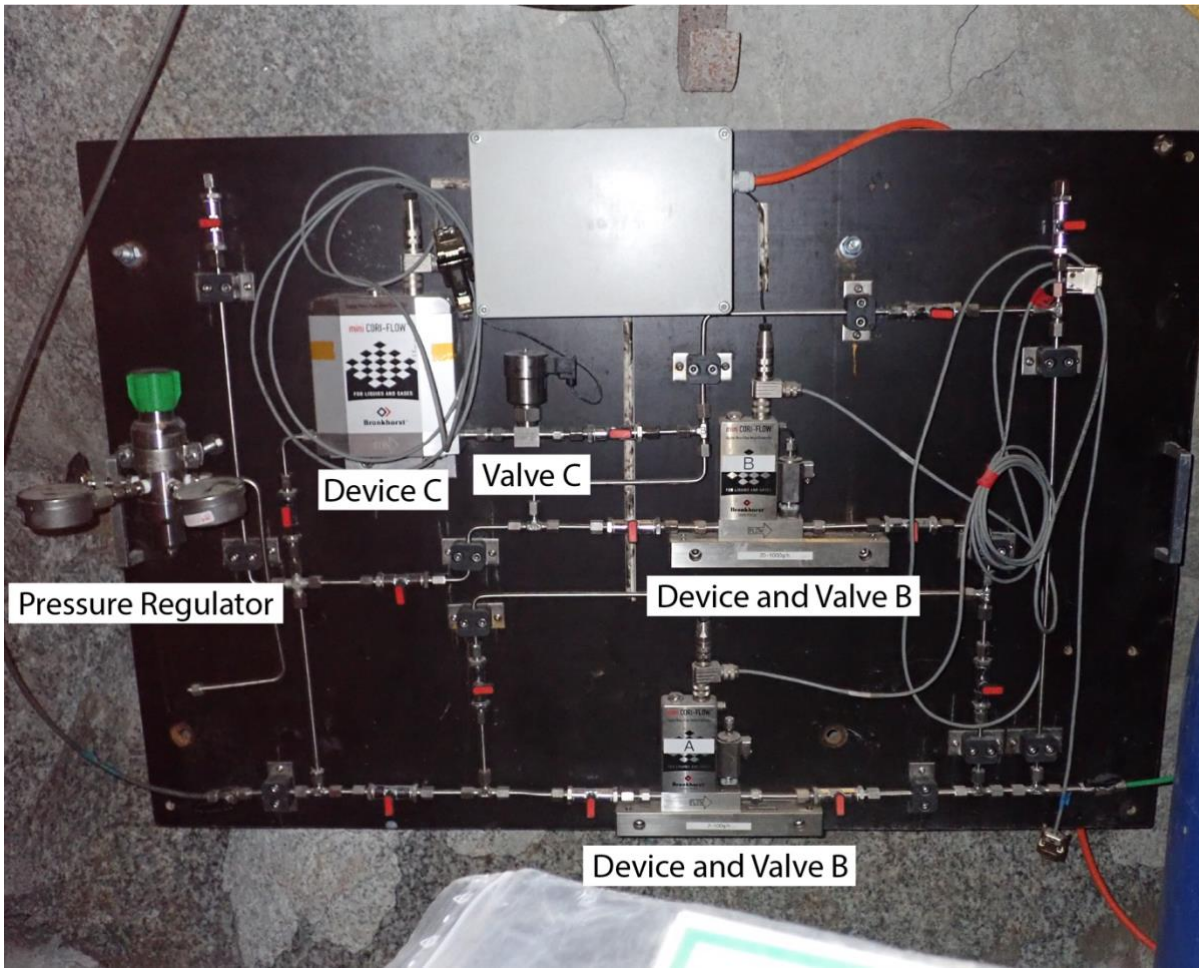

Fig. 10.13. Flow board with three used flow controllers (flow meter and corresponding automatic valves) and the pressure regulator.

Appendix J: Pulse Test, Curve Fitting, Results

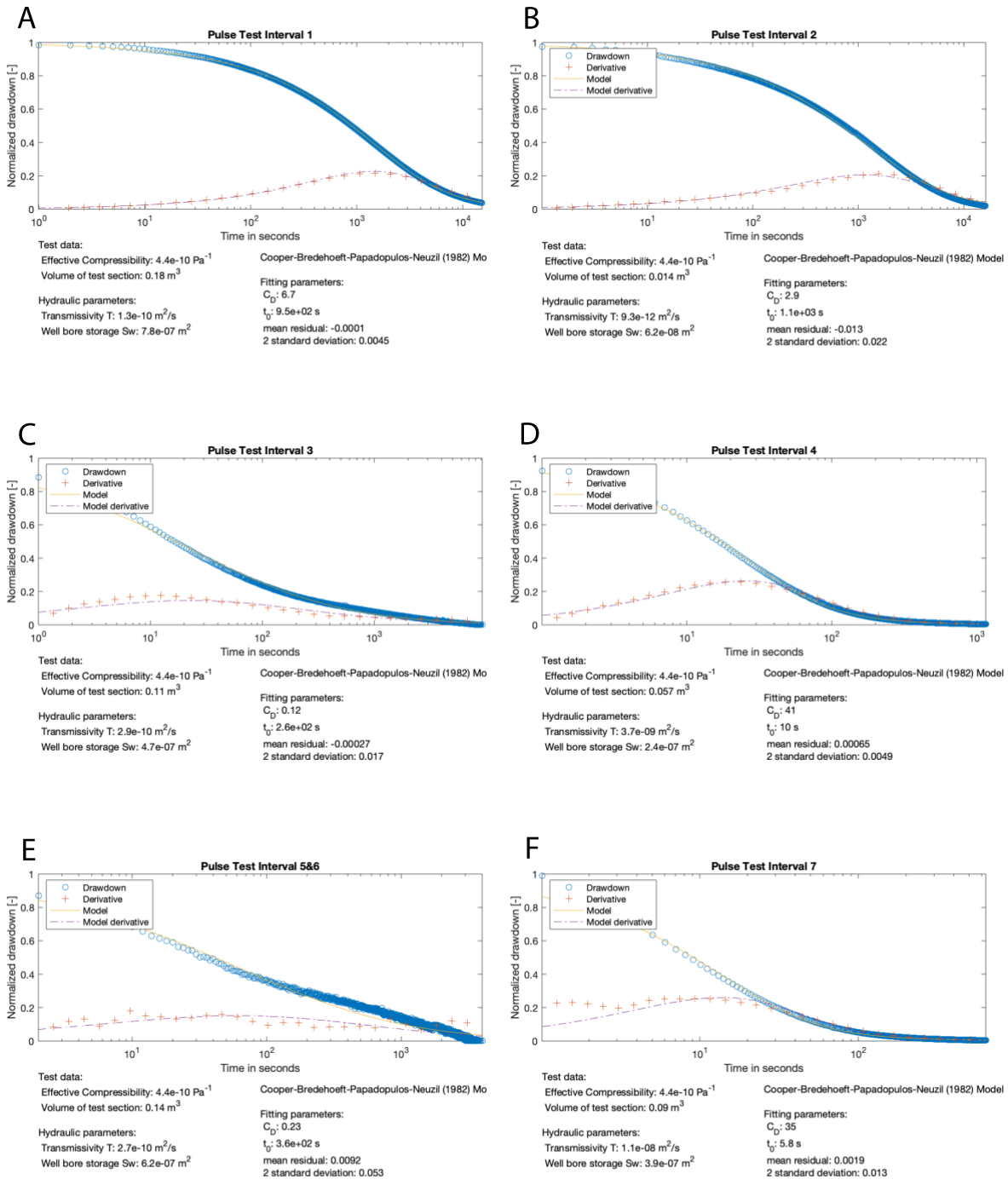

Fig. 10.14. Results of curve fitting for the pulse tests in Interval 1 (A), Interval 2 (B), Interval 3 (C), Interval 4 (D), Interval 5&6 (E) and Interval 7 (F).

Appendix K: Constant rate test pressure curves, drawdown (with flow rate) and buildup

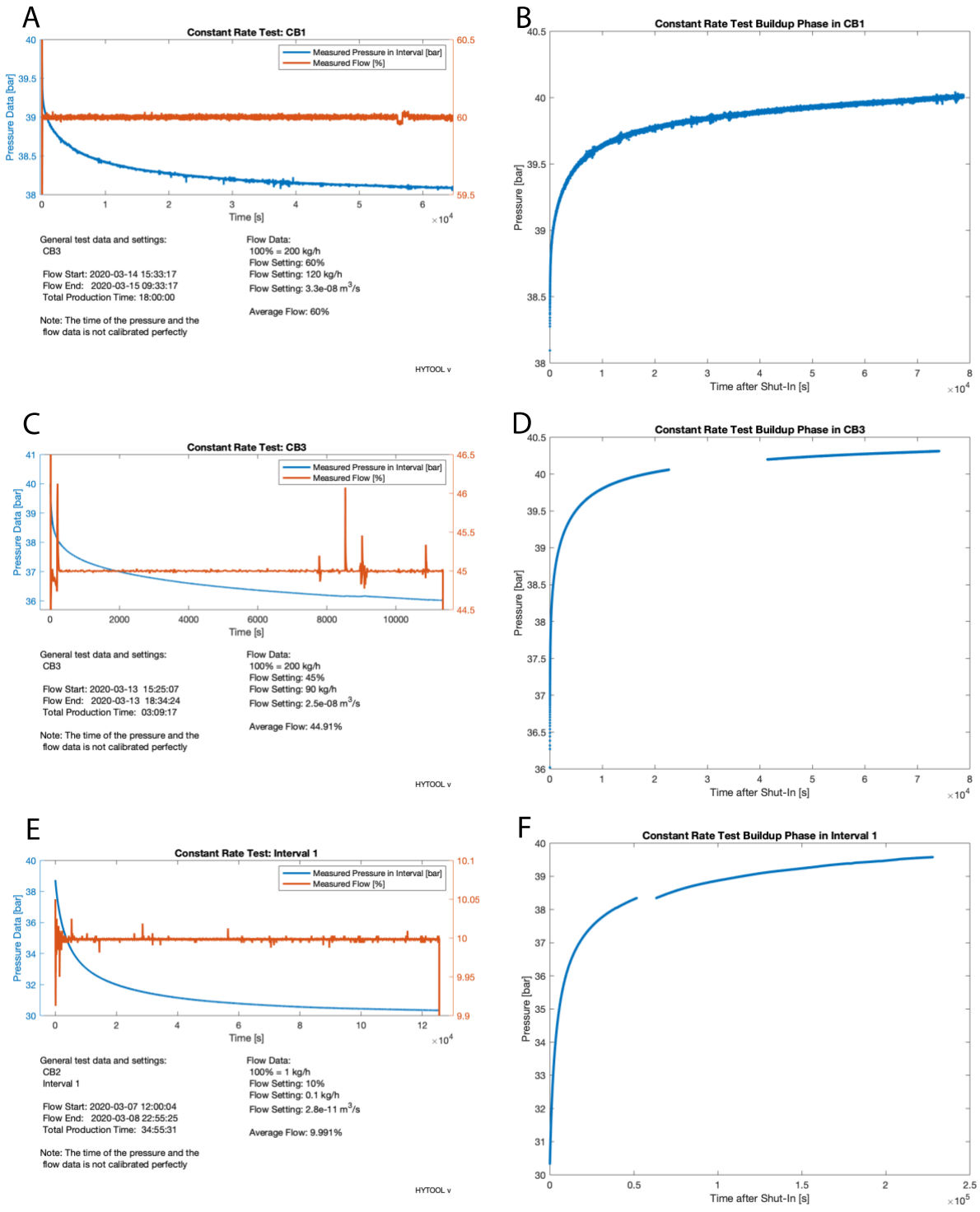

Fig. 10.15. Pressure curve of drawdown phase with flow rates and buildup phase of constant rate tests in CB1 (A,B), CB3 (C,D) and Interval 1 (E,F).

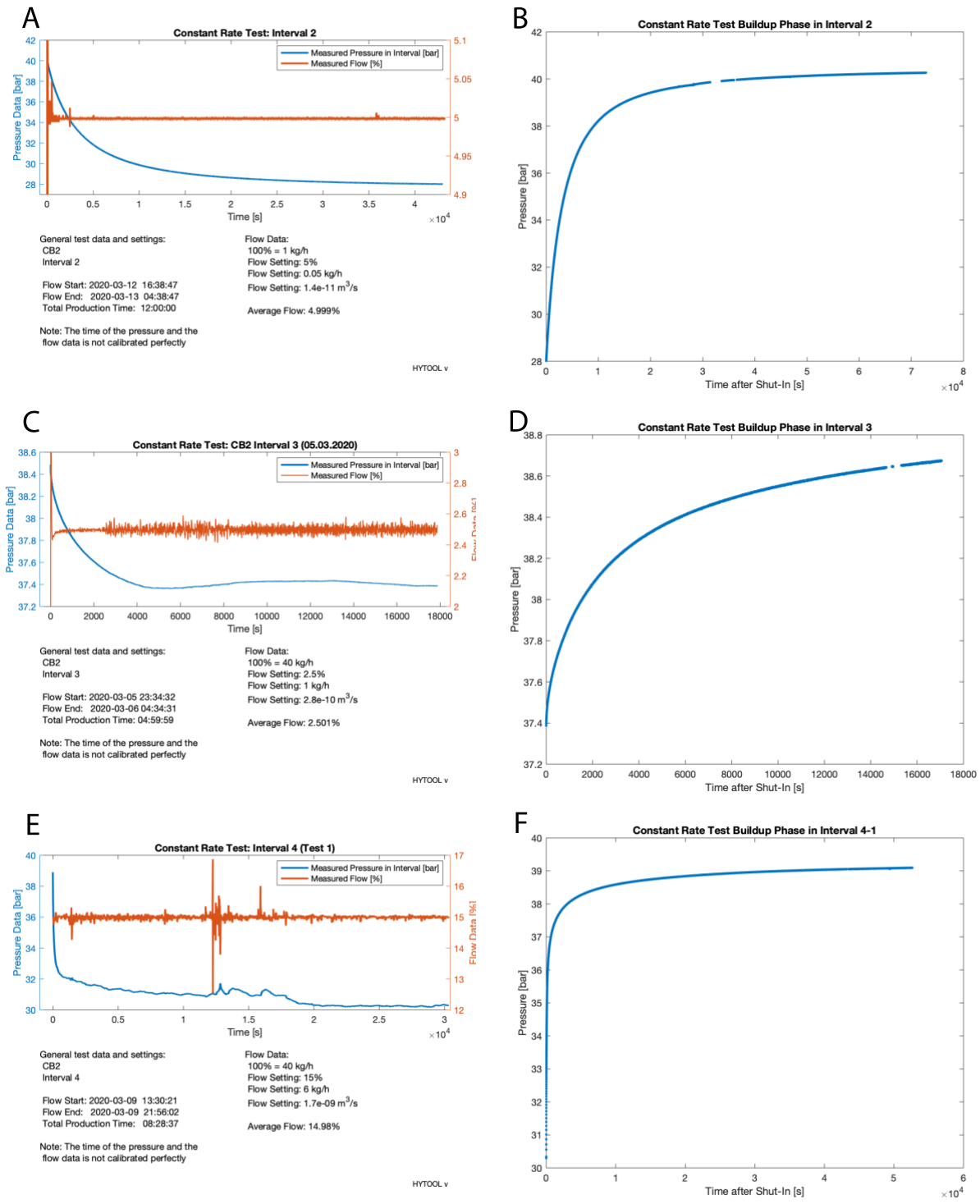

Fig. 10.16. Pressure curve of drawdown phase with flow rates and buildup phase of constant rate tests in Interval 2 (A,B), Interval 3 (C,D) and Interval 4-1 (E,F).

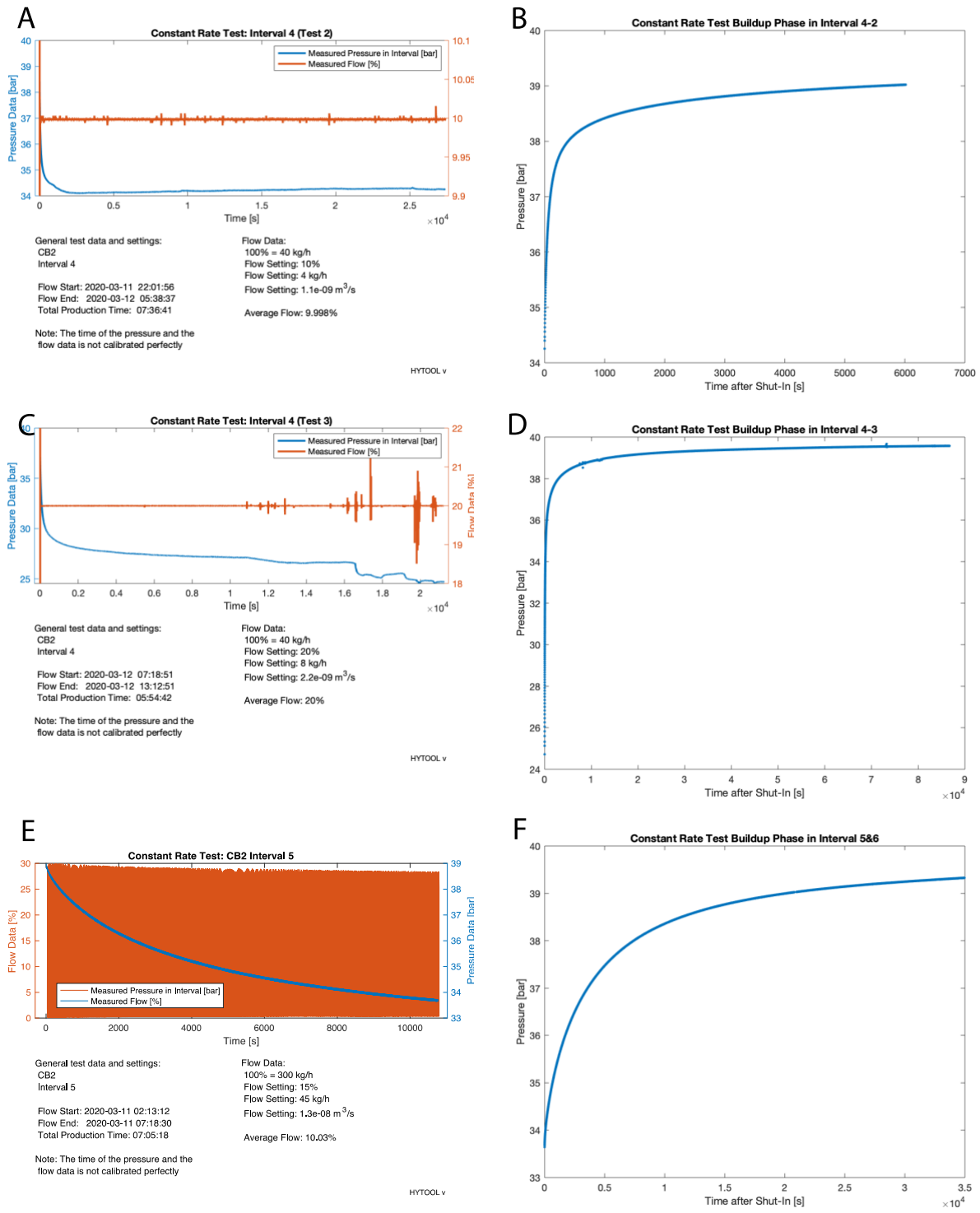

Fig. 10.17. Pressure curve of drawdown phase with flow rates and buildup phase of constant rate tests in Interval 4-2 (A,B), Interval 4-3 (C,D) and Interval 5&6 (E,F).

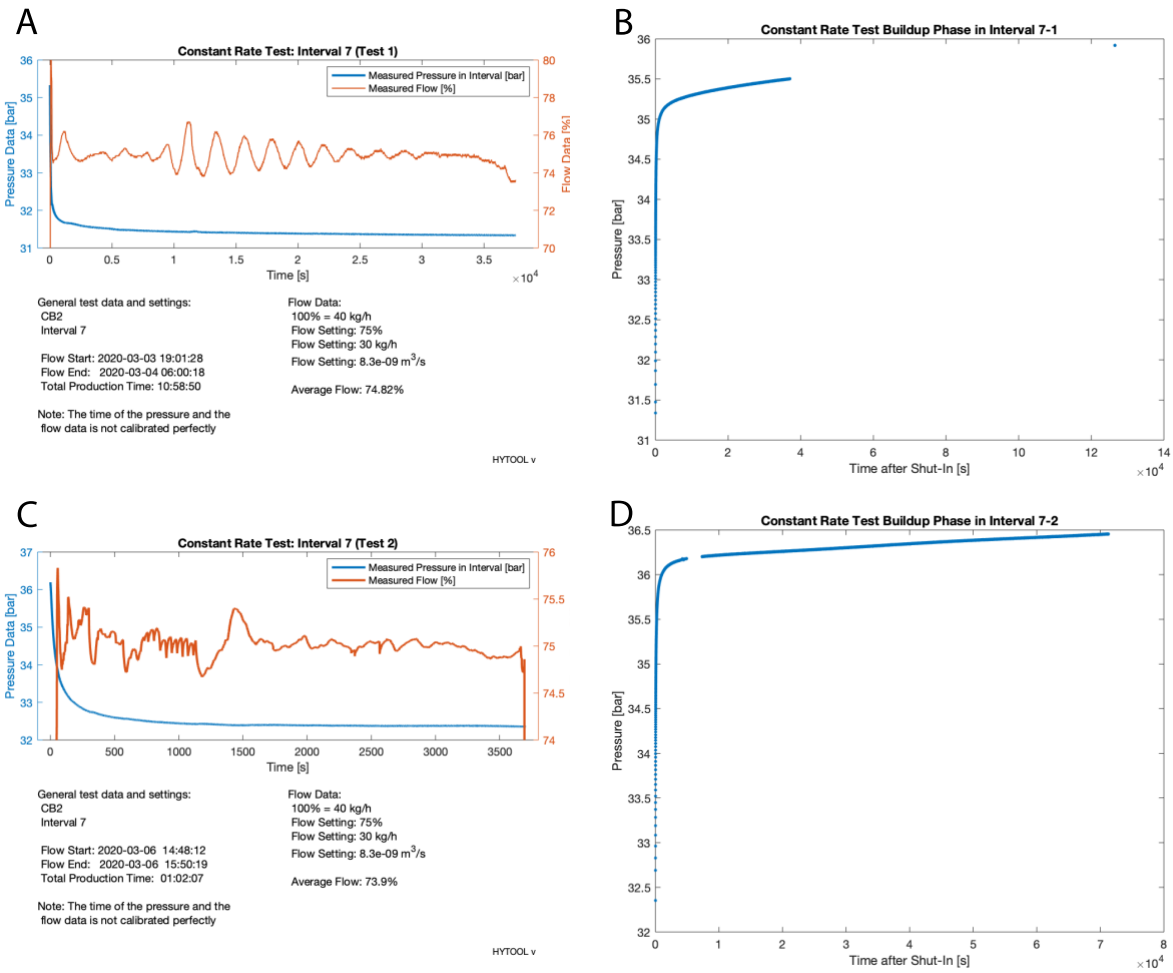

Fig. 10.18. Pressure curve of drawdown phase with flow rates and buildup phase of constant rate tests in Interval 7-1 (A,B) and Interval 7-2 (C,D).

Appendix L: Results of single well test analyses of the constant rate tests

Tab. 10.5. Results of the single well test analyses of the constant rate tests performed in CB1, CB3 and the intervals in CB2 analyzed with the Theis (1935) solution.

Interval / Borehole	Transmissivity (T) [m^2/s]		Storativity (S) [–]		Radius of Investigation R_i [m]		Mean Residual of Fit [m]		2*Standard Deviation of Mean Residual [m]	
	Drawdown	Buildup	Drawdown	Buildup	Draw-down	Build-up	Draw-down	Build-up	Draw-down	Build-up
CB1	$1.5 \cdot 10^{-6}$	$1.4 \cdot 10^{-6}$	$4.2 \cdot 10^{-3}$	$4.6 \cdot 10^{-3}$	9.6	9.8	0.44	0.26	0.61	0.39
CB3	$4.1 \cdot 10^{-7}$	$4. \cdot 10^{-7}$	$1.5 \cdot 10^{-3}$	$9.4 \cdot 10^{-4}$	3.6	12	0.43	-1.2	1.1	2.8
1	$1.4 \cdot 10^{-10}$	$1.4 \cdot 10^{-10}$	$4.5 \cdot 10^{-5}$	$4.3 \cdot 10^{-5}$	1.3	1.7	-1.7	-2.2	7.6	7.8
2	$4.1 \cdot 10^{-11}$	$4.4 \cdot 10^{-11}$	$1.1 \cdot 10^{-5}$	$1.1 \cdot 10^{-5}$	11	0.79	-1.9	-4	13	18
3	$1.1 \cdot 10^{-8}$	$8.4 \cdot 10^{-9}$	$3.7 \cdot 10^{-4}$	$1.1 \cdot 10^{-3}$	1.5	0.73	-0.27	0.13	2	0.45
4-1	$1.4 \cdot 10^{-8}$	$1.5 \cdot 10^{-8}$	$1.5 \cdot 10^{-5}$	$1.3 \cdot 10^{-5}$	11	15	-4.9	-5.9	7.9	9.4
4-2	$1.7 \cdot 10^{-8}$	$1.3 \cdot 10^{-8}$	$3.9 \cdot 10^{-6}$	$2.6 \cdot 10^{-5}$	22	2.5	-5.4	-1.8	9.5	4.6
4-3	$1.2 \cdot 10^{-8}$	$1.2 \cdot 10^{-8}$	$1.2 \cdot 10^{-5}$	$7.3 \cdot 10^{-6}$	6.8	24	-5.7	-14	13	19
5&6	$8.4 \cdot 10^{-8}$	$8.5 \cdot 10^{-8}$	$9.7 \cdot 10^{-3}$	$1.7 \cdot 10^{-2}$	0.61	0.83	0.12	-0.0093	2.3	2.9
7-1	$2.1 \cdot 10^{-7}$	$1.8 \cdot 10^{-7}$	$4.3 \cdot 10^{-6}$	$2.1 \cdot 10^{-5}$	80	36	-2.9	-3.1	4.1	4.4
7-2	$1.2 \cdot 10^{-7}$	$2.0 \cdot 10^{-7}$	$1.5 \cdot 10^{-4}$	$8.5 \cdot 10^{-6}$	2.4	83	-2.4	-3.7	6.5	4

Tab. 10.6. Results of the single well test analyses of the constant rate tests performed in CB1, CB3 and the intervals in CB2 analyzed with the GRF model (Barker, 1988).

Interval / Borehole	Transmissivity (T) [m^2/s]		Storativity (S) [–]		Flow Dimension (n) [–]		Mean Residual of Fit [m]		2*Standard Deviation of Mean Residual [m]	
	Drawdown	Buildup	Drawdown	Buildup	Draw-down	Build-up	Draw-down	Build-up	Draw-down	Build-up
CB1	$2.8 \cdot 10^{-6}$	$2.2 \cdot 10^{-6}$	$1.5 \cdot 10^{-3}$	$2.1 \cdot 10^{-3}$	1.8	1.9	-0.0883	-0.14	0.748	0.764
CB3	$5.7 \cdot 10^{-7}$	$3.7 \cdot 10^{-8}$	$9.8 \cdot 10^{-4}$	$1.3 \cdot 10^{-3}$	1.9	2.1	-0.00004	-0.437	0.265	1.82
1	$8.7 \cdot 10^{-11}$	$8.3 \cdot 10^{-11}$	$6.1 \cdot 10^{-5}$	$6.3 \cdot 10^{-5}$	2.4	2.4	-0.428	-0.408	3.33	2.2
2	$1.4 \cdot 10^{-11}$	$1.2 \cdot 10^{-11}$	$2.1 \cdot 10^{-5}$	$2.3 \cdot 10^{-5}$	3.2	3.4	0.0821	0.0396	3.38	2.68
3	$8.6 \cdot 10^{-9}$	$6.9 \cdot 10^{-9}$	$4.5 \cdot 10^{-4}$	$1.42 \cdot 10^{-3}$	2.2	2.1	0.0137	-0.0136	1.79	0.71
4-1	$9.5 \cdot 10^{-9}$	$4.9 \cdot 10^{-9}$	$1.5 \cdot 10^{-5}$	$5.6 \cdot 10^{-5}$	2.2	2.6	-0.0265	-0.0336	4.84	0.252
4-2	$2.0 \cdot 10^{-9}$	$5.4 \cdot 10^{-9}$	$9.2 \cdot 10^{-5}$	$6.4 \cdot 10^{-5}$	3.7	2.6	-0.5	-0.103	1.6	0.403
4-3	$4.8 \cdot 10^{-9}$	$3.4 \cdot 10^{-9}$	$3.8 \cdot 10^{-5}$	$4.6 \cdot 10^{-5}$	2.5	2.7	-0.799	-0.462	2.18	0.87
5&6	$1.3 \cdot 10^{-7}$	$4.1 \cdot 10^{-8}$	$9.8 \cdot 10^{-3}$	$2.9 \cdot 10^{-2}$	1.6	2.6	0.0274	0.0282	1.71	1.46
7-1	$5.4 \cdot 10^{-8}$	$4.6 \cdot 10^{-8}$	$8.1 \cdot 10^{-5}$	$2.7 \cdot 10^{-4}$	2.6	2.7	-0.0748	-0.328	0.244	0.702
7-2	$2.7 \cdot 10^{-8}$	$4.2 \cdot 10^{-8}$	$5.5 \cdot 10^{-4}$	$2.6 \cdot 10^{-}$	3.2	2.8	-0.2	-0.107	0.774	0.827

Appendix M: Horner plots, with manual linear fit on late time data

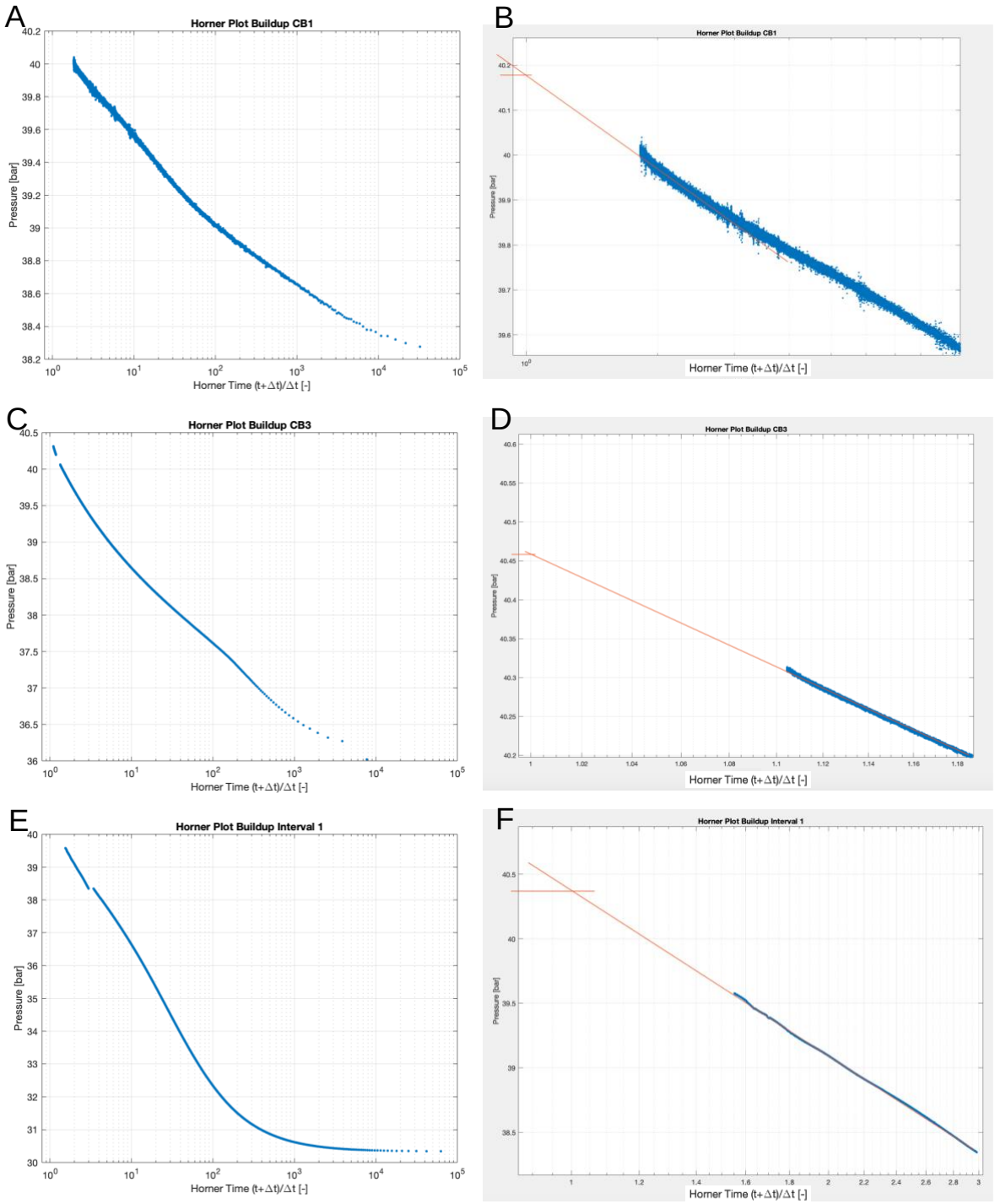

Fig. 10.19. Horner plots and late time section of Horner plots with manual linear fit for the constant rate test in CB1 (A,B), CB3 (C,D) and Interval 1 (E,F).

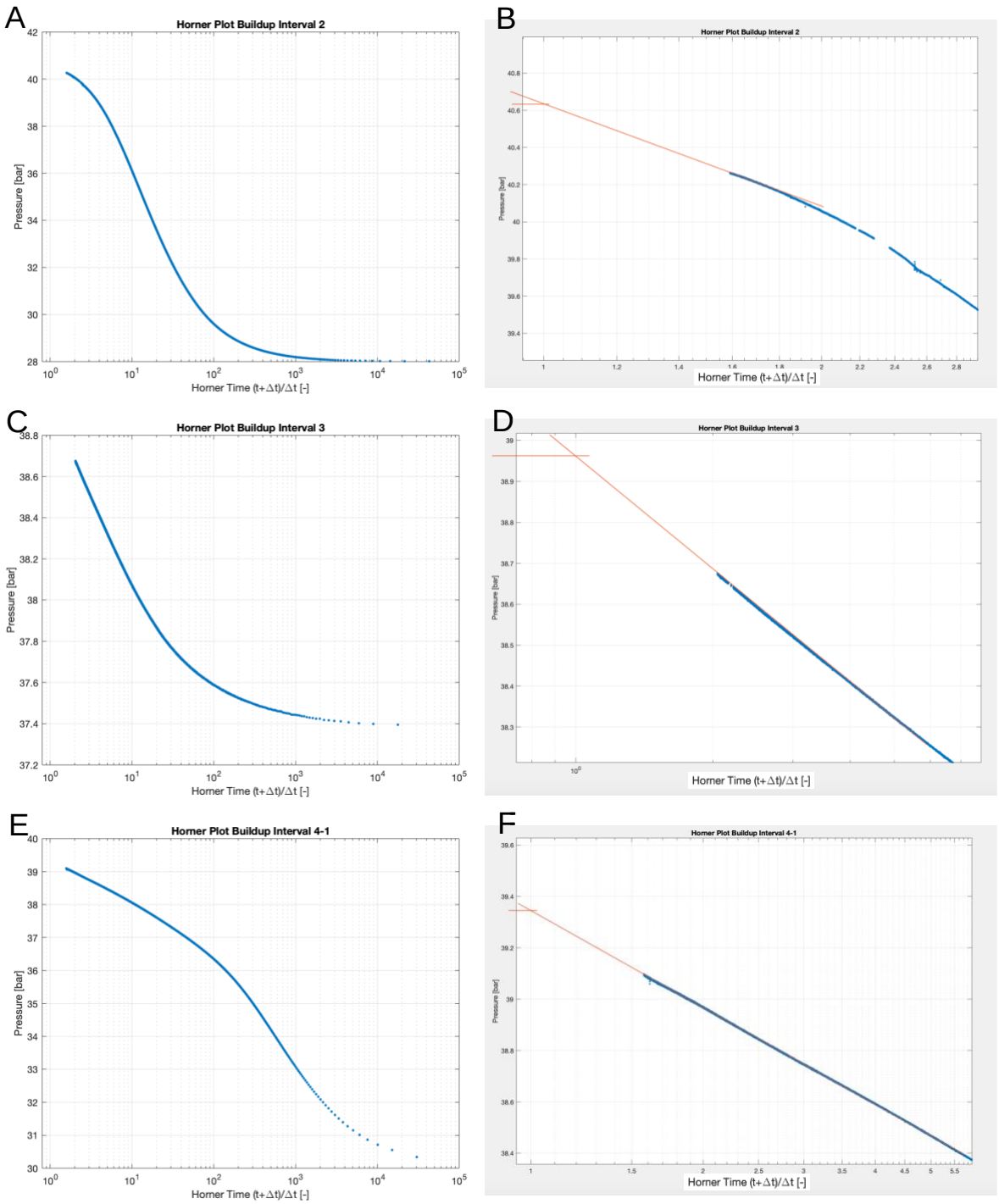

Fig. 10.20. Horner plots and late time section of Horner plots with manual linear fit for the constant rate test in Interval 2 (A,B), Interval 3 (C,D) and Interval 4-1 (E,F).

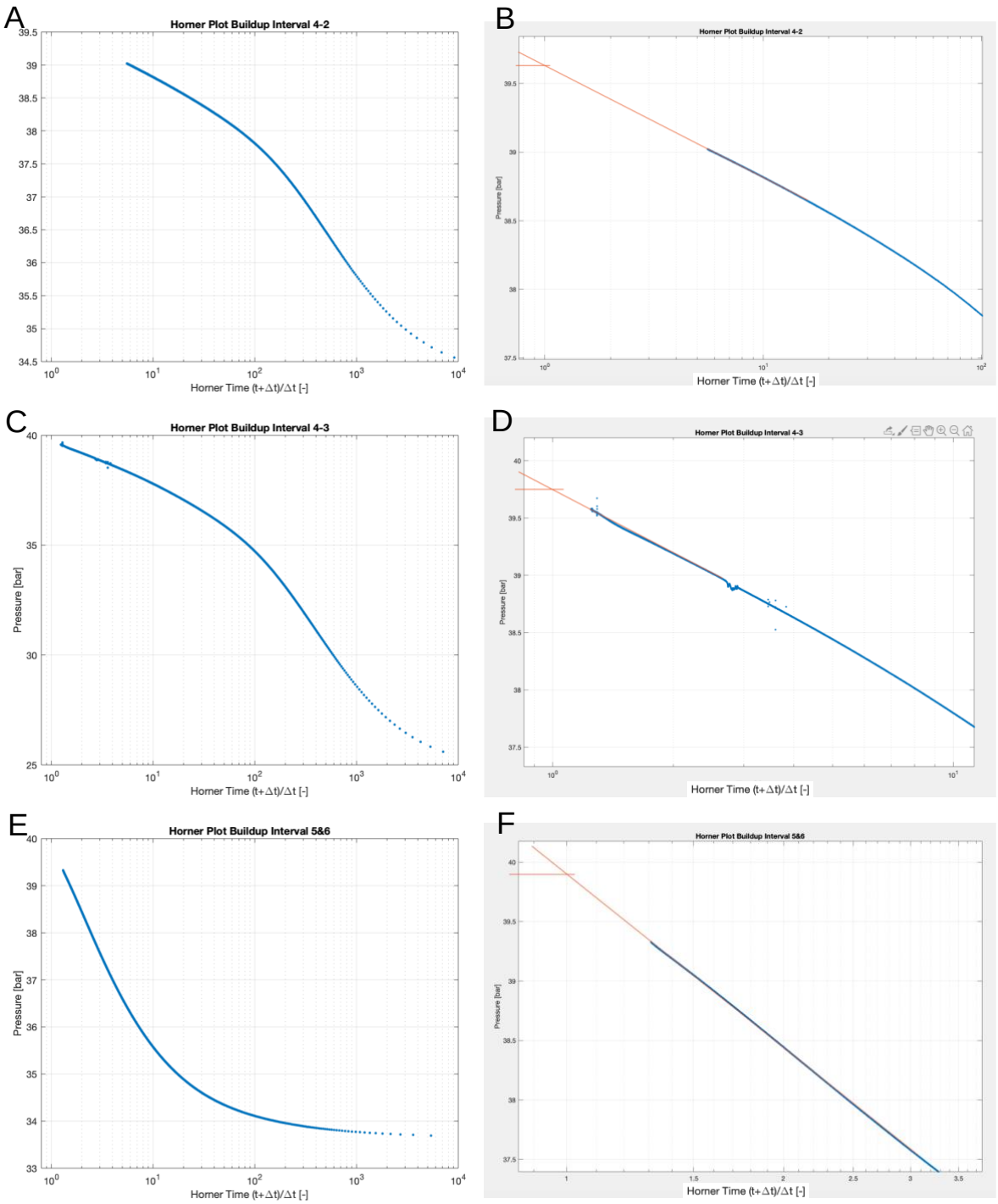

Fig. 10.21. Horner plots and late time section of Horner plots with manual linear fit for the constant rate test in Interval 4-2 (A,B), Interval 4-3 (C,D) and Interval 5&6 (E,F).

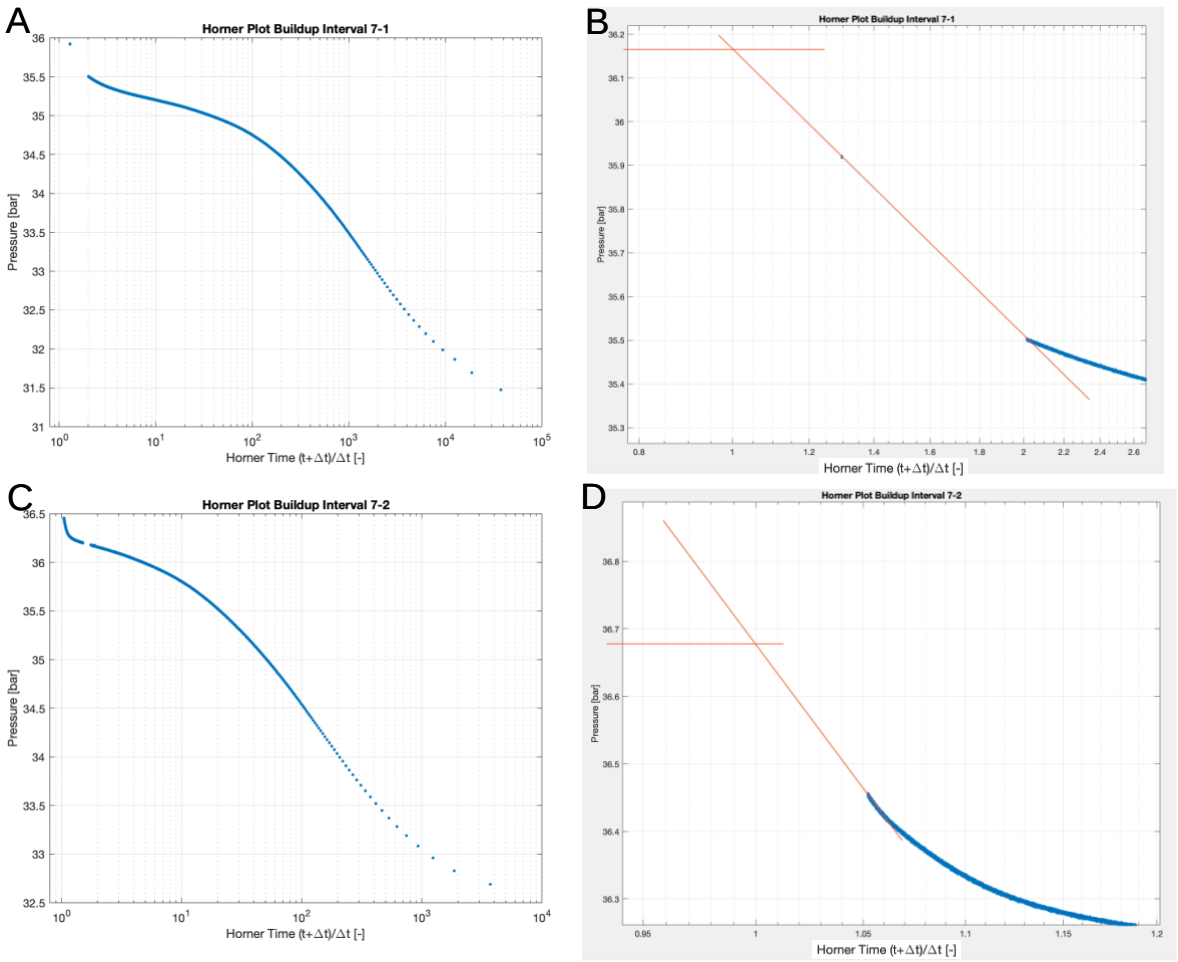

Fig. 10.22. Horner plots and late time section of Horner plots with manual linear fit for the constant rate test in Interval 7-1 (A,B) and Interval 7-2 (C,D).

Appendix N: Diagnostic plots, single well test, drawdown

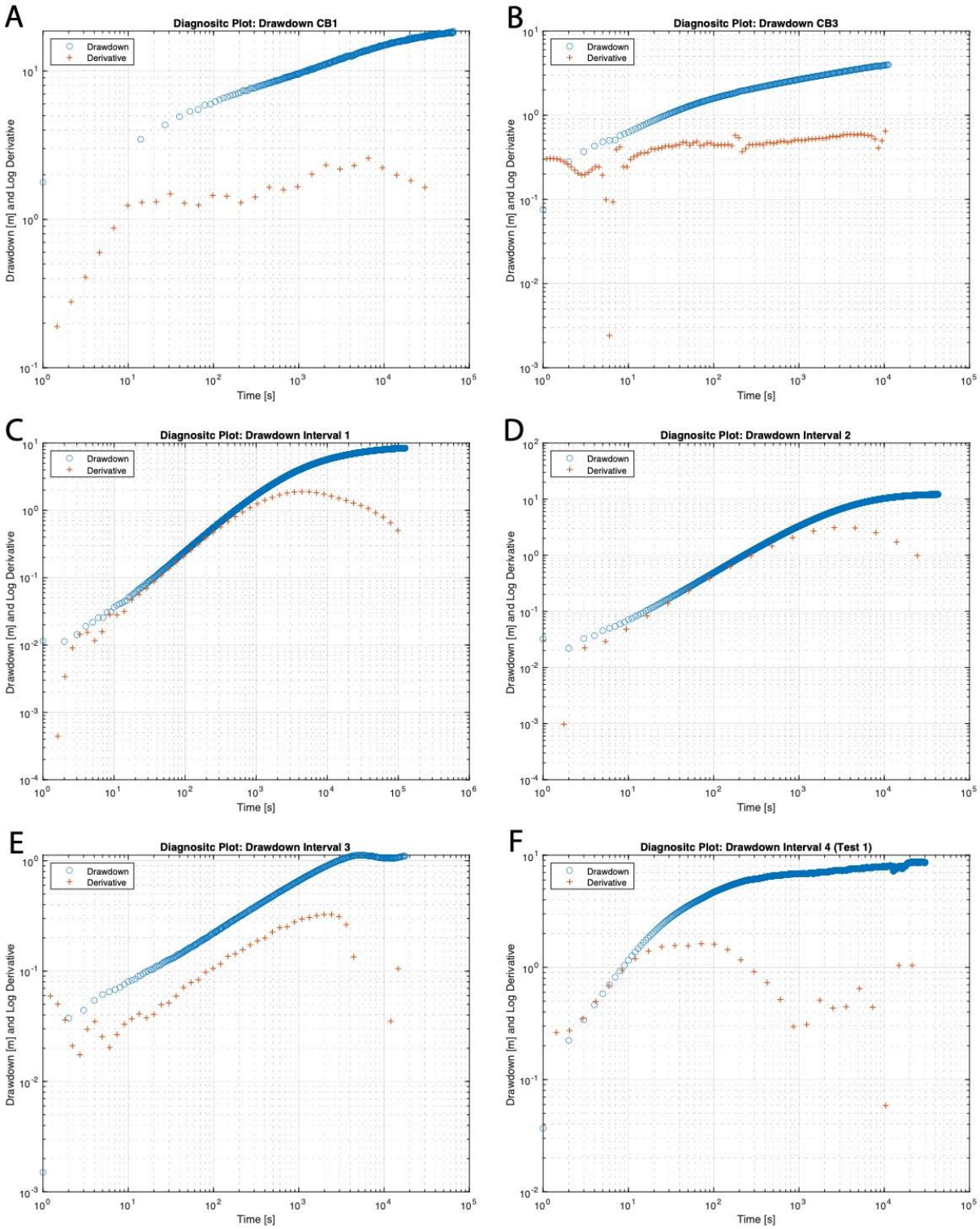

Fig. 10.23. Diagnostic plots for single well test analysis of the drawdown phases of the constant rate test in CB1 (A), CB3 (B), Interval 1 (C), Interval 2 (D), Interval 3 (E), and Interval 4-1 (F).

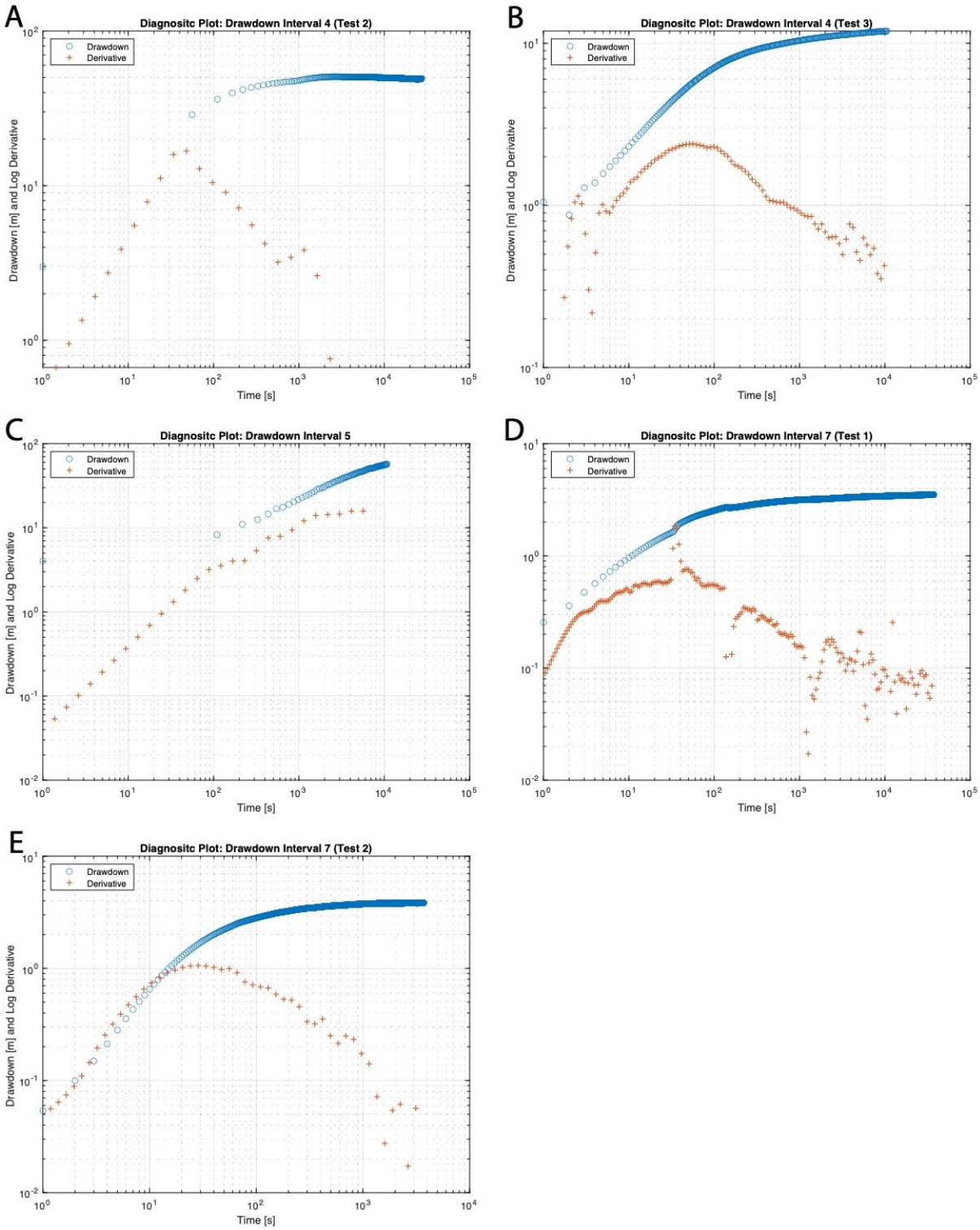

Fig. 10.24. Diagnostic plots for single well test analysis of the drawdown phases of the constant rate test in Interval 4-2 (A), Interval 4-3 (B), Interval 5&6 (C), Interval 7-1 (D) and Interval 7-2 (E).

Appendix O: Diagnostic plots, single well test, buildup

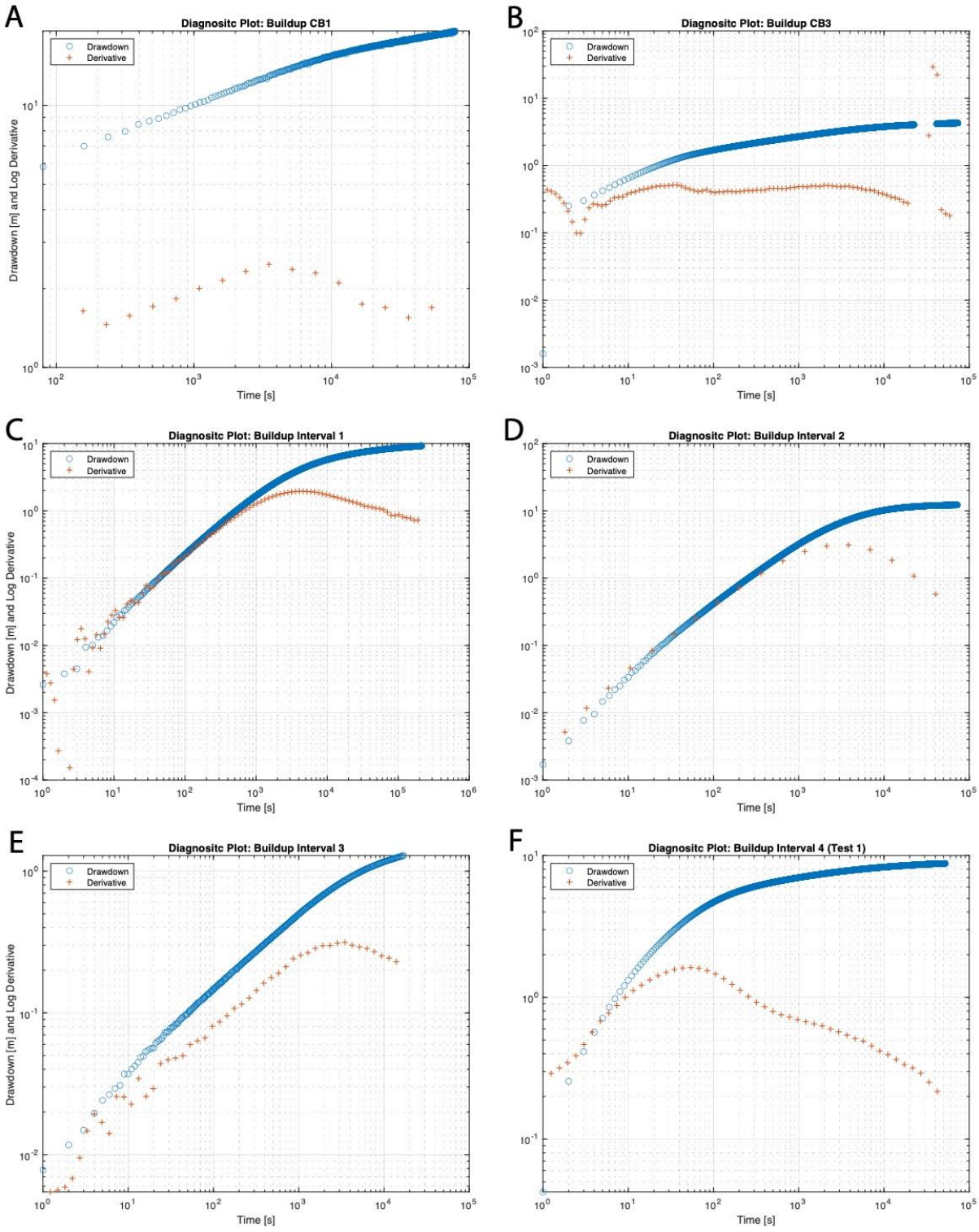

Fig. 10.25. Diagnostic plots for single well test analysis of the buildup phases of the constant rate test in CB1 (A), CB3 (B), Interval 1 (C), Interval 2 (D), Interval 3 (E), and Interval 4-1 (F).

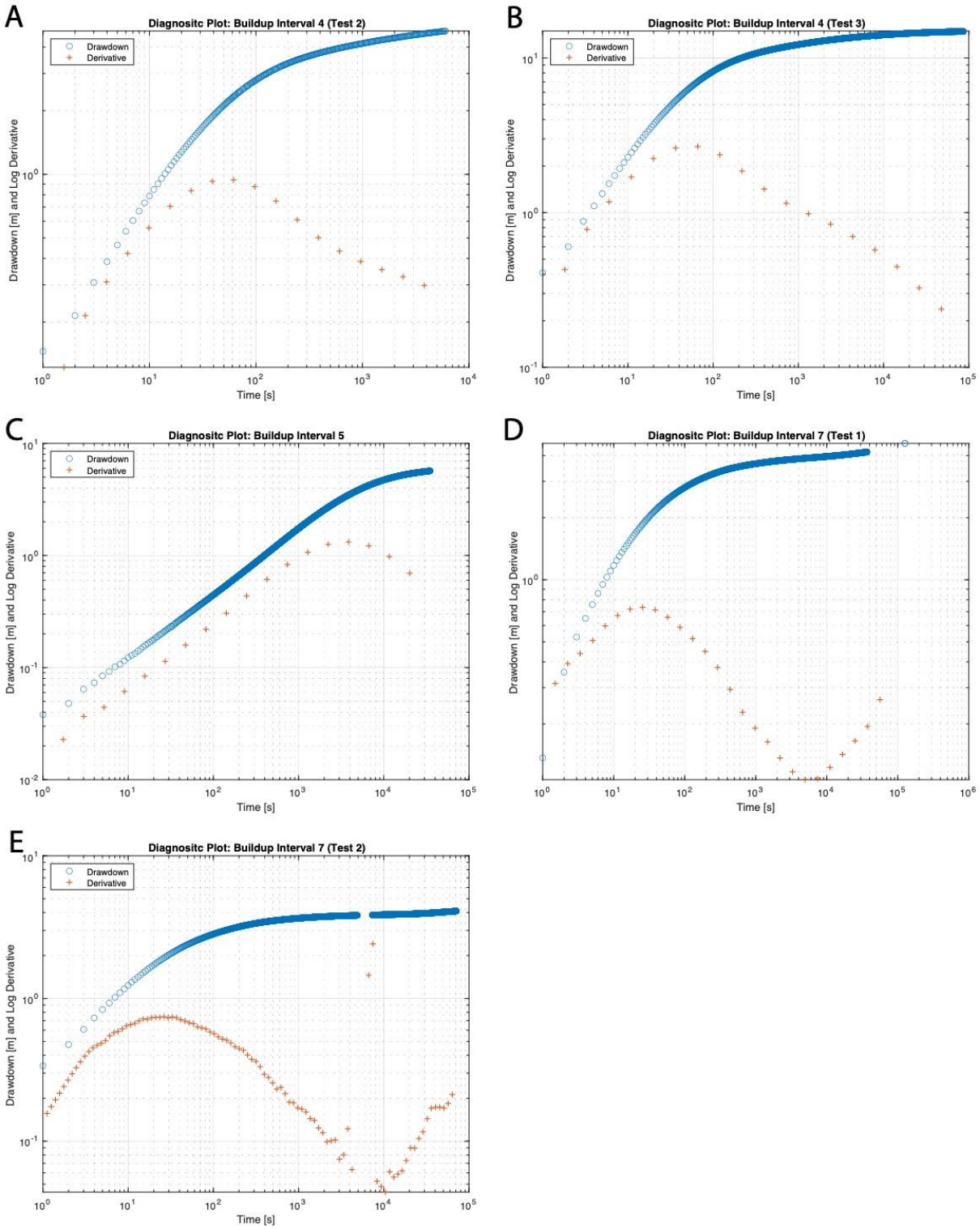

Fig. 10.26. Diagnostic plots for single well test analysis of the buildup phases of the constant rate test in Interval 4-2 (A), Interval 4-3 (B), Interval 5&6 (C), Interval 7-1 (D) and Interval 7-2 (E).

Appendix P: Pressure Responses to constant rate tests

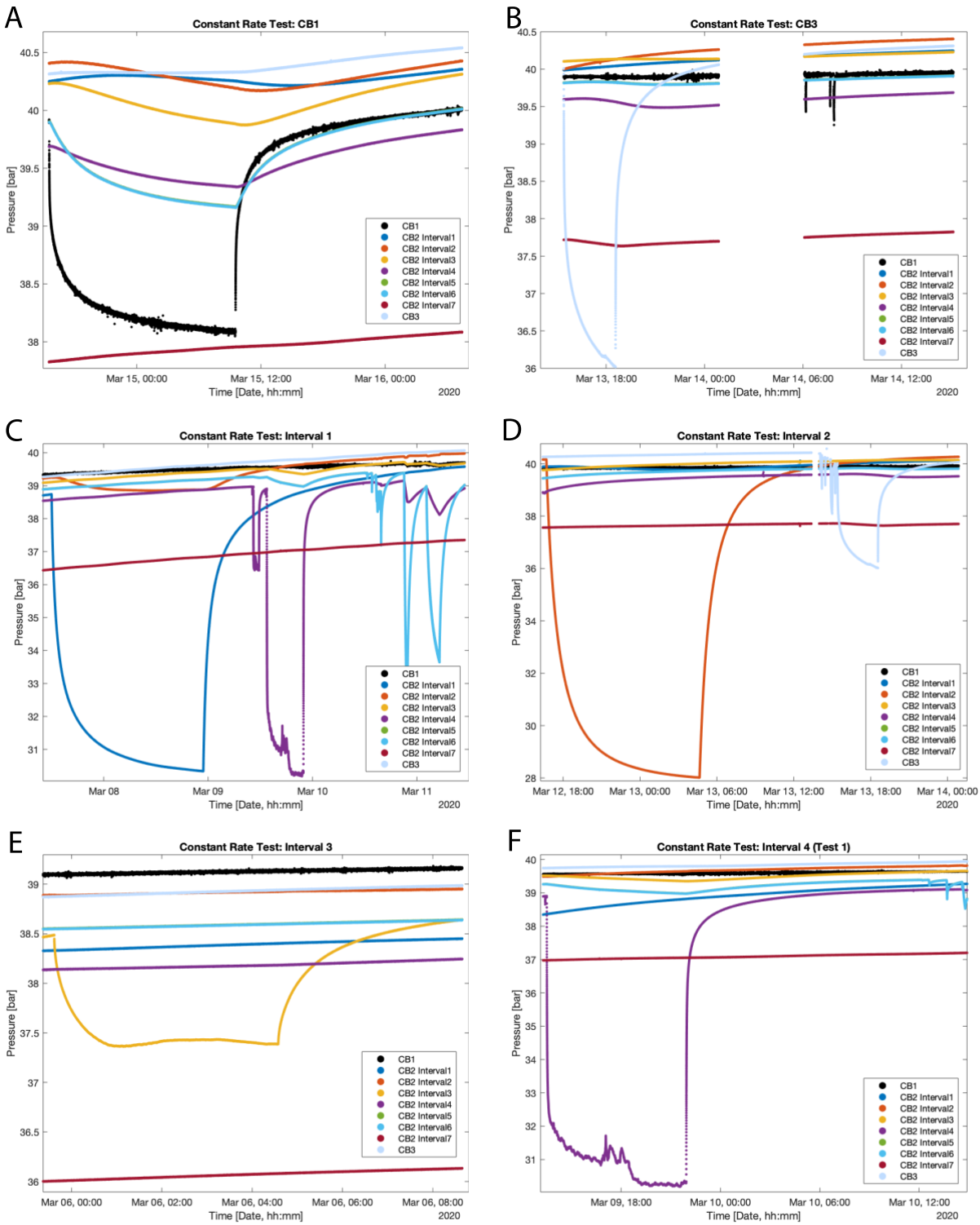

Fig. 10.27. Pressure curve from constant rate tests in CB1 (A), CB3 (B), Interval 1 (C), Interval 2 (D), Interval 3 (E), and Interval 4-1 (F).

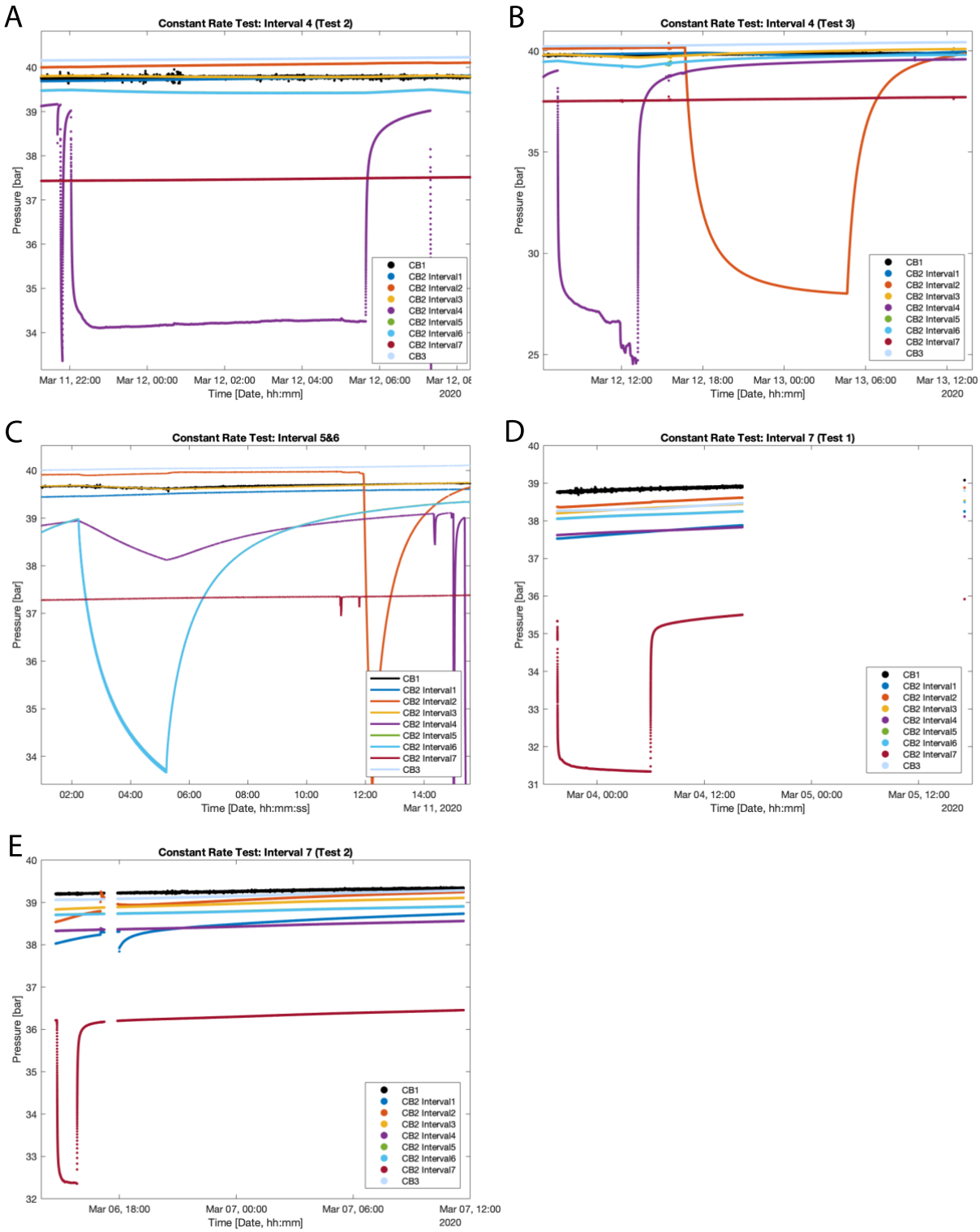

Fig. 10.28. Pressure curve from constant rate tests (drawdown and buildup) in Interval 4-2 (A), Interval 4-3 (B), Interval 5&6 (C), Interval 7-1 (D) and Interval 7-2 (E).

Appendix Q: Diagnostic plots, cross-hole responses to drawdown in CB1

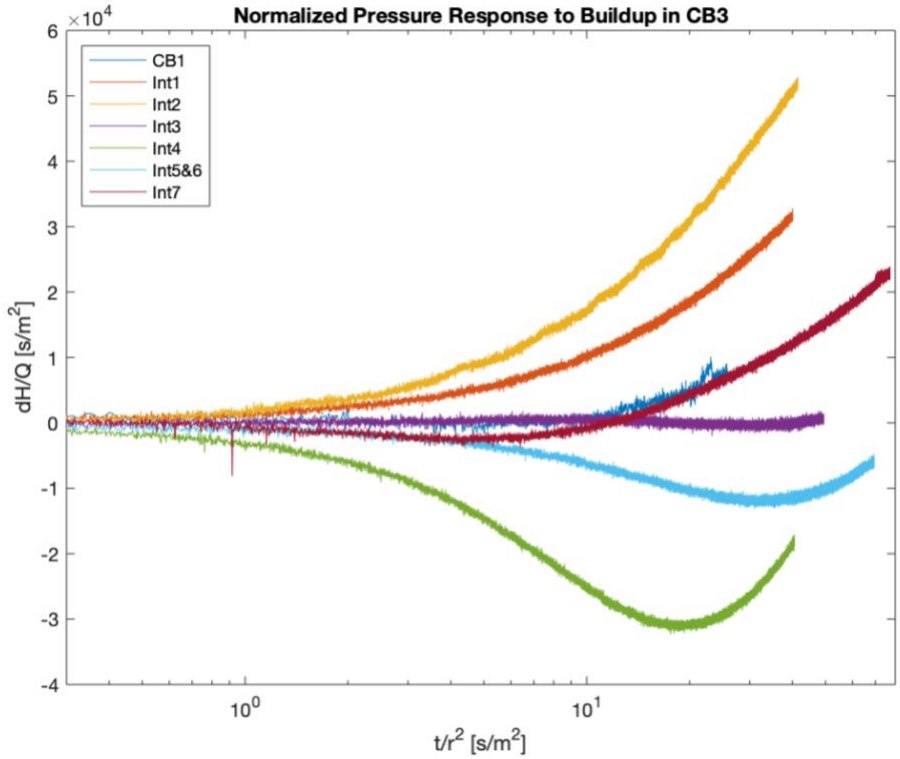

Fig. 10.29. Normalized (time by squared distance between active and observation borehole/interval; differential head by production rate) pressure response plot for the responses to the buildup in CB3.

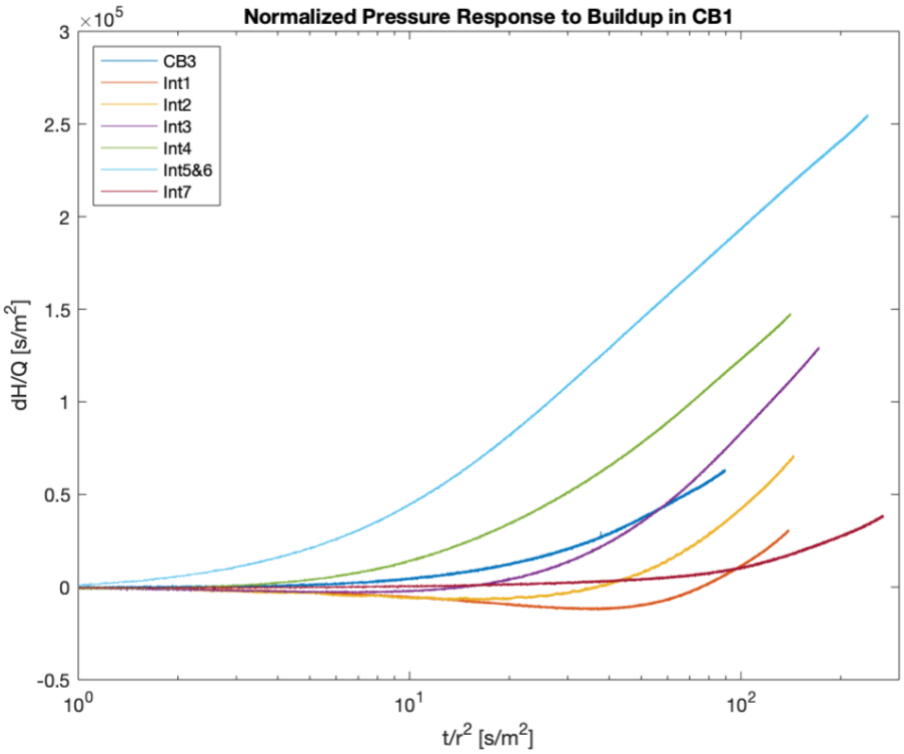

Fig. 10.30. Normalized (time by squared distance between active and observation borehole/interval; differential head by production rate) pressure response plot for the responses to the buildup in CB1.

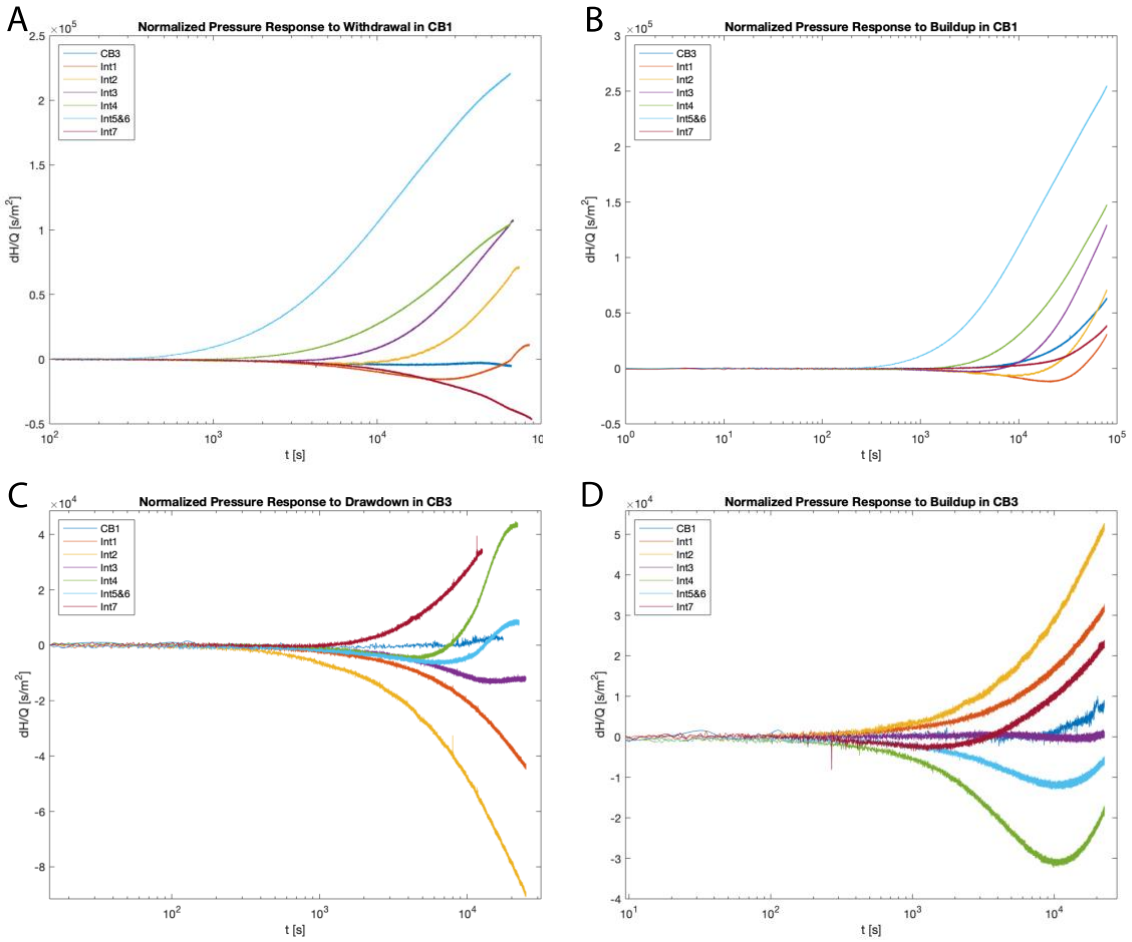

Fig. 10.31. Normalized (differential head by production rate) pressure response plot for the responses to the drawdown and the buildup phase in CB1 and CB3, respectively.

Appendix R: Diagnostic plots, cross-hole responses to drawdown in CB1

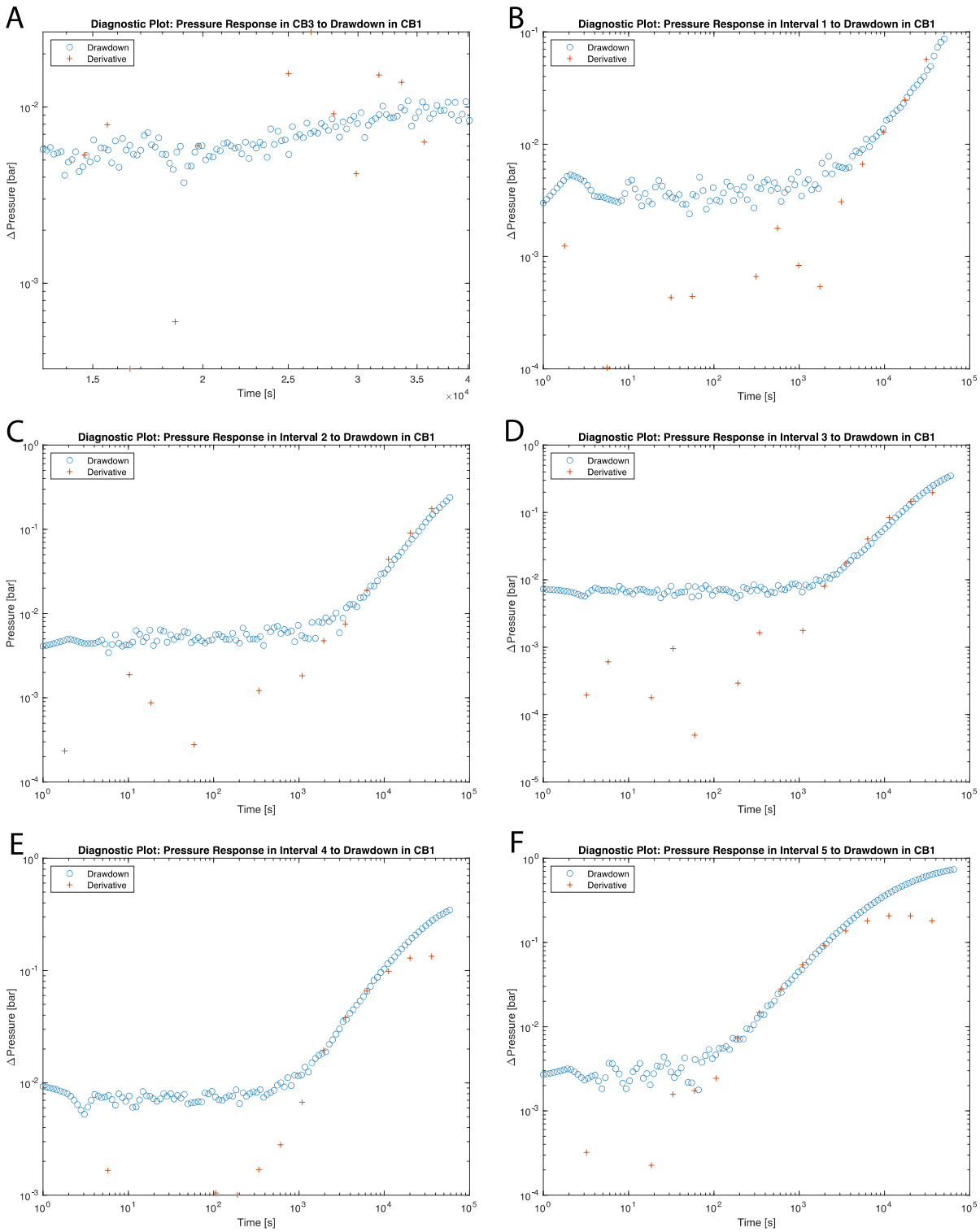

Fig. 10.32. Diagnostic plots for the cross-hole responses in CB3 (A), Interval 1 (B), Interval 2 (C), Interval 3 (D), Interval 4 (E) and Interval 5&6 (F) to the drawdown in CB1.

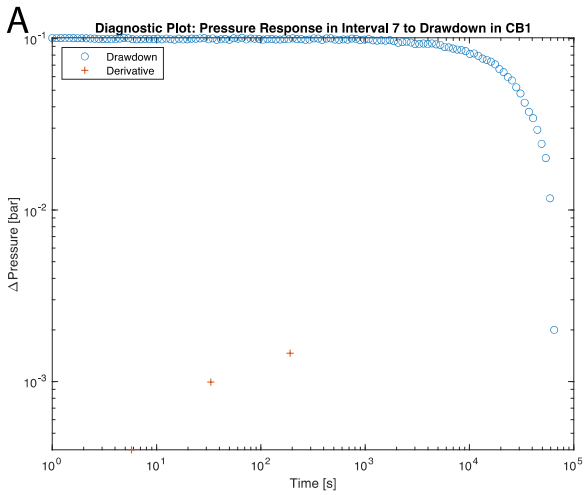

Fig. 10.33. Diagnostic plots for the cross-hole responses in Interval 7 (A) to the drawdown in CB1.

Appendix S: Diagnostic plots, cross-hole responses to buildup in CB1

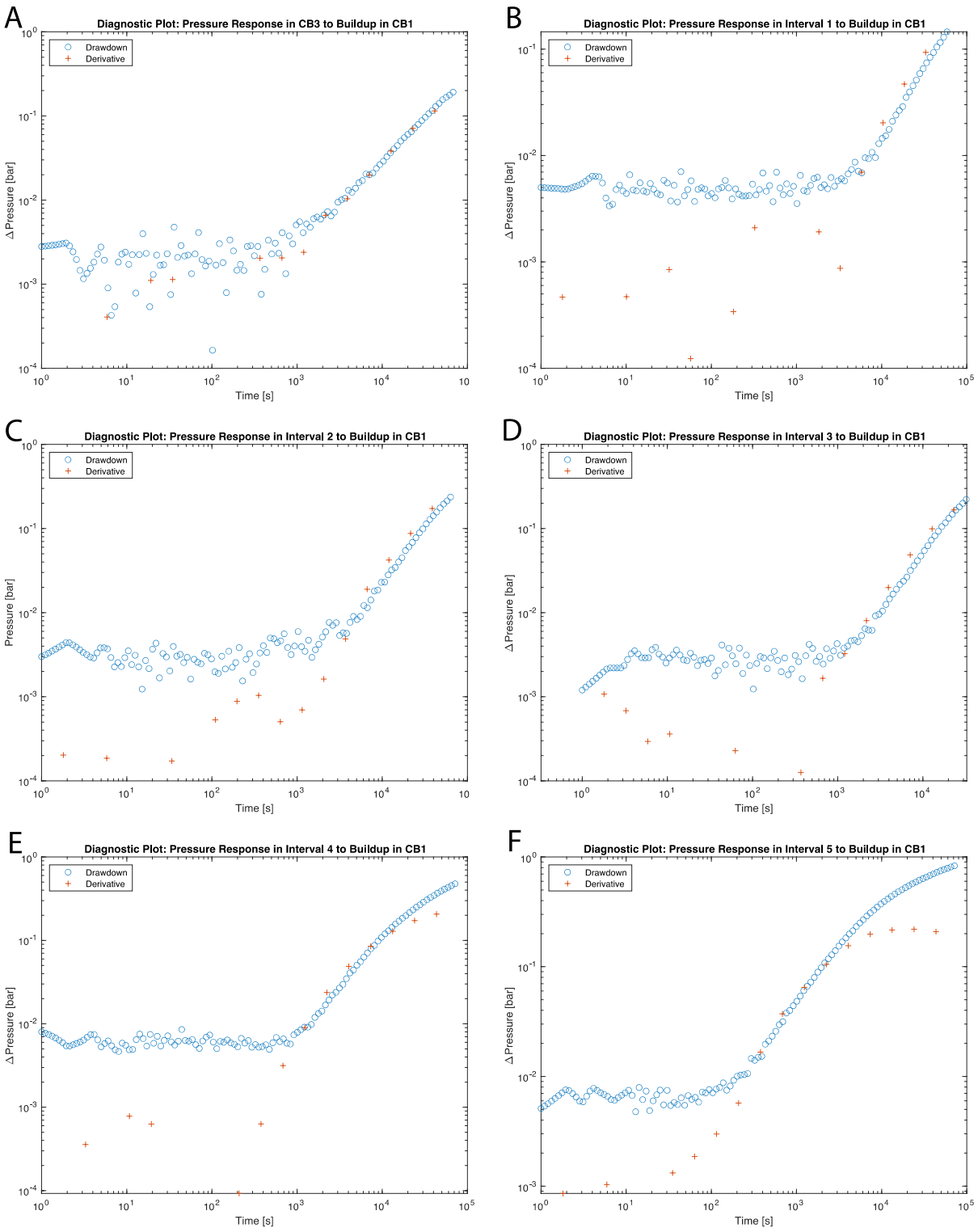

Fig. 10.34. Diagnostic plots from the cross-hole responses to the buildup in CB1 for CB3 (A), Interval 1 (B), Interval 2 (C), Interval 3 (D), Interval 4 (E) and Interval 5&6 (F).

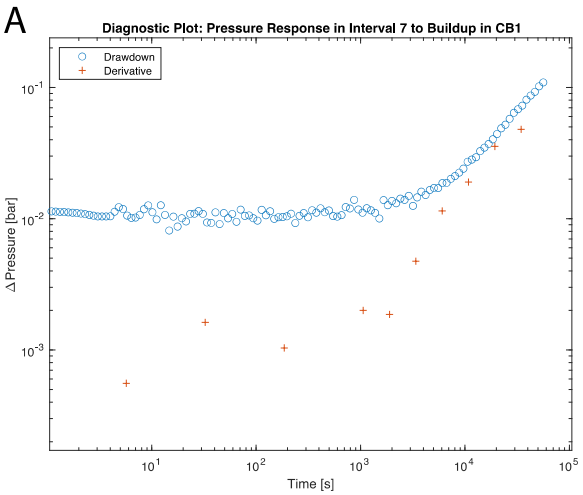

Fig. 10.35. Diagnostic plots from the cross-hole responses to the buildup in CB1 for Interval 7 (A).

Appendix T: Diagnostic plots, cross-hole responses to drawdown in CB3

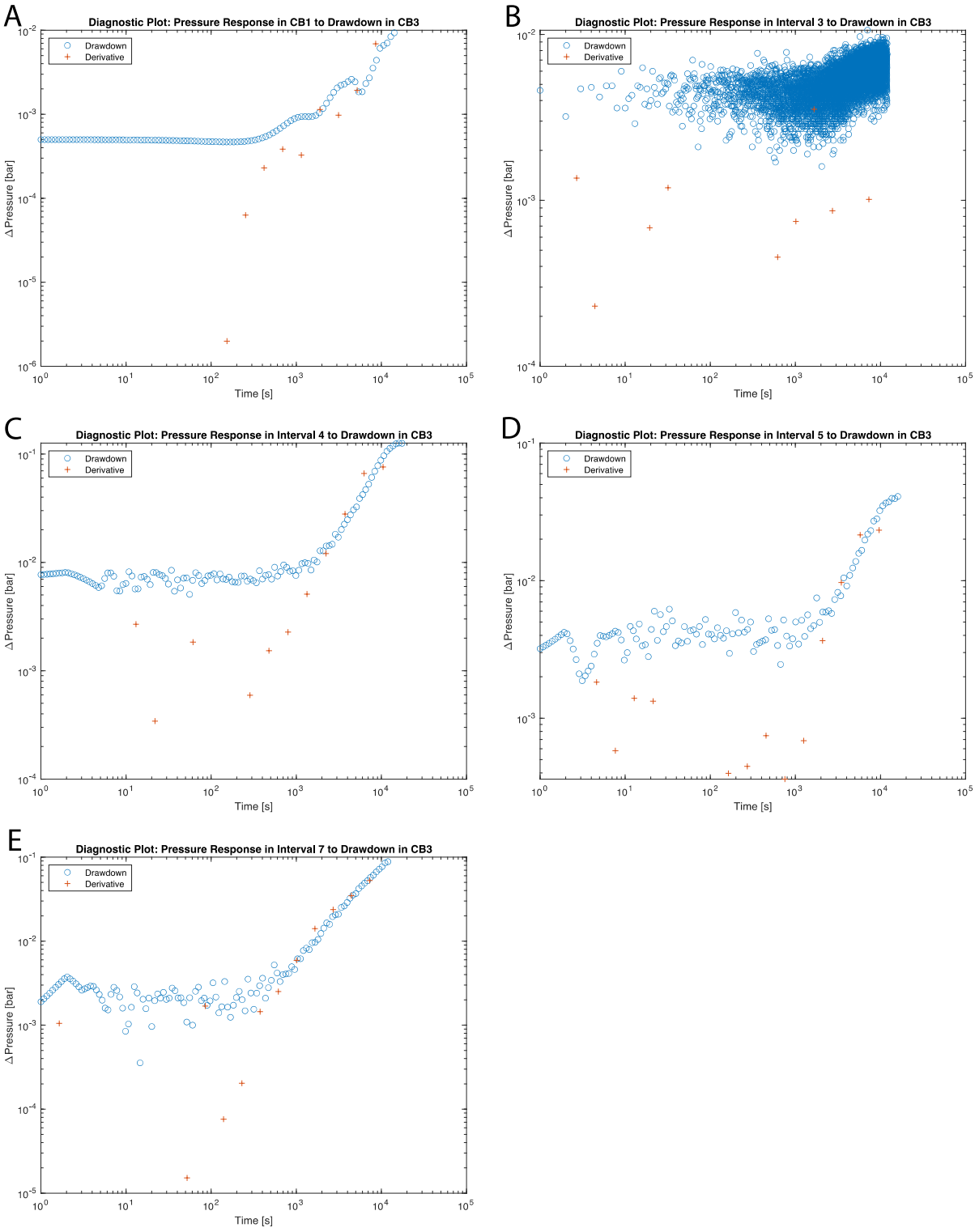

Fig. 10.36. Diagnostic plots from the cross-hole responses to the drawdown in CB3 for CB1 (A), Interval 3 (B), Interval 4 (C), Interval 5&6 (D) and Interval 7 (E).

Appendix U: Diagnostic plots, cross-hole responses to buildup in CB3

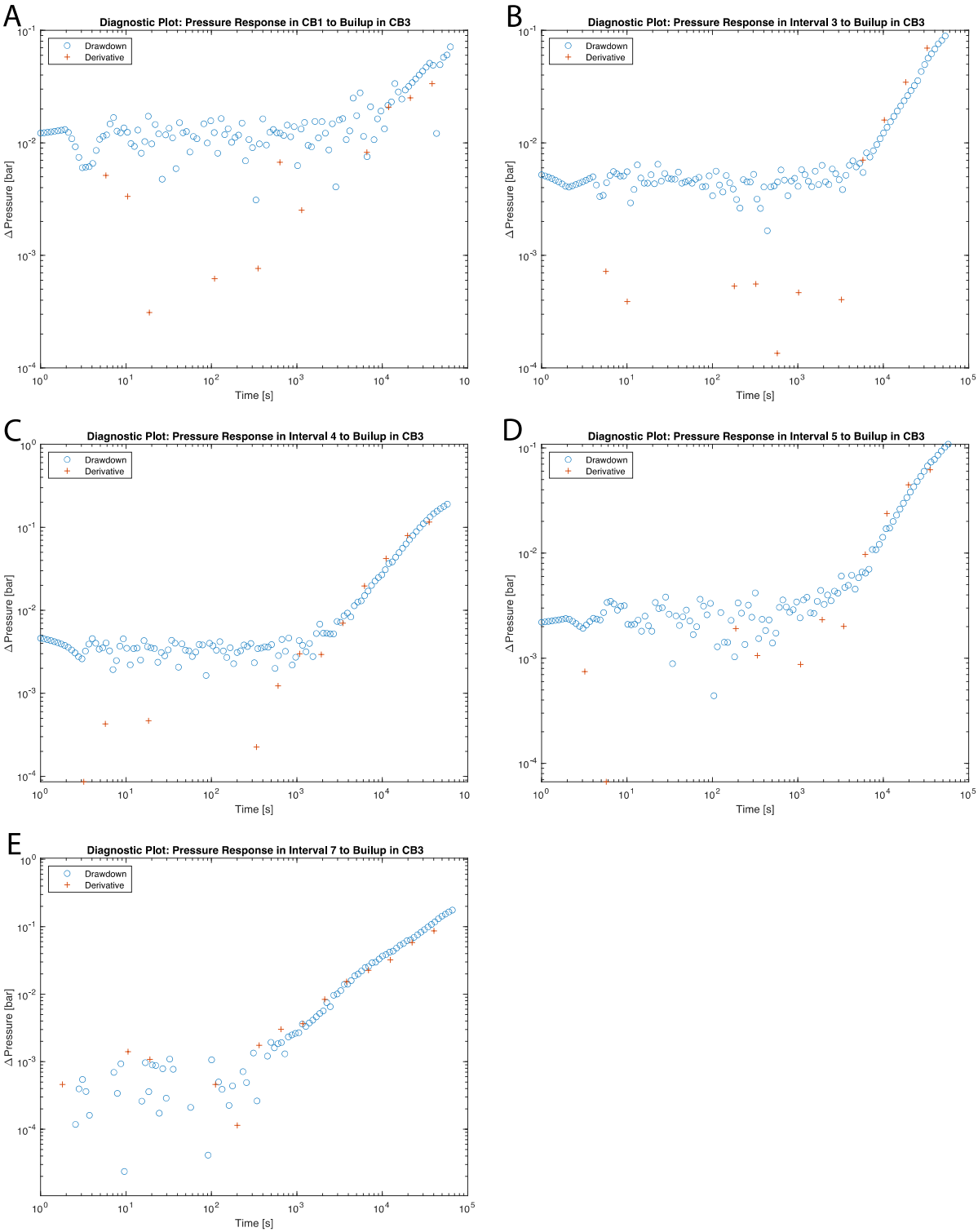

Fig. 10.37. Diagnostic plots from the cross-hole responses to the buildup in CB3 for CB1 (A), Interval 3 (B), Interval 4 (C), Interval 5&6 (D) and Interval 7 (E).

Appendix V: Transmissivity and storativity values from cross-hole responses analyses

Tab. 10.7. Results of the analyses of the cross-hole responses (drawdown/buildup) in CB1, CB3 and the intervals in CB2 to the constant rate tests in CB1 resp. CB3, analyzed Theis (1935) solution.

Interval / Borehole	Transmissivity (T) [m^2/s]				Storativity (S) [–]			
	Drawdown in CB1	Buildup in CB1	Drawdown in CB3	Buildup in CB3	Drawdown in CB1	Buildup in CB1	Drawdown in CB3	Buildup in CB3
CB1	s	s	t	$6.0 \cdot 10^{-6}$	s	s	t	$3.4 \cdot 10^{-4}$
CB3	t	$1.5 \cdot 10^{-6}$	s	s	t	$1.6 \cdot 10^{-4}$	S	s
1	t	$1.4 \cdot 10^{-6}$	t	n	t	$3.2 \cdot 10^{-3}$	t	n
2	t	$9.7 \cdot 10^{-7}$	t	n	t	$1.9 \cdot 10^{-4}$	t	n
3	t	$8.3 \cdot 10^{-7}$	t	$1.6 \cdot 10^{-6}$	t	$2.6 \cdot 10^{-4}$	t	$6.7 \cdot 10^{-5}$
4	$1.6 \cdot 10^{-6}$	$1.1 \cdot 10^{-6}$	t	$1.2 \cdot 10^{-6}$	$5.6 \cdot 10^{-4}$	$5.1 \cdot 10^{-4}$	t	$3.8 \cdot 10^{-5}$
5&6	$1.2 \cdot 10^{-6}$	$1.1 \cdot 10^{-6}$	t	$1.9 \cdot 10^{-6}$	$5.9 \cdot 10^{-5}$	$5.7 \cdot 10^{-5}$	t	$1.0 \cdot 10^{-4}$
7	t	$3.3 \cdot 10^{-6}$	t	$1.9 \cdot 10^{-6}$	t	$7.9 \cdot 10^{-3}$	t	$1.2 \cdot 10^{-4}$

s: single well test; t: too short data for IARF; n: no response observed

*Tab. 10.8. Mean residuals and their 2*standard deviations for the curve fitting to data from the cross-hole responses (drawdown/buildup) in CB1, CB3 and the intervals in CB2 to the constant rate tests in CB1 and CB3, respectively, analyzed Theis (1935) solution.*

Interval / Borehole	Mean Residual [m]				2*Standard Deviation of Mean Residual			
	Drawdown in CB1	Buildup in CB1	Drawdown in CB3	Buildup in CB3	Drawdown in CB1	Buildup in CB1	Drawdown in CB3	Buildup in CB3
CB1	s	s	t	0.0065	s	s	t	0.12
CB3	t	0.0055	s	s	t	0.074	S	s
1	t	0.0018	t	n	t	0.048	t	n
2	t	0.0062	t	n	t	0.097	t	n
3	t	0.0099	t	0.0023	t	0.091	t	0.028
4	0.0063	0.013	t	0.0037	0.074	0.12	t	0.046
5&6	-0.012	-0.0034	t	0.0026	0.23	0.091	t	0.033
7	t	0.0035	t	0.017	t	0.063	t	0.16

s: single well test; t: too short data for IARF; n: no response observed

Tab. 10.9. Results of the analyses of the cross-hole responses (drawdown/buildup) in CB1, CB3 and the intervals in CB2 to the constant rate tests in CB1 resp. CB3, analyzed Agarwal et al. (1970) solution.

Interval	Transmissivity (T) [m^2/s]				Storativity (S) [–]			
	Drawdown in CB1	Buildup in CB1	Drawdown in CB3	Buildup in CB3	Drawdown in CB1	Buildup in CB1	Drawdown in CB3	Buildup in CB3
CB1	s	s	t	$5.7 \cdot 10^{-6}$	s	s	t	$3.4 \cdot 10^{-4}$
CB3	t	$1.2 \cdot 10^{-6}$	s	s	t	$1.7 \cdot 10^{-4}$	s	s
1	t	$2.2 \cdot 10^{-6}$	t	n	t	$6.8 \cdot 10^{-5}$	t	n
2	t	$1.7 \cdot 10^{-6}$	t	n	t	$2.2 \cdot 10^{-5}$	t	n
3	t	$1.9 \cdot 10^{-6}$	t	$2.8 \cdot 10^{-6}$	t	$3.8 \cdot 10^{-5}$	t	$2.2 \cdot 10^{-5}$
4	$1.5 \cdot 10^{-6}$	$1.1 \cdot 10^{-6}$	t	$2.5 \cdot 10^{-6}$	$5.7 \cdot 10^{-4}$	$5.2 \cdot 10^{-4}$	t	$1.0 \cdot 10^{-5}$
5&6	$1.4 \cdot 10^{-6}$	$1.2 \cdot 10^{-6}$	t	$1.6 \cdot 10^{-6}$	$3.5 \cdot 10^{-5}$	$4.1 \cdot 10^{-5}$	t	$1.0 \cdot 10^{-4}$
7	t	$2.9 \cdot 10^{-6}$	t	$1.6 \cdot 10^{-6}$	t	$8.5 \cdot 10^{-3}$	t	$1.3 \cdot 10^{-4}$

s: single well test; t: too short data for IARF; n: no response observed

*Tab. 10.10. Mean residuals and their 2*standard deviations for the curve fitting to data from the cross-hole responses (drawdown/buildup) in CB1, CB3 and the intervals in CB2 to the constant rate tests in CB1 and CB3, respectively, analyzed Agarwal et al. (1970) solution.*

Interval / Borehole	Mean Residual [m]				2*Standard Deviation of Mean Residual			
	Drawdown in CB1	Buildup in CB1	Drawdown in CB3	Buildup in CB3	Drawdown in CB1	Buildup in CB1	Drawdown in CB3	Buildup in CB3
CB1	s	s	t	0.0048	s	s	t	0.12
CB3	t	0.0014	s	s	t	0.033	S	s
1	t	-0.0007	t	n	t	0.017	t	n
2	t	-0.0001	t	n	t	0.026	t	n
3	t	0.0013	t	0.0021	t	0.019	t	0.021
4	0.0009	0.0029	t	0.0019	0.068	0.046	t	0.031
5&6	-0.0005	-0.0011	t	0.0016	0.14	0.032	t	0.023
7	t	0.003	t	0.01	t	0.046	t	0.12

s: single well test; t: too short data for IARF; n: no response observed

Appendix W: Diffusivity values from single well test and cross-hole response analyses

Tab. 10.11. Diffusivity values obtained from the diffusion plot reading

Interval / Borehole	Diffusivity values [m^2/s] from diffusion plot reading from the responses to the recovery	
	in CB1	in CB3
CB1	–	2.40E-02
CB3	1.00E-02	–
1	1.20E-02	no response observed
2	1.50E-02	no response observed
3	2.40E-02	6.00E-02
4	2.20E-02	9.50E-02
5&6	7.00E-02	2.10E-02
7	5.30E-03	2.30E-02

Tab. 10.12. Diffusivity values obtained from the calculation with the transmissivity and storativity values resulted from the single well test analyses.

Interval / Borehole	Diffusivity Values from Single Well Test Analyses			
	Drawdown		Buildup	
	Theis	GRF (Barker)	Theis	GRF (Barker)
CB1	3.53E-04	1.90E-03	3.05E-04	1.07E-03
CB3	2.83E-04	5.79E-04	4.78E-04	2.88E-04
1	3.17E-06	1.44E-06	3.32E-06	1.32E-06
2	3.60E-06	6.62E-07	4.23E-06	5.11E-07
3	3.01E-05	1.94E-05	7.84E-06	4.83E-06
4	2.16E-03	2.65E-04	1.09E-03	8.23E-05
5&6	8.73E-06	1.34E-05	4.98E-06	1.38E-06
7	2.42E-02	5.09E-05	1.62E-02	1.66E-04

Tab. 10.13. Diffusivity values obtained from the calculation with the transmissivity and storativity values resulted from the cross-hole response analyses.

Interval / Borehole	Diffusivity Values from Cross-Hole Response Analyses					
	Response to Drawdown in CB1		Response to Buildup in CB1		Response to Buildup in CB3	
	Theis	Agarwal	Theis	Agarwal	Theis	Agarwal
CB1	–	–	–	–	1.79E-02	1.68E-02
CB3	n.a.	n.a.	9.60E-03	7.06E-03	–	–
1	n.a.	n.a.	4.30E-04	3.24E-02	n.r.	n.r.
2	n.a.	n.a.	5.20E-03	7.73E-02	n.r.	n.r.
3	n.a.	n.a.	3.20E-03	5.00E-02	2.31E-02	1.27E-01
4	2.77E-03	2.63E-03	2.20E-03	2.12E-03	3.15E-02	2.50E-01
5&6	1.96E-02	4.00E-02	1.90E-02	2.93E-02	0.0189	1.60E-02
7	n.a.	n.a.	4.20E-04	3.41E-04	1.67E-02	1.23E-02

n.a.: Not Analyzed; n.r.: No Response observed